國 立 交 通 大 學

機 械 工 程 學 系

碩 士 論 文

放置可移動擾動銅粒子在一水平加熱銅板上對 FC-72 池沸騰熱傳增強研究

Enhancement of Subcooled FC-72 Pool Boiling Heat Transfer by Movable Copper Particles on a Horizontal Plate

研 究 生：薛 正 宏

指 導 老 師：林 清 發 教授

中 華 民 國 102 年 7 月

放置可移動擾動銅粒子在一水平加熱銅板上對次冷態 FC-72 池沸騰熱傳增強研究

Enhancement of Subcooled FC-72 Pool Boiling Heat Transfer by Movable Copper Particles on a Horizontal Plate

研 究 生 ： 薛 正 宏　　Student：Cheng-Hung Hsueh

指導教授 ： 林 清 發　　Advisor：Prof. Tsing-Fa Lin

國立交通大學

機械工程學系

碩士論文

A Thesis

Submitted to Department of Mechanical Engineering

College of Engineering

National Chiao Tung University

In partial Fulfillment of the Requirements

For the Degree of

Master of Science

In

Mechanical Engineering

July 2013

Hsinchu, Taiwan, Republic of China

中華民國 102 年 7 月

放置可移動擾動粒子在依水平加熱銅板上對 FC-72 持沸騰熱傳增強研究

研究生: 薛 正 宏　　指導老師:林 清 發　教授

國立交通大學機械工程學系

摘要

本論文乃針對放置可移動的擾動銅粒子在一沉浸於次冷態 FC-72 中的加熱銅板之池沸騰熱傳增強研究。在本實驗中，我們探討了流體次冷度、擾動粒子的直徑、擾動粒子的數目，以及所施加之熱通量之間的關係。其中，次冷度範圍從 5℃到 20℃，輸入熱通量 q 從 0.1 到 6W/cm^2，銅粒子的直徑分別有 1.0 和 1.5mm 兩種，在小粒徑時數量從 100 至 1800 顆，而大粒徑時數量從 100 到 800 顆。

實驗結果分別以沸騰曲線和 h-T 圖表示，並且把加上擾動粒子的結果和光滑銅表面作相互比較。實驗結果發現，當我們在銅板上加上了擾動粒子，熱傳效果在低和中熱通量時，會有明顯的增強效果，而隨著放置於加熱銅板上的粒子量越多，熱傳效果會變得越來越好。在本實驗中，最好的一組熱傳效果大約產生相較於光滑表面之 400%的提升，而熱傳效果也會因為參數的相互組合不同而有所變化。另外，在高熱通量的情形下，熱傳效果會有明顯的下降趨勢，這個效果主要歸因於擾動粒子對於氣泡的脫離產生了阻擋的負面效果。在本實驗中，熱傳降低的幅度最大約光滑表面的 20%。而理想的熱傳效果，必須搭配選用適當的擾動粒子粒徑、數目、以及流體次冷度才能達到。

Enhancement of Subcooled FC-72 Pool Boiling Heat Transfer by Movable Copper Particles on a Horizontal Plate

Student: Cheng-Hung Hsueh **Advisor: Prof. Tsing-Fa Lin**

National Chiao Tung University

ABSTRACT

An experiment is carried out here to investigate how subcooled pool boiling heat transfer of liquid FC-72 over a horizontal heated copper plate is affected by placing a large number of copper particles above the plate surface, intending to explore the possible pool boiling heat transfer enhancement by the moving particles. During the experiment, the copper particles are freely placed above the heated plate with a rectangular acryl fence surrounding the plate so that the particles can be moved by the force induced by the boiling flow without been blown away from the heating plate. In the experiment the liquid subcooling ranges from 5℃ to 20℃ and the imposed heat flux is varied from 0.1 to 6 W/cm^2 for the diameter of the moving metallic particles fixed at 1.0 and 1.5 mm. Besides, the total particle number placed on the plate ranges from 100 to 1800 and from 200 to 800 respectively for the small and large particles. The measured data are presented in terms of boiling curves and boiling heat transfer coefficients for the heating surface with the presence and absence of the particles. The experimental parameters include the liquid subcooling, imposed heat flux level, and the size and number of the particles.

Results obtained from the present study for the subcooled pool boiling of

FC-72 show that placing the movable copper particles can significantly increase the pool boiling heat transfer at low liquid subcooling for $\Delta T_{sub} \leq 10℃$. For the small copper particles at liquid subcooling ΔT_{sub}=10℃ and N_p=1600, the enhancement can be up to 200% over that for a bare surface for a certain combination of the experimental parameters. The best enhancement in this study can be as high as 300% for the small copper particles at the liquid subcooling of 5℃ and N_p=1400 & 1800. Even when more than one layer of particles are placed on the plate, relatively significant boiling heat transfer enhancement can be obtained. However, the boiling heat transfer enhancement varies nonmonotonically with the liquid subcooling, particle size and number, and the heat flux applied, reflecting the complex mutual influences of the movable particles and bubble motion near the heated surface. We also note that at higher liquid subcooling, the copper particles are less effective in augmenting the boiling heat transfer. For the high ΔT_{sub} of 20℃ the boiling heat transfer is retarded by the copper particles especially when a large number of the particles are placed on the plate. Besides, the wall superheat for the incipient boiling can be substantially reduced by the moving metallic particles in some cases for $N_p / N_{pf} \geq 1.0$ and $\Delta T_{sub} \leq 10℃$. However, at high heat flux (wall superheat) placing the particles on the plate can substantially reduce the boiling heat transfer especially for the large particles.

The results from the visualization of the boiling flow over the copper plate indicate that placing the movable particles above the plate produce two opposite effects of enhancing and retarding the boiling heat transfer. At high heat flux the retarding effect is strong and boiling heat transfer is impeded by the particles.

TABLE OF CONTENTS

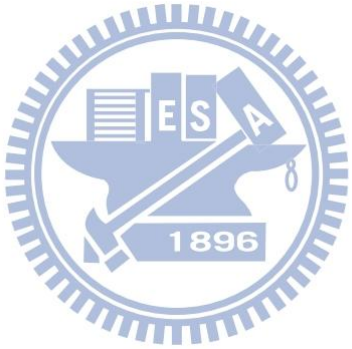

LIST OF TABLES

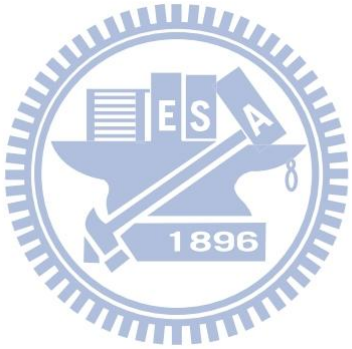

LIST OF FIGURES

Experimental Apparatus

Data Reduction

Subcooled Pool Boiling Heat Transfer

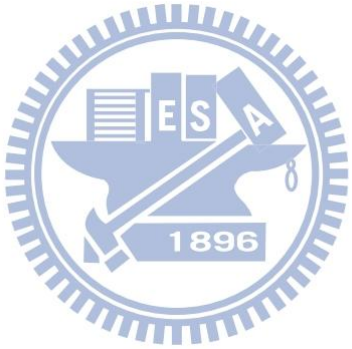

NOMENCLATURE

A	area, mm^2
d_p	diameters of particles, mm
N_p	numbers of particles
h	heat transfer coefficient, $W/m^2 \cdot K$
I	measured current from DC power supply, A
V	measured voltage from DC power supply, V
k	thermal conductivity, W/m·K
L	characteristic length, m
Nu_L	Nusselt number, $Nu_L = \frac{hL}{k_\ell}$
P	system pressure, kPa
Q	heat transfer rate, W
q_n	net wall heat flux, W/cm^2
Ra	Rayleigh number
T	temperature, ^oC
t	time, sec
W	plate width, cm
C_p	specific heat, J/kg·°C
ρ_{Cu}	copper density (ρ_{cu}=8989.9), kg/m^3
ΔT_{sub}	subcooling degree, $\Delta T_{sub} = T_{sat} - T_{bulk}$, K
ΔT_w	wall superheat, $\Delta T_w = T_w - T_{bulk}$, K

Greek Symbols

ν	kinematic viscosity, m^2/s
ρ_ℓ	liquid density, kg/m^3

μ	absolute viscosity, kg/m·s
β	coefficient of expansion, /°C
σ	surface tension, N/m
δ	the distance between the thermocouple tips and the upper surface of the copper plate, m

Subscripts

Cu	copper
t	total

CHAPTER 1

INTRODUCTION

1.1 Motive of the Present Study

Considering the enormous and still increasing needs for electronic products in recent years, the electronics industry rapidly develop tiny integrate circuits including nano components to improve product performance. As a consequence, relatively large amount of heat is generated in the integrate circuits during the device operation. How to effectively remove this large amount of the dissipating heat from the micro processors poses a great challenge to heat transfer research community. In order to transfer the large quantity of the dissipating heat from the chips with an ultra-high microelectronic component density, highly efficient heat transfer methods are required to control their temperatures at allowable level. Although air cooling has been used most commonly over a long period of time, this method has reached its upper performance limit and is unable to handle the huge amount of dissipating heat encountered in the current electronics industry [1]. Therefore, we need a better heat transfer method to solve the problem confronted. Cooling methods based on liquid convection and liquid-vapor phase-change heat transfer have been considered. Among these, boiling heat transfer is regarded as one of the most effective methods in electronics cooling comparing with the methods based on single-phase heat transfer because of the exchange of latent heat involved in the boiling processes which can take away a great quantity of heat. Besides, larger heat transfer rate can be produced by boiling of subcooled liquid due to the larger temperature difference between the coolant and heat dissipating surface. Furthermore, to meet the future need, methods to augment the boiling heat transfer have received increasing attention in the heat transfer research.

Over the past decades considerable effort has been devoted to investigating how the

changes in the heating surface structure can enhance the pool boiling heat transfer. Typical methods include adding the micro-structures, micro-pin fins and grooves to the surfaces. Besides, coating the surfaces with particles and covering the surfaces with screens have been shown to be effective. These enhancement methods are based on various forms of extended surface fixed firmly onto the surfaces or directly fabricated on the surfaces. In the present study, enhancement of pool boiling heat transfer by placing movable particles above the heating plate will be explored. The particle motion is driven by the two-phase boiling flow near the plate. The particles are confined in a rectangular enclosure surrounding the heating plate in order to avoid the particles to move away from the plate, that would decrease the particle number density on the plate.

The working fluid FC-72 used here is a dielectric fluorocarbon liquid manufactured by the 3M Company and gains popularity in electronics cooling application. It not only has suitable phase-change temperature for thermal control of I.C. components but also owns the quality that does not foul the boiling surface. Most importantly, FC-72 has less impact on our environment than alternative liquids like chlorofluorocarbons or organic liquids. Copper has properties of better thermal conductivity than most metals and is often considered to be suitable for heat dissipating elements. Thus the heat transfer enhancement characteristics of pool boiling of the dielectric liquid on a copper plate by placing movable particles above the heating surface immersed in FC-72 liquid are explored in the present study. In an earlier attempt [2] Wei in our laboratory obtained significant enhancement in pool boiling heat transfer of saturated FC-72 over a horizontal heated copper plate by placing copper and stainless steel particles on the plate when the, size and number of particles are suitably chosen for low and medium wall superheats. In this study we move further to investigate the possibility of enhancing subcooled pool boiling heat transfer of FC-72 by the movable copper particles.

1.2 Literature Review

In what follows the literature relevant to the present study is briefly reviewed. Pool boiling heat transfer is a process of vigorous heat transfer resulting from latent heat exchange associated with liquid-to-vapor phase change in a quiescent liquid. Nukiyama [3] conducted a pioneering pool boiling experiment in 1934 and arranged the experimental heat transfer data as a form of the wall superheat versus the heat flux, which is known as the "boiling curve" today. After that, the pool boiling heat transfer research has received considerable attention.

The state of the art cooling technologies for handling heat dissipation in microelectronic equipments have been developed extensively over the past 30 years. Several products were released including Air-Cooled Modules, High Thermal Conduction Modules, and Liquid-Cooled Modules, as discussed by Bar-Cohen [4].

In an early attempt to improve pool boiling heat transfer by using a micro-configured surface, Miller et al. [5] found that vapor retention could be a function of the scale and geometry of the micro-configurations. They pointed out that the relation between the stability of the potential nucleation sites and the micro-configuration size and geometry required further investigation, so that the size and the site density of the cavities could be optimized for boiling heat transfer enhancement.

Slightly later a few studies were carried out to examine the influences of the surface fabricated microstructures on the pool boiling heat transfer. These include boiling of FC-72 on micro-porous surfaces with particle coating tested by Chang and You [6] and by Vemuri and Kim[7], adding micro-porous pin-fins along with coating particles to the surface investigated by Rainey and You [8,9], and fabricating micro-pin-fins and submicron-scale roughness on the surfaces by Honda et al. [10] and Wei et al. [11]. The study of Rainey and You [8] concluded that the microporous coating can significantly enhance the boiling heat transfer performance over the pin-finned surfaces. For the subcooled boiling on the micro-porous surface [9], Rainey et al found that at increasing subcooling/pressure, the CHF could be increased as well.

In examining the pool boiling on the micro-pin-fin surfaces, Honda et al. [10] and Wei et al. [11] noted that the boiling curves were characterized by that a very small increase in the wall superheat could cause a large increase in the heat flux. And increasing the fin height was found to provide better heat transfer in the nucleate boiling regime and resulted in a higher critical heat flux. Nucleation site interaction in pool boiling on an artificial surface was investigated by Zhang and Shoji [12] and by Yu et al. [13]. The hydrodynamic interaction can be also influenced by some factors, such as the liquid properties, subcooling, system pressure. The study of Yu et al. [13] concluded that the critical heat flux was dependent on the cavity density. The evaporation/boiling heat transfer regimes in the capillary wicking structures were identified and discussed by Li et al.[14] and Li and Peterson[15]. Anderson and Mudawar [16] reported that microstructures in the forms of fins, studs, grooves and vapor-trapping cavities on the boiling surface significantly shifted the boiling curve toward lower superheats while increasing the incipience excursion. Their results also suggest that the maximum boiling heat flux is a function of surface geometry and orientation but independent of the initial conditions, surface roughness, or the presence of large artificial cavities. Intending to augment boiling heat transfer, O'Connor and You [17] painted silver flakes on the boiling surface. Their experimental data show that the incipience boiling superheats are 70-85% lower and the nucleate boiling superheats are 70-80% lower than the bare surface. Besides, the critical heat flux is increased by 109%. O'Connor et al. [18] then compared two methods of generating surface microstructures, "spraying" and "painting", for pool boiling heat transfer enhancement. They noted that for saturated FC-72, the incipient boiling superheat showed 33-55% reduction for the sprayed alumina and 63-85% reduction for the painted diamond. The enhancement in the critical heat flux can be up to 45% for the sprayed alumina and 61% for the painted diamond microstructures. While for the subcooled boiling of FC-72, the critical heat flux was increased about 101% and 87% for the diamond paint and sprayed alumina microstructures, respectively. Chang and You [19] further studied the effects of coating different sizes of the

diamond particles on the pool boiling heat transfer performances. They classified the coating thickness into two groups. For coatings thinner than 100 μm, increasing the coating thickness would generate a higher active nucleation density. But for coatings thicker than 100 μm, a further increase in the coating thickness does not always enhance the pool boiling heat transfer. They attributed this result to higher impedance for liquid-vapor exchange channels and higher thermal resistance for the thicker coating. Jung and Kwak [20] investigated the effects of submicron-scale roughness on the subcooled boiling heat transfer over a boiling surface anodized in DMF (dimethylforamide) and HF (hydrofluoric acid). Both surface treatments were found to increase the effective boiling area and served for increasing the nucleation sites and hence showed considerable enhancement in the boiling heat transfer. The critical heat flux also increases linearly. Honda and Wei [21] reviewed recent advances in enhancing boiling heat transfer from electronic components immersed in dielectric liquids through the use of surface microstructures. They concluded that most of the surface microstructures were effective in decreasing the wall superheat at the boiling incipience. The nucleate boiling heat transfer also can be improved and the critical heat flux is raised almost linearly with increasing the liquid subcooling for ΔT_{sub} in the range of 0 to 40K. Rainey and You [22] and Rainey et al. [23] respectively studied the effects of the orientation and pressure on the pool boiling heat transfer from microporous surface. Their data show that nucleate boiling performance increases slightly for the surface inclined from 0^{o}(horizontal) to 45^{o} and then decreases for the inclination angle ranging from 90^{o} to 180^{o}. Moreover, for the plain and microporous surfaces increases in boiling performance and critical heat flux and decrease in the incipience wall superheat were noted as the pressure increased.

Chou et al. [24] arranged several grooved patterns on surfaces intending to enhance boiling heat transfer of distilled water. Their experimental data reveal that the radial grooved pattern has the best enhanced boiling heat transfer performance and the spiral or concentric grooved pattern has poorer boiling heat transfer coefficient. The worst performance is noted

for the grid or the spotted grooved pattern. All grooved patterns they investigated have better heat transfer performance than the plain surface and the denser groove is better than the sparser one for the same patterns.

Hasegawa et al. [25] covered a heat pipe with a woven screen to investigate the associated boiling characteristics and burnout phenomena. Their results disclose that the additional screen produces two opposite effects of inhibiting and enhancing the boiling heat transfer. Tsay et al. [26] explored pool boiling heat transfer enhancement by covering the boiling surface with a screen in distilled water. They found that the screen coverage could raise bubble generation frequency and enhance the boiling heat transfer. But the screen can also cover some nucleation sites and hence may retard the boiling heat transfer. They also noted that the boiling heat transfer became poorer at lowering the liquid level. They concluded that covering the heated surface with a screen could augment the pool boiling heat transfer if the mesh size was comparable with the bubble departure diameter. In boiling of methanol and HFE-7100, Liu et al. [27] pointed out that placing a fine mesh layer on the boiling surface enhanced nucleate boiling heat transfer at low wall superheat (ΔT_{sat}<8-10K) but an opposite trend resulted at high superheat (ΔT_{sat}>8-10K). They also reported that the heat transfer in nucleate boiling always became worse with a coarse mesh on the boiling surface. On the other hand, for smooth surface the increase of liquid subcooling results in lower wall superheat which can be considered as enhancement in heat transfer. Watwe et al. [28] also investigate the pressure and subcooling effects from a PPGA chip package. They concluded that the CHF increased linearly with the subcooling for FC-72 at atmospheric pressure. Moreover, Franco et al. [29] used dielectric refrigerant R141b to investigate enhancement in the boiling heat transfer performance by covering the heated surface with wire meshes. The boiling heat transfer coefficient was noted to increase significantly, especially at relatively low heat fluxes. They also found that the wire mesh coverage on the heating surface resulted in slower transition to steady film boiling. In studying the effects of the wall superheat and the mesh

layer covering on boiling heat transfer, Kurihara and Myers [30] tested several working fluids including water, acetone, n-hexane, carbon tetrachloride, and carbon disulfide. They found that active nucleation sites on the heating plate increased due to the mesh covering and the boiling heat transfer coefficient was proportional to the one-third power of the bubble column numbers at high numbers.

Pool boiling heat transfer in liquid saturated particle bed and fluidized bed of distilled water was investigated by Shi et al. [31]. The tests were conducted for glass beads, steel balls, fine sand and Al_2O_3 particles. They showed that boiling heat transfer could be enhanced greatly by adding the solid particles into the liquid whether in fixed particle bed or in fluidized particle bed. The boiling heat transfer enhancement is closely related to the particle size (d_p=0.5, 1.0 and 2.0 mm), initial bed depth (H_p=3.0, 6.5, 9.5 and 13.4 mm) and heat flux applied. The best heat transfer enhancement is 120% for the particle diameter d_p=1.0 mm and bed height H_p=9.5 mm. A similar study was conducted by Matijevic et al. [32] using lead spheres to cover a heating surface. The spheres were packed as closely as possible into a single layer. They noted that boiling heat transfer from the heating surface to water could be enhanced substantially by the metallic spheres (d=3.0, 3.5, 3.6, 4.0 and 4.5 mm), and the smaller spheres resulted in a better enhancement of boiling heat transfer.

Mohamed et al. [33] carried out a series of experiments to examine boiling of subcooled HFE-7100 fluid. He found that compared to the saturated state, a higher degree of liquid subcooling caused obviously higher critical heat flux (CHF) and lower surface superheat to initiate boiling on the porous graphite surface and smooth flat copper surface. For the case of the saturated liquid on the smooth flat copper surface, the critical heat flux and surface superheat to initial boiling for saturation state are respectively 21.5 W/cm^2 and 10.9 K. While at a subcooling of 30℃ the CHF and initial boiling temperature are individually 37.3W/cm^2 and 5 K, an increase of more than 73% for CHF and a decrease of 54% for the ONB temperature.

Recently, Coulibaly et al. [34] examined bubble coalescence during subcooled nucleate pool boiling of FC-72. They showed that the coalesced bubble moved and oscillated on the heater surface with significant heat transfer variations prior to departure. Bubble departure size and departure frequency decreased as the subcooling increased. Harada et al. [35] also studied bubble behavior in subcooled boiling. Their results showed that when bubbles were lifted-off the heated surface in subcooled liquid, the life time of bubbles was significantly shorten because the bubbles collapsed rapidly due to vapor condensation.

Heat transfer enhancement by the usage of nanofluids has become very popular recently. In nanofluids a very large number of nano particles (diameters smaller than 100 nm) are added into a working fluid which is considered to significantly increase thermal conductivity of the fluid. Wen and Ding [36] reported an enhancement of boiling heat transfer coefficient for about 40% with alumina water based nanofluids. On the other hand, by using the same nanoparticles in the same fluid, Bang and Chang [37] found that the boiling heat transfer coefficient deteriorated for about 20% when the nanoparticles are added.

Some active techniques to enhance boiling heat transfer were also proposed in the literature. Jeong and Kwon [38] found that the CHF augmentation in pool boiling of water due to ultrasonic vibration was closely related to its effects on increasing bubble generation and its departure. They noted that the rate of increase in CHF for downward facing surface ranged from 87~126% as the water subcooling varied from 5 to 40℃. When ultrasonic wave is applied, the rate of CHF augmentation increased as the water subcooling increases. This is caused by an increase in cavitation bubble population, which contributed to fluid mixing, for an increase in subcooling. Cipriani et al. [39] imposed electric field on pool boiling of FC-72 over a heated platinum wire (d=0.1 and 0.2 mm)and found that the boiling heat transfer was strongly influenced by the presence of the electric field at a low wire superheat. An increase of the boiling heat transfer coefficient up to 400% was encountered with the maximum applied voltage. But it is almost unaffected by the electrical force at high wire superheat. Through

heated surface vibration, Navruzov et al. [40] demonstrated that boiling heat transfer of ethanol could be substantially enhanced at low imposed heat flux. The amplitude of the surface vibration is found to be a governing parameter for heat transfer enhancement at low-frequency vibrations. Besides, the vibration of the heat transfer surface significantly alters the heat transfer process both in subcooled boiling and in free convection. The single-phase heat transfer curves are 70-80% above the basic curve at increasing heat loads.

1.3 Objective of Present Study

Literature review conducted above clearly discloses that considerable works have been carried out in the past to investigate the enhancement in the pool boiling heat transfer over a surface by passive methods through fabricating surface microstructures such as roughness and micro-pin-fins and by covering the surface with mesh screens and particle coating. All these microstructures are fixed firmly onto the boiling surface. Besides, some effective active heat transfer augmentation methods such as vibrating or rotating heating surface and/or fluid and applying electric field to vibrate a heating surface have been suggested. Following the previous work on the enhancement of saturated pool boiling heat transfer [2], an experiment is conducted here to explore the possible enhancement in the subcooled FC-72 pool boiling heat transfer by placing movable copper particles on the boiling surface. The vigorous motion of the bubbles in the boiling flow can cause violent movement of the particles. Meanwhile, this violently moving particles can significantly affect the bubble dynamics near the surface. Thus we expect the boiling heat transfer from the surface can be enhanced. The method proposed here is passive in nature. However, it behaves like an active heat transfer enhancement method.

CHAPTER 2

EXPERIMENTAL APPARATUS AND PROCEDURES

A schematic arrangement of the experimental apparatus for the present investigation of the subcooled pool boiling heat transfer enhancement by movable metallic particles driven by the boiling flow is similar to that employed in the previous study [2] and is shown in Fig. 2.1. The experimental system includes a main test chamber, a test heater assembly, and other auxiliary parts such as a D.C. power supply, a data acquisition unit and a high-speed photographic unit. The working fluid, FC-72, is a highly wetting dielectric fluorocarbon liquid produced by 3M Industrial Chemical Products Division, which has been considered as a good candidate fluid for liquid immersion cooling applications. It is chemically stable, dielectric, and has a relatively low boiling point (T_{sat}=56°C at atmospheric pressure). Some thermophysical properties of FC-72 are given in Table 2.1.

2.1 Main Test Chamber

The main test chamber is a hermetic stainless steel pressure vessel of 205 mm in height and 216 mm in diameter. An internal water condenser is installed inside the chamber and connects with a thermostat (LAUDA RK20) to maintain the bulk temperature of the working fluid in the chamber at the preset level. The maximum cooling power of the thermostat is 180W (at 20°C). We further use an external temperature controller (FENWAL MYSPEC Digital Temperature Controller) to control the bulk temperature of FC-72 in the test chamber with an accuracy of ± 0.1°C. Besides, a cartridge heater is located near the bottom of the test chamber to provide additional heating during the degassing process. In order to prevent the heat

loss from the vessel to the ambient, a superlon layer of 10-mm thick is wrapped around the chamber. Moreover, a pressure transducer with an operating range of 0-200 kPa is located at the gate valve to measure the pressure of the work fluid. Meanwhile, the working fluid temperature is measured by two resistance temperature detectors (RTDs) located at the gate valve and at a selected location 5 cm above the bottom surface of the chamber with a calibrated accuracy of ± 0.1°C. An auxiliary tank of 10-liter liquid FC-72 is placed right above the test vessel and it is only used for the subcooled pool boiling experiment to prevent regassing of the working fluid after degassing. A pressure transducer and a RTD are placed in the auxiliary tank to measure the internal gas pressure and liquid temperature. In addition, a test heater assembly is mounted to a stainless steel shelf to fix the PEEK (Polyether Ether Ketone) substrate. The working fluid is maintained at approximately 80 mm above the heated surface in the experiment.

2.2 Test Heater Assembly

A schematic of the test heater assembly is shown in Fig. 2.2. The assembly consists mainly of a film heater and it is adhered to the lower surface of a square copper plate by epoxy Omegabond 200. The plate is 10-mm thick with 30x30 mm^2 in surface area. The heater supplies the required power input to the copper plate. The copper plate is flush mounted onto a much larger PEEK block. Liquid FC-72 boils on the upper surface of the copper plate. More specifically, the copper plate is heated by D.C. current delivered from a D.C. power supply to the film heater. Besides, three calibrated copper-constantan thermocouples (T-type) with a calibrated accuracy of $\pm$ 0.2°C are installed at selected locations in the copper plate right below the boiling surface. They are used for the control and determination of the boiling surface

temperature. The detailed locations of the thermocouples in the copper plate are shown in Fig. 2.3. Note that the whole copper plate is inserted into a PEEK block which serves as a heat insulator ($k_T \approx 0.25 \mathrm{W/m \cdot K}$), intending to reduce the heat loss from the lateral and bottom surfaces of the plate to the ambient. Besides, the locations of thermocouples in the PEEK block which installed for the estimation of heat loss are shown in Fig. 2.4.

2.3 Confinement of Particles and Experimental Parameters

Solid particles of the same material and uniform size are placed freely on the upper surface of the copper plate, as schematically shown in Fig. 2.5. In order to insure that the particles would not be blown away by the vigorous motion of the bubbles, we install an acryl fence of 2-cm high and 1-cm thick around the edges of the heating copper plate. In the present study tests will be conducted for copper particles. The density of copper is measured before the experiment with $\rho_{cu} = 8990\ kg/m^3$. The copper particle is chosen here because the copper have much higher density than liquid FC-72 and is used widely in the industry for its excellent conductivity which may enhance the thermal conduction from the plate. Besides, the chosen particles should not be too small so that they float in the liquid above the plate and do not contact the heating surface. Moreover, they should not be too large and cannot be moved by the boiling flow. Here, the particle diameter is selected to be 1.0 and 1.5 mm. On the other hand, the liquid FC-72 subcooling is varied from 5℃ to 20℃. More specifically, four different liquid subcoolings at ΔT_{sub}=5℃, 10℃, 15℃ and 20℃ are tested. The chosen particle size and number for the cases covered here are summarized in Table 2.2. The measured data expressed in terms of boiling curves and boiling heat transfer coefficients will be compared with that of a bare heating surface.

2.4 DC Power Supply

The power generated in the film heater in the test heater assembly is provided by a programmable D.C. power supply (Gpc 3030D). It offers a maximum D.C. power of 180W for an output voltage of 60V and an output current of 3A. The power input to the copper block is transmitted through a GPIB interface to a personal computer. In order to measure the D.C. current, a precision ammeter (KYORITSU A.C./D.C. DIGITAL CLAMP METER) is arranged in series connection with the electric circuit. Besides, a YOKOGAWA data recorder is used to measure the voltage drop across the test heater assembly. All the voltage, current and power measurement devices are calibrated by a YOKOGAWA WT200 power meter according to the Center of Measurement Standards in Industrial Technology Research Institute of Taiwan.

2.5 Data Acquisition

A 20-channel YOKOGAWA data recorder (MX-100) combined with a personal computer is used to acquire and process the data from various transducers. All signals detected from the T-type thermocouples, RTDs, pressure transducer, ammeter, data recorders and power meter are all collected and converted by the internal calibration equations in the computer during the data acquisition.

2.6 Optical Measurement Technique

A high-speed camera along with a microscope is installed in front of the observation window to observe the boiling activity in the flow. The photographic apparatus consists mainly of a high speed digital video camera (IDT High-speed

CMOS Camera), a micro-lens (Optem Zoom 16), and a three-dimensional positioning mechanism. The high-speed motion analyzer can take photographs up to 143,307 frames/sec. In the present experiment the recording rate is 1000 frames/sec. After the experimental system reaches a statistical state, we start capturing the images of the particles and bubble in the boiling flow. Besides, we store and display the images in the personal computer through an image-capturing software.

2.7 Experimental Procedures

Before the experiment, the boiling surface is polished by fine sand paper (Number 3000, 2000 and 1000) and cleaned by ethyl alcohol. In each test, we need to remove non-condensable gases existing in the empty test chamber by running a vacuum pump for about 15 minutes and then fill the FC-72 liquid into the chamber until the liquid level is higher than the heating plate for about 80 mm. Next, the FC-72 liquid in the test chamber is heated to 65℃ and boiled vigorously for about 1 hour to further remove the dissolved non-condensable gases in the dielectric liquid. During the process, the temperature in the chamber is detected and maintained by a digital temperature controller. After the working fluid pressure and temperature stabilize to one atmosphere and at the preset subcooled state, we turn on the test heater. The imposed heat flux on the boiling surface is adjusted by controlling the electric current delivered to the heater from the D.C. power supply. Upon reaching the statistical state, we begin collecting the required heat transfer data and visualizing the boiling activity. After the experiment for the case of bare surface is finished, we put the chosen number and size of the copper particles on the copper plate and repeat the procedure described above. In order to keep the particles on the copper plate, we also place an acrylic rectangular enclosure onto the PEEK block around the edge of copper plate.

Effects of the particle size, number and subcooling of the working fluid on the possible boiling heat transfer enhancement will be investigated in the experiment.

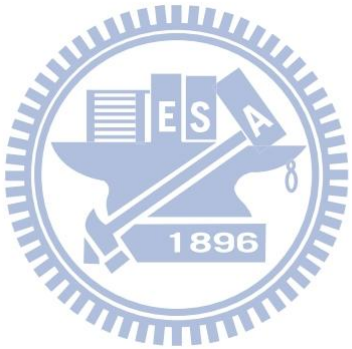

Table 2.1 Thermophysical properties of FC-72.

Properties at 25°C	**FC-72**
Appearance	Clear, colorless
Average Molecular Weight	338
Boiling Point (1atm)	56°C
Pour Point (1atm)	-90°C
Estimated Critical Temperature	449K
Estimated Critical Pressure	1.83×10^6 Pa
Vapor Pressure	3.09×10^4 Pa
Latent Heat of Vaporization h_{fg} (at normal boiling point)	88 J/g
Liquid Density ρ_ℓ	1680 kg/m^3
Absolute Viscosity μ	6.4×10^{-3} poises ; 6.4×10^{-4} kg/m·s
Kinematic Viscosity ν	3.8×10^{-3} stokes ; 3.8×10^{-7} m^2/ s
Liquid Specific Heat c_p	1100 J/kg·°C
Liquid Thermal Conductivity k	0.057 W/m·°C
Coefficient of Expansion β	0.00156 /°C
Surface Tension σ	10 dynes/cm ; 10^{-2} N/m

Table 2.2 Cases covered in present study for 1.0 mm copper particle

Material	Subcooling Degrees	N_p	
Copper (1mm)	5℃	100	1000
		200	1100
		300	1200
		400	1300
		500	1400
		600	1500
		700	1600
		800	1700
		900	1800
	10℃	200	1200
		400	1400
		600	1600
		800	1800
		1000	
	15℃	200	800
		400	1200
		600	
	20℃	800	1200

Table 2.3 Cases covered in present study for 1.5 mm copper particle

Material	Subcooling Degrees	N_p	
Copper (1.5mm)	5℃	200	600
		400	800
	10℃	200	600
		400	800
	15℃	200	600
		400	800
	20℃	200	600
		400	800

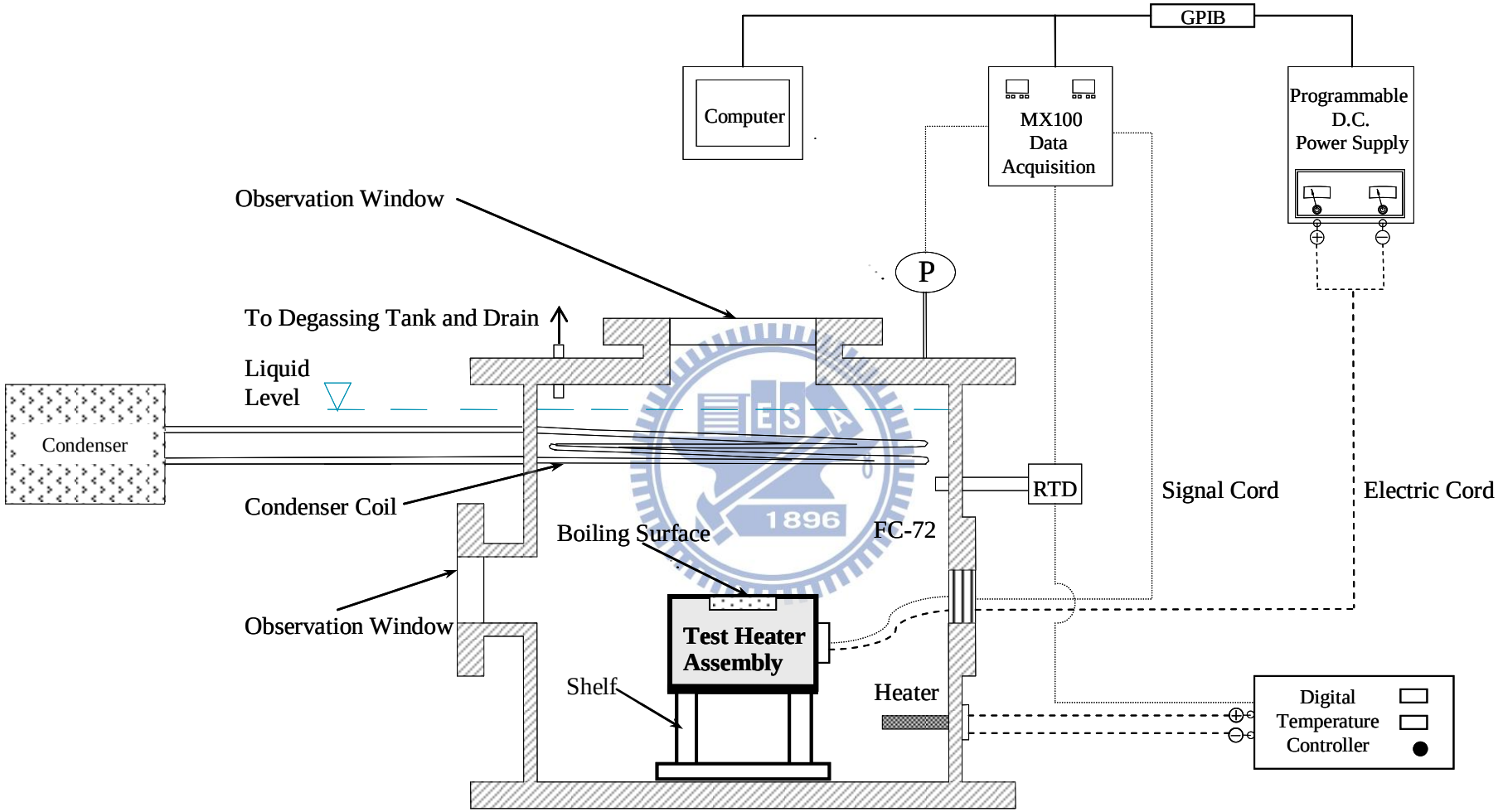

Fig. 2.1 Schematic diagram of the test apparatus.

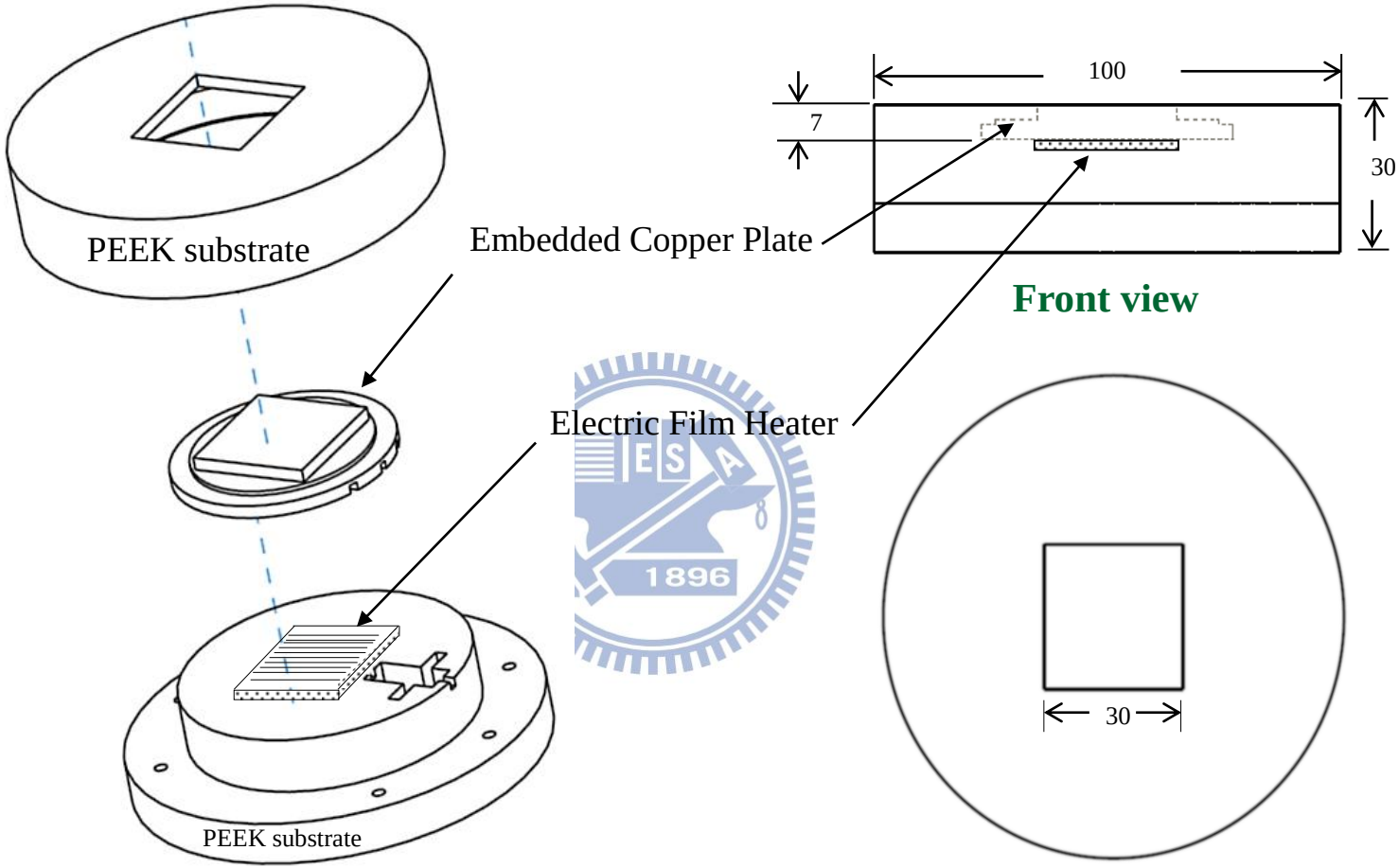

Fig. 2.2 Schematic diagram of the test heater assembly (not to scale).

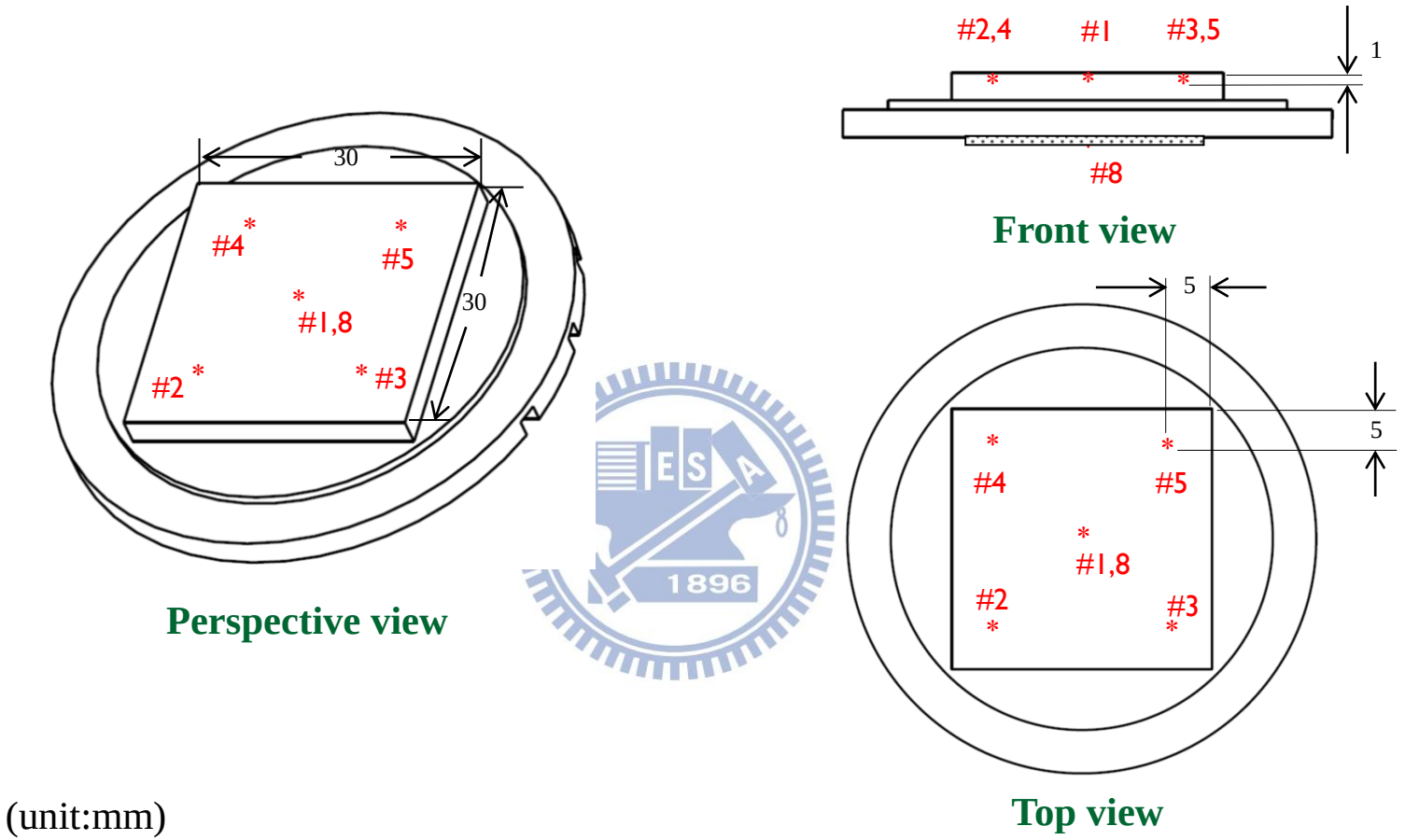

Fig. 2.3 Locations of three thermocouples in the copper plate and one thermocouple below the heater (not to scale).

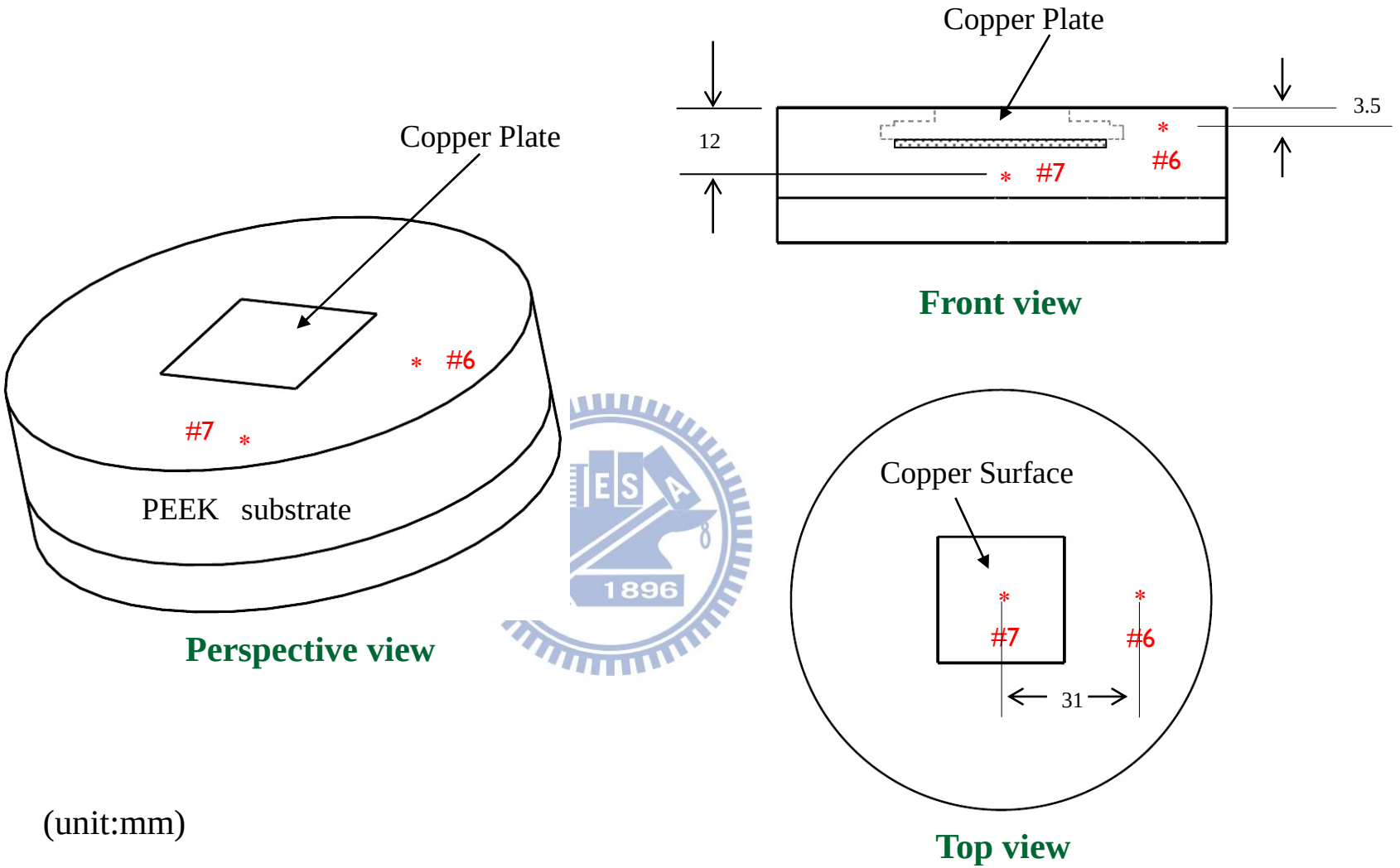

Fig. 2.4 Locations of two thermocouples in the PEEK (not to scale).

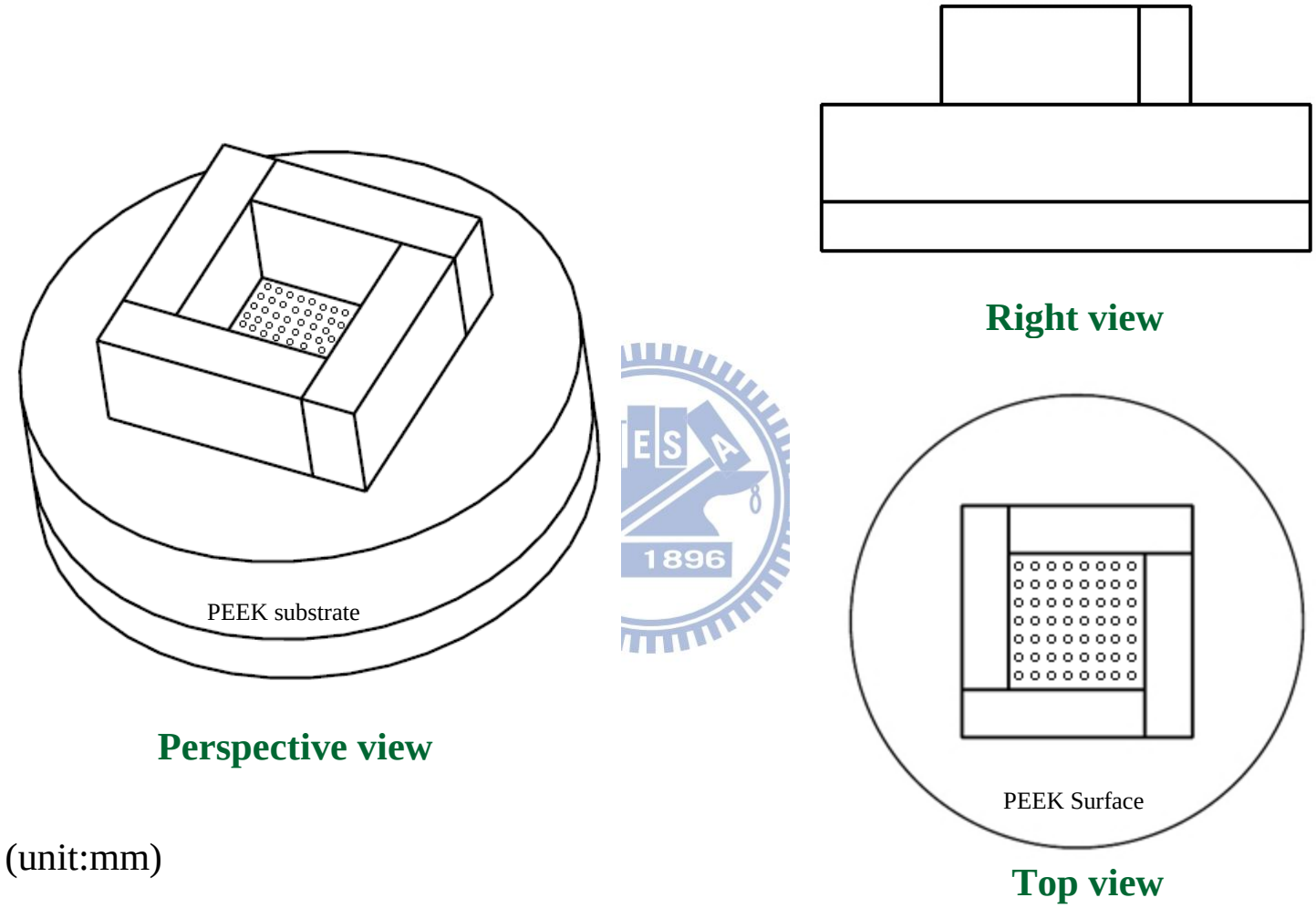

Fig. 2.5 Schematic diagram of placing movable particles on heating surface with acryl rectangular enclosure (not to scale).

CHAPTER 3

DATA REDUCTION

3.1 Boiling Heat Transfer Coefficient

The space-average natural convection and boiling heat transfer coefficients over the upper surface of the heated square copper plate when the flow is at a statistical state are both defined as

$$\mathrm{h} = {}^{q_n}/_{\Delta T_w} \tag{3.1}$$

where q_n is the net heat flux imposed on the upper surface and ΔT_w is the wall superheat defined as the difference between the average surface temperature and the bulk liquid temperature of FC-72 which can be written as:

$$\Delta T_w = T_w - T_b \tag{3.2}$$

The average heated surface temperature T_w is estimated from the measured average temperature from the thermocouples installed at different locations near the upper surface of the copper plate according to the steady-state one-dimensional conduction heat transfer. Specifically,

$$T_w = T_{Cu} - \left(q_n \times \frac{\delta}{k_{Cu}} \right) \tag{3.3}$$

where

T_{Cu} = the average measured temperature from the thermocouples installed in the copper plate (°C)

k_{Cu} = the thermal conductivity of copper (W/m·K)

δ = the vertical distance between the thermocouple tips and the upper surface of the copper plate (m)

The total power input Q_t to the copper plate can be obtained from the measured voltage drop across the film heater in the test heater assembly and the current passing through it,

$$Q_t = I \cdot V \tag{3.4}$$

where

Q_t = total power input to the upper surface of the copper plate (W)

I = electric current passing through the film heater (Amp.)

V = voltage drop across the film heater (Volts)

The substrate of the test section is made from PEEK, which have a much lower thermal conductivity ($k_T \approx 0.25 \mathrm{W/m \cdot K}$) than the copper ($k \approx 386 \mathrm{W/m \cdot K}$). In evaluating total heat loss from the heater assembly, we focus on heat transfer from the heater and copper plate surface to the PEEK. Figures 2.3 and 2.4 are the schematic diagrams of the thermocouples buried in the copper plate and PEEK. The heat dissipation model used to estimate the heat loss is shown in Fig. 3.1, and the total heat loss can be estimated as follows:

$$\mathrm{Q_{loss}} = \mathrm{k_p} \cdot \frac{(\mathrm{T_8 - T_7})}{\mathrm{L_1}} \cdot \mathrm{A_1} + 4 \cdot \mathrm{k_p} \cdot \frac{(\mathrm{T_{cu} - T_6})}{\mathrm{L_2}} \cdot \mathrm{A_2} + \frac{2\pi \cdot \mathrm{k_p} \cdot \mathrm{L_3} \cdot (\mathrm{T_{cu} - T_6})}{\ln(\frac{\mathrm{r_6}}{\mathrm{r_{cu,2}}})} + \frac{2\pi \cdot \mathrm{k_p} \cdot \mathrm{L_4} \cdot (\mathrm{T_{cu} - T_6})}{\ln(\frac{\mathrm{r_6}}{\mathrm{r_{cu,3}}})} + \mathrm{k_p} \cdot \frac{(\mathrm{T_{cu} - T'_5})}{\mathrm{L_5}} \cdot \mathrm{A_5} + \mathrm{k_p} \cdot \frac{(\mathrm{T_{cu} - T'_6})}{\mathrm{L_6}} \cdot \mathrm{A_6} \tag{3.5}$$

where

T_6 , T_7 , T_8 : the average measured temperatures from the thermocouples inside the PEEK insulator, as schematically shown in Figs. 2.3 & 2.4

L_1, L_2 , L_3 , L_4 , L_5 , L_6: shortest distances between locations No.1~No.6 and the

film heater or copper plate (m)

A_1 , A_2, A_3, A_4, A_5, A_6 : bottom and lateral surface areas of the copper plate

T'_5 , T'_6 : these two temperatures are calculated by using interpolation method based on T_6, as schematically shown in Fig. 3.2

Finally, the net imposed input heat flux to the upper surface of copper plate can be evaluated from the relation

$$q_n = \frac{Q_t - Q_{loss}}{A_{Cu}} \tag{3.6}$$

where A_{Cu} is the area of the upper surface of the copper plate.

3.2 Uncertainty Analysis

An uncertainty analysis is carried out here to estimate the uncertainty levels in the experiment. Kline and McClintock [41] proposed a formula for evaluating the uncertainty in the result F as a function of independent variables, X_1, X_2, X_3……X_n,

$$F=F\ (X_1\ ,X_2,\ X_3\cdots\cdots\cdots X_n) \tag{3.7}$$

The absolute uncertainty of F is expressed as

$$\delta F = \left\{\left[\left(\frac{\partial F}{\partial X_1}\right)\delta X_1\right]^2 + \left[\left(\frac{\partial F}{\partial X_2}\right)\delta X_2\right]^2 + \left[\left(\frac{\partial F}{\partial X_3}\right)\delta X_3\right]^2 + \cdots + \left[\left(\frac{\partial F}{\partial X_n}\right)\delta X_n\right]^2\right\}^{\frac{1}{2}} \tag{3.8}$$

and the relative uncertainty of F is

$$\frac{\delta F}{F} = \left\{\left[\left(\frac{\partial \ell nF}{\partial \ell nX_1}\right)\left(\frac{\delta X_1}{X_1}\right)\right]^2 + \left[\left(\frac{\partial \ell nF}{\partial \ell nX_2}\right)\left(\frac{\delta X_2}{X_2}\right)\right]^2 + \left[\left(\frac{\partial \ell nF}{\partial \ell nX_3}\right)\left(\frac{\delta X_3}{X_3}\right)\right]^2 + \cdots + \left[\left(\frac{\partial \ell nF}{\partial \ell nX_n}\right)\left(\frac{\delta X_n}{X_n}\right)\right]^2\right\}^{\frac{1}{2}} \tag{3.9}$$

If $F = X_1^a X_2^b X_3^c$..... , then the relative uncertainty is

$$\frac{\delta F}{F}=\left\{\left[a\left(\frac{\delta X_1}{X_1}\right)\right]^2+\left[b\left(\frac{\delta X_2}{X_2}\right)\right]^2+\left[c\left(\frac{\delta X_3}{X_3}\right)\right]^2+\cdots\cdots\right\}^{\frac{1}{2}} \tag{3.10}$$

where $\frac{\partial F}{\partial X_i}$ and ∂X_i are, respectively, the sensitivity coefficient and uncertainty level associated with the variable X_i. The values of the uncertainty intervals ∂X_i are obtained by a root-mean-square combination of the precision uncertainty of the instruments and the unsteadiness uncertainty, as recommended by Moffat [42]. The choice of the variable X_i to be included in the calculation of the total uncertainty level of the result *F* depends on the purpose of the analysis.

The uncertainties of the parameters in the present study are calculated as follows:

(1) Uncertainty of temperature difference, $\Delta T_w=T_w-T_b$

$$\begin{aligned}\frac{\delta(T_w-T_b)}{(T_w-T_b)}&=\left\{\left[\left(\frac{\partial \ell n(T_w-T_b)}{\partial \ell n T_w}\right)\left(\frac{\delta T_w}{T_w}\right)\right]^2+\left[\left(\frac{\partial \ell n(T_w-T_b)}{\partial \ell n T_b}\right)\left(\frac{\delta T_b}{T_b}\right)\right]^2\right\}^{\frac{1}{2}}\\&=\left\{\left[\left(\frac{T_w}{T_w-T_b}\right)\left(\frac{\delta T_w}{T_w}\right)\right]^2+\left[\left(\frac{T_b}{T_w-T_b}\right)\left(\frac{\delta T_b}{T_b}\right)\right]^2\right\}^{\frac{1}{2}}\\&=\left\{\left[\frac{\delta T_w}{T_w-T_b}\right]^2+\left[\frac{\delta T_b}{T_w-T_b}\right]^2\right\}^{\frac{1}{2}}\end{aligned} \tag{3.11}$$

(2) Uncertainty of total power input, Q_t

$$Q_t=I\cdot V \tag{3.4}$$

and $$\frac{\delta Q_t}{Q_t}=\left[\left(\frac{\delta I}{I}\right)^2+\left(\frac{\delta V}{V}\right)^2\right]^{\frac{1}{2}} \tag{3.12}$$

(3) Uncertainty of net wall heat flux, q_n

$$q_n = \frac{Q_t - Q_{loss}}{A_{Cu}} \tag{3.6}$$

and

$$\frac{\delta q_n}{q_n} = \left\{ \left[\left(\frac{\partial \ell n q_n}{\partial \ell n A_{Cu}} \right) \left(\frac{\delta A_{Cu}}{A_{Cu}} \right) \right]^2 + \left[\left(\frac{\partial \ell n q_n}{\partial \ell n Q_t} \right) \left(\frac{\delta Q_t}{Q_t} \right) \right]^2 + \left[\left(\frac{\partial \ell n q_n}{\partial \ell n Q_{loss}} \right) \left(\frac{\delta Q_{loss}}{Q_{loss}} \right) \right]^2 \right\}^{\frac{1}{2}}$$

$$= \left\{ \left[1 \cdot \left(\frac{\delta A_{Cu}}{A_{Cu}} \right) \right]^2 + \left[\left(\frac{Q_t}{Q_t - Q_{loss}} \right) \left(\frac{\delta Q_t}{Q_t} \right) \right]^2 + \left[\left(\frac{Q_{loss}}{Q_t - Q_{loss}} \right) \left(\frac{\delta Q_{loss}}{Q_{loss}} \right) \right]^2 \right\}^{\frac{1}{2}}$$

$$= \left\{ \left[\frac{\delta A_{Cu}}{A_{Cu}} \right]^2 + \left[\frac{\delta Q_t}{Q_t - Q_{loss}} \right]^2 + \left[\frac{\delta Q_{loss}}{Q_t - Q_{loss}} \right]^2 \right\}^{\frac{1}{2}} \tag{3.13}$$

Where

$$Q_{loss} = k_p \cdot \frac{(T_8 - T_7)}{L_1} \cdot A_1 + 4 \cdot k_p \cdot \frac{(T_{cu} - T_6)}{L_2} \cdot A_2 + \frac{2\pi \cdot k_p \cdot L_3 \cdot (T_{cu} - T_6)}{\ln(\frac{r_6}{r_{cu,2}})} + \frac{2\pi \cdot k_p \cdot L_4 \cdot (T_{cu} - T_6)}{\ln(\frac{r_6}{r_{cu,3}})} + k_p \cdot \frac{(T_{cu} - T'_5)}{L_5} \cdot A_5 + k_p \cdot \frac{(T_{cu} - T'_6)}{L_6} \cdot A_6 \tag{3.5}$$

(4) Uncertainty of space-average heat transfer coefficient, *h*

$$h = q_n / \Delta T_w \tag{3.1}$$

And

$$\frac{\delta h}{h} = \left\{ \left[\left(\frac{\partial \ell n h}{\partial \ell n q_n} \right) \left(\frac{\delta q_n}{q_n} \right) \right]^2 + \left[\left(\frac{\partial \ell n h}{\partial \ell n (T_w - T_b)} \right) \left(\frac{\delta (T_w - T_b)}{T_w - T_b} \right) \right]^2 \right\}^{\frac{1}{2}}$$

$$= \left\{ \left[1 \cdot \left(\frac{\delta q_n}{q_n} \right) \right]^2 + \left[-1 \cdot \left(\frac{\delta (T_w - T_b)}{T_w - T_b} \right) \right]^2 \right\}^{\frac{1}{2}}$$

$$= \left\{ \left[\frac{\delta q_n}{q_n} \right]^2 + \left[\frac{\delta (T_w - T_b)}{T_w - T_b} \right]^2 \right\}^{\frac{1}{2}} \tag{3.13}$$

A summary of the results from the present uncertaintly analysis is given in Table 3.1.

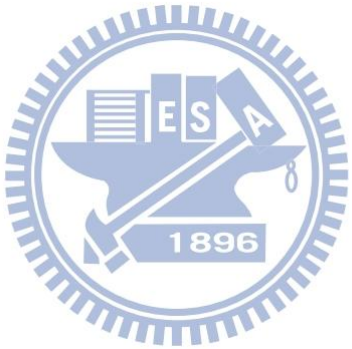

Table 3.1 Summary of the results from the uncertainty analysis.

Parameter	**Uncertainty**
Geometry	
Length & thickness (%)	± 0.167%
Area (%)	± 0.334%
Particle diameter (%)	± 10.0%
Particle density(%)	± 13.4%
Parameter measurement	
Temperature, T (°C)	± 0.05
Temperature difference, ΔT_w (°C)	± 0.36
System pressure, P (kPa)	± 0.5
Boiling heat transfer on the copper flat plate	
Total power input, Q_t (%)	± 5.9%
Imposed net heat flux, q_n(%)	± 8.3%
Heat transfer coefficient, h (%)	± 11.0%

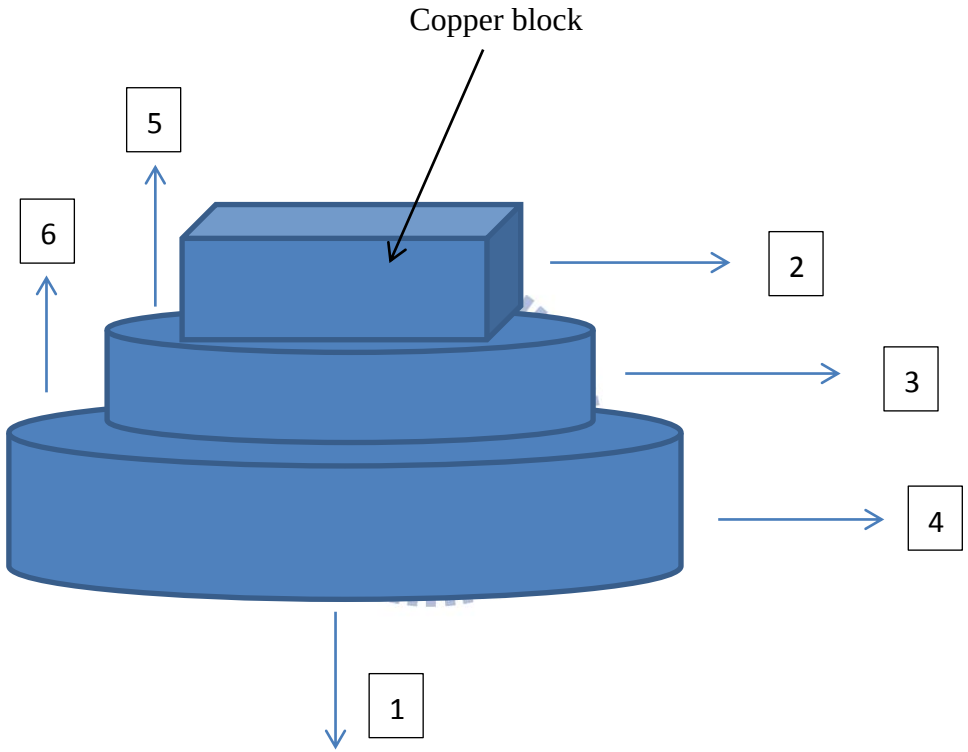

Fig. 3.1 Schematic diagram of six main directions of the heat loss.

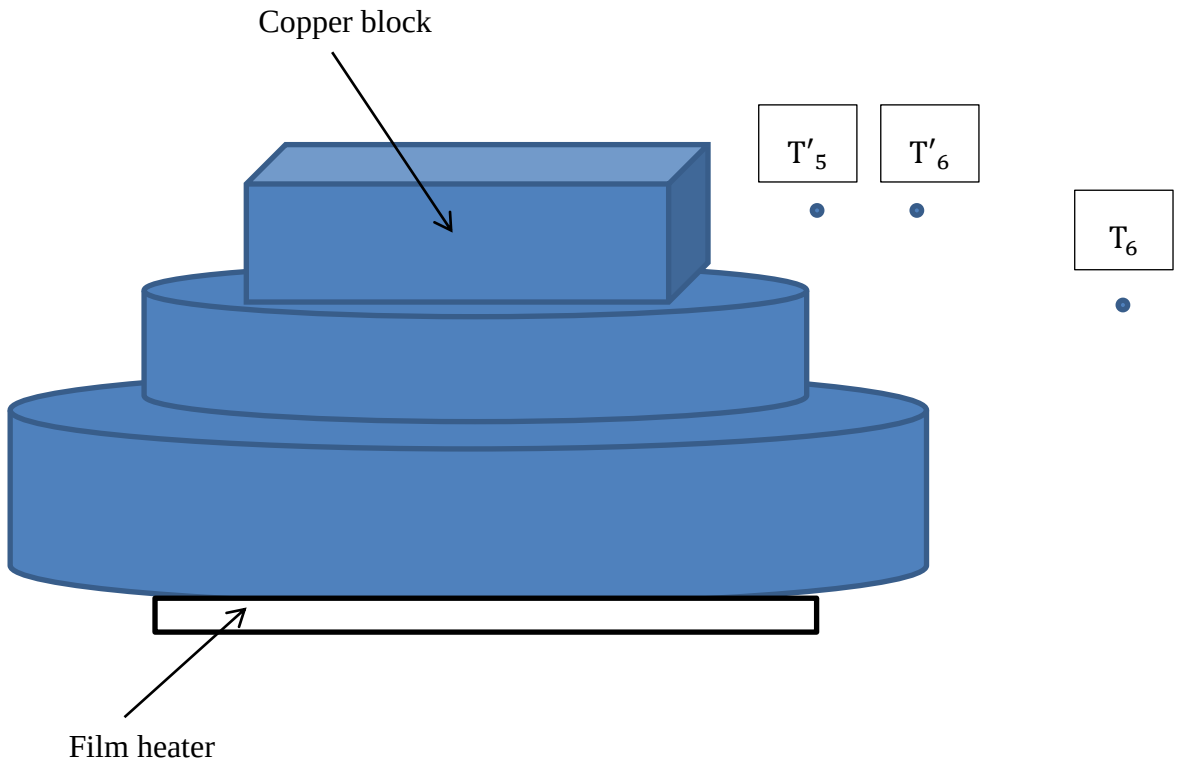

Fig. 3.2 Schematic diagram of T'$_5$ and T'$_6$

CHAPTER 4

POSSIBLE SUBCOOLED POOL BOILING HEAT TRANSFER ENHANCEMENT OF FC-72 OVER HEATED COPPER SURFACE

The experimental results to illustrate possible enhancement of subcooled pool boiling heat transfer of FC-72 by placing movable particles on the heating surface obtained in the present study are examined in this chapter. The present experiments are carried out for the liquid subcooled temperature set at ΔT_{sub}=5℃, 10℃, 15℃ and 20℃. The diameter of the particles d_p is fixed at 1.0 and 1.5 mm, and the total number of particles N_p varied from 100 to 1800 for the particles with the diameter 1.0 mm or from 100 to 800 for the particles with the diameter 1.5 mm. The FC-72 liquid in the test chamber is maintained at subcooled liquid state corresponding to the atmospheric pressure. Note that the maximum numbers of particles forming a single closely packed particle layer over the boiling surface N_{pf} are 900 and 400 respectively for the particles with the diameter of 1.0 mm and 1.5 mm when each particle contact directly with neighboring particles. In the experiment tests are also conducted for the particle number well exceeds N_{pf} and many particles are on top of the other particles. The measured data are presented in terms of the boiling curves and boiling heat transfer coefficients for various diameters and numbers of the copper particles. Effects of the experimental parameters on the possible subcooled boiling heat transfer enhancement will be examined in detail. Selected data are presented in the following to illustrate the possible pool boiling heat transfer enhancement by the boiling flow driven metallic particles.

4.1 Single-phase Natural Convection Heat Transfer

Before conducting the pool boiling experiment, we first measure steady natural convection heat transfer of FC-72 liquid over the heated copper surface without the presence of any particles which prevails at low imposed heat flux, intending to verify the present experimental setup. The measured data for the natural convection heat transfer coefficient are compared with the empirical correlation of Radziemska and Lewandowski [43] in Fig. 4.1. Their correlation is

$$Nu_L=(2.1e^{-48W}+1.2)Ra_L^{0.2} \tag{4.1}$$

where w is the width of the heating plate (m). The correlation given in Eq.(4.1) is based on the data for a small horizontal plate heated from below for $10^5<Ra_L<10^8$. Note that the characteristic length L used in defining the dimensionless groups in the above equation is chosen to be the ratio of the heated surface area and its perimeter, and the Nusselt and Rayleigh numbers are respectively defined as

$$Nu_L=\frac{hL}{k_\ell} \tag{4.2}$$

and

$$Ra_L=\frac{g\beta(\Delta T_{sat})L^3}{\alpha\nu} \tag{4.3}$$

The results in Fig. 4.1 indicate that our natural convection data are in good agreement with that calculated from Eq. (4.1). Thus the experimental system established here is considered to be suitable for the present study.

4.2 Saturated Pool Boiling on Bare Copper Surface

To further verify the suitability of the present experimental system, we first measured boiling curve for saturated pool boiling of liquid FC-72 on the bare heated copper plate ($N_p = 0$). These data are compared with that from Rainey and You [22] in Fig. 4.2 for pool boiling of FC-72 on a square copper plate of 5×5 cm^2 in surface

area. Note that the present saturated pool boiling data are in good agreement with theirs.

4.3 Effect of Surface Aging on Boiling over Bare Copper Plate

It is well known that the change of the boiling surface properties with time, the so called “aging effect”, can be significant in affecting the boiling heat transfer from a surface after the surface has been used over certain period of time. Obviously, the measured boiling heat transfer data for the cases with and without the presence of the particles on the surface can be meaningfully compared only when the surface aging effect is small. Thus tests are carried out here to investigate the aging effect of subcooled FC-72 liquid boiling on the present heated surface. The results show that the boiling curves and heat transfer coefficients measured over a time interval of 6 hours do not differ to a noticeable degree, as seen from Fig. 4.3. But a significant aging effect is found for an interval of 24 hours. Thus in the present experiment the boiling heat transfer data for the corresponding cases with and without the presence of particles on the surface are obtained within 6 hours.

4.4 Effects of Moving Copper Particles on Boiling Heat Transfer

Possible FC-72 boiling heat transfer enhancement by the copper particles moving on the heated surface is then examined. Results are presented first for the small liquid subcooling with ΔT_{sub}=5℃ by showing the boiling heat transfer data for the bare surface and for the surface with copper particles on it for d_p=1 mm and various N_p in Figs. 4.4-4.18. The results in Figs. 4.4-4.6 for d_p=1.0 mm and N_p=100 to 300 indicate that at a small particle number the boiling heat transfer can be slightly enhanced by the copper particles only at low wall superheat near the onset of

nucleate boiling. The enhancement gets smaller at increasing wall superheat. Besides, the moving copper particles does not affect the boiling heat transfer to a significant degree in the single-phase flow at very low wall superheat and in the fully developed nucleate boiling region at high wall superheat. Moreover, a slight reduction in the boiling heat transfer by the copper particles is noted at an even higher wall superheat.

As the total number of the copper particles is increased to 400, 500 and 600, noticeable augmentation in the boiling heat transfer by the motion of the copper particles appears at low wall superheat (Figs. 4.7-4.9). On the other hand, the degradation in the boiling heat transfer at high wall superheat is not noticeably increased. For a further increase in the number of the copper particles to 700-900, the particles on the copper plate are rather crowded. However, enhancement in the boiling heat transfer by the copper particles is even more significant at low ΔT_{sat} (Figs. 4.10-4.12), implying strong interactions between the particles and boiling flow at this large N_p. Note that when N_p>700, the boiling heat transfer at high wall superheat starts to degenerate to a significant degree. In fact, substantial retardation in the boiling heat transfer by the copper particles exists at high ΔT_w. It is of interest to note from the data given in Figs. 4.13-4.18 that even when the total number of the copper particles well exceeds N_{pf} for $N_p \geq 1{,}000$ the boiling heat transfer enhancement by the copper particles is still significant at low ΔT_w. This suggests that the presence of a large number of the copper particles on top of the other particles does not lower the boiling heat transfer performance at low wall superheat.

To be more quantitative on the boiling heat transfer affected by the copper particles presented above for ΔT_{sub}=5℃ and d_p=1.0 mm, the ratios of the boiling heat transfer coefficients for the cases with to that without the presence of the particles h_p/h are shown in Fig. 4.19 for various ΔT_w and N_p. Note that the

enhancement in the boiling heat transfer can exceed 200% for $N_p \geq 800$. The best enhancement for these cases is 300% for N_p=1800 at $\Delta T_w \approx 16.3$K. Note that the best enhancement usually occurs at very low ΔT_w near the onset of nucleate boiling. Beyond this low ΔT_w the case with N_p=1600 has the best average heat transfer over the whole boiling process. Besides, for $N_p \geq 1200$ the onset of nucleate boiling takes place much earlier than the bare surface. For instance, at N_p=1400 a 28% reduction in the incipient boiling wall superheat can be obtained by the moving particles. On the contrary the reduction in the boiling heat transfer at high ΔT_w can be as high as 20%. Note that for the FC-72 saturated pool boiling examined by Wei [2], the reduction can be even higher at 25%. Moreover, in the single-phase natural convection flow the change in the heat transfer coefficient by the particles is within $\pm$13% of that for the bare surface.

Aside from the boiling heat transfer, the above results also show that the presence of the copper particles can substantially lower the wall superheat needed for the onset of nucleate boiling for most cases (Table 4.1). This will cause lower operating temperature and is also beneficial in electronics cooling by employing moving metallic particles on the boiling surface.

Next, the measured heat transfer data for the higher degree of the liquid subcooling with ΔT_{sub}=10℃ are given in Figs. 4.20-4.28 for N_p ranging from 200 to 1800. By and large, these results are similar to those for ΔT_{sub}=5℃ presented above. However, some noted differences do exist. Due to the bulk temperature in the chamber is lower, the onset of nucleate boiling occurs at a higher wall superheat. In Fig. 4.29 we find that the best enhancement can reach 200% for N_p= 1600, which is much lower than that for ΔT_{sub}=5℃. On the other hand, the reduction in boiling heat transfer at high wall superheat is slightly lower.

But for the cases with even higher degree of liquid subcooling, results are quite different. The data in Figs. 4.30-4.32 indicate that there are nearly no heat transfer enhancement for ΔT_{sub}=15℃ for N_p ranging from 200 to 600. Only when $N_p \geq 800$, heat transfer can be enhanced slightly (Fig.4.33 & 4.34). For an even higher liquid subcooling at ΔT_{sub}=20℃ the boiling heat transfer is reduced by the copper particles, as evident from Figs. 3.35 & 3.36. No heat transfer augmentation by the particles is found. Besides, the incipience boiling wall superheat can be even higher with the presence of the particles.

Attention is then turned to the data shown in Figs. 4.37-4.57 for the larger copper particles with $d_p = 1.5$ mm. The results clearly indicate that the effects of the larger copper particles on the boiling heat transfer exhibit similar trend to the smaller particles presented above. At ΔT_{sub}=5℃, the boiling heat transfer enhancement can be up to 292% for N_p=800 at low wall superheat.

4.5 Effects of Subcooling Degree in the Bulk Liquid

To illustrate the effects of the copper particles on the boiling heat transfer enhancement for various degrees of the bulk liquid subcooling, we compare the measured heat transfer data h & h_p/h for ΔT_{sub} ranging from 0℃ to 20℃ in Fig. 4.58-4.65 at selected N_p. The data in Fig.4.58-4.61 manifest that for a given N_p the wall superheat for the boiling onset is noticeably higher for a higher liquid subcooling and the boiling heat transfer enhancement is smaller. In fact, at ΔT_{sub}=15℃ the enhancement is nearly negligible. According to our flow observation, the bubbles departing from the heated surface is fewer and smaller at a higher ΔT_{sub}. The resulting thrust acting on the particles by the bubbles are weaker, leading to a smaller boiling heat transfer augmentation. Note that at the high liquid subcooling with

ΔT_{sub}=20℃, the boiling heat transfer is retarded by the copper particles for all N_p tested here (Fig. 4.62-4.65). The boiling heat transfer retardation is more pronounced for a larger larger N_p.

During the course of this study we also test copper particles of much smaller size with d_p=0.5 mm to find whether there is any enhancement in such high liquid subcooling situation. Results from such test shown in Figs. 4.66-4.69 indicate that for ΔT_{sub}=15℃ and N_p=1800 & 3600 there is a slight enhancement after the onset of boiling but no positive effect for ΔT_{sub}=20℃. We can conclude that when there is high liquid subcooling, the departing bubbles will become very fewer and smaller and the particle motion is relatively weak. The boiling heat transfer enhancement by the particles is not significant.

4.6 Interactions between Particles and Boiling Flow

To delineate the complicate effects of the moving copper particles on the boiling heat transfer, motions of the particles and bubbles in the boiling flow are visualized. The results from this visualization for selected cases are presented in Figs. 4.70-4.76. More specifically, photos taken from the side view of the subcooled boiling flow in a small region above the heating plate are shown in Fig. 4.70 for the small copper particles with N_p =600 at low imposed heat flux of 0.78 $^{w}/_{m^2}$ and ΔT_{sub}=5℃. In these figures, the symbol "t=0" denotes an arbitrary time instant in the statistical state. At high heat flux the vigorous motions of the particles and bubbles and their strong interactions are prone to overshadow each other, causing the top view photos to be rather ambiguous. Thus only the side view photos are shown here.

Our flow visualization reveals that when a given heat flux slightly higher than that needed for ONB is imposed to the boiling surface the fast growth of bubbles after

their incipience on the heated surface can push the surrounding particles to move away from their original sites horizontally over a certain distance. As the particles move on the heated surface, they in turn can push the bubbles along their path to depart from the heating surface, resulting in earlier bubble departure. Besides, the moving particles can collide with other particles. At higher imposed heat flux more bubbles nucleate from the heated plate and force resulting from the growth of bubbles can be very strong. Consequently, the particles can be lifted directly up by the growing bubbles too. Later, the heavy metallic particles may drop back to the plate due to gravity and the surrounding bubbles and liquid can be pushed away. Besides, collision between the particles is frequent. These mutual particle-bubble interactions in the boiling flow schematically shown in Fig. 4.77 get more intense at increasing heat flux, causing the three-phase liquid-vapor-particle flow over the heated surface to become highly turbulent and tending to enhance boiling heat transfer from the plate. It is also noted that at a higher liquid subcooling the bubble growth is slower and the bubbles departing from the heated surface are smaller and at a lower rate. Thus the bubble- particle interactions are weaker and their effects on the boiling heat transfer diminish.

However, at an even higher heat flux a very large number of bubbles nucleate at the heated surface and the copper particles can impede the bubbles of certain size to grow further and depart from the heated surface. The bubbles are then trapped beneath the particles, as schematically illustrated in Fig. 4.78. Meanwhile, the particles can reduce the inrush of the bulk liquid to the heated surface especially at large particle number. Therefore the boiling heat transfer is retarded by the particles. These heat transfer retarding effects are more severe at higher heat flux when more particles are placed on the heated plate.

4.7 Proposed Correlations

The data for h_p/h presented in Figs. 4.19, 4.29, 4.42 and 4.47 can be correlated empirically as

$$\frac{h_p}{h} = \left\{A + B\left(\frac{N_{pf}}{N_p}\right)^2\right\} \cdot \left[\frac{C_{pl}(\Delta T_w - \Delta T_{ONB,b})}{i_{lv}}\right]^{\left[C+D\left(\frac{N_{pf}}{N_p}\right)^2\right]} \tag{4.4}$$

$$A = \left[0.7 - 0.57\left(\frac{T_b}{T_{sat}}\right)\right] + \left[-0.0055 + 0.0033\left(\frac{T_b}{T_{sat}}\right)\right]\left(\mathrm{d_p}/\sqrt{\sigma/\mathrm{g}\Delta\rho}\right)$$

$$B = \left[-0.62523 + 0.753\left(\frac{T_b}{T_{sat}}\right)\right] + \left[0.015 - 0.0173\left(\frac{T_b}{T_{sat}}\right)\right]\left(d_p/\sqrt{\sigma/\mathrm{g}\Delta\rho}\right)$$

$$C = \left[0.07 - 1.56\left(\frac{T_b}{T_{sat}}\right)\right] + \left[0.0874 - 0.097\left(\frac{T_b}{T_{sat}}\right)\right]\left(\mathrm{d_p}/\sqrt{\sigma/\mathrm{g}\Delta\rho}\right)$$

$$D = \left[-1.04 + 1.377\left(\frac{T_b}{T_{sat}}\right)\right] + \left[0.0128 - 0.0158\left(\frac{T_b}{T_{sat}}\right)\right]\left(\mathrm{d_p}/\sqrt{\sigma/\mathrm{g}\Delta\rho}\right)$$

The mean absolute error (MAE) for the above correlation for h_p/h when compared with the present data is 20.7%.

Finally, we illustrate the ranges of the experimental parameters in which the boiling heat transfer can be enhanced by placing the copper particles on the heated surface in Fig. 4.79-4.82. The results manifest that the lower bounds of the imposed heat flux for enhancing boiling heat transfer do not significantly vary with the ratio of the particle number placed on the plate to the maximum particle number forming a single particle layer on the plate N_p/N_{pf} and with the particle size. But the lower bounds for the wall superheat decrease noticeably with N_p/N_{pf} (Fig. 4.79 (b) and Fig. 4.80 (b)). The upper bounds of q and ΔT_w for enhancing boiling heat transfer, however, show nonmonotonic variations with N_p/N_{pf}, particle size and subcooling. Note that in Fig. 7.82 for ΔT_{sub}=20℃ the boiling heat transfer can not be enhanced by the moving copper particles in the present attempt.

Table 4.1 Wall superheats at onset of nuclear boiling for 1.0 mm copper particles

Particle Diameter	Subcooling Degree	N_p	$(\Delta T_w)_{ONB}$(℃)	$(\Delta T_w)_{ONB}$(℃) for bare surface
$d_{p=}$1.0 (mm)	5℃	100	15.9	16.1
		200	15.6	15.8
		300	14.8	15.9
		400	14.7	15.8
		500	15.1	16.0
		600	14.3	15.9
		700	15.0	15.7
		800	14.6	16.0
		900	14.6	16.2
		1000	14.4	16.1
		1100	14.1	16.0
		1200	13.6	16.1
		1400	11.8	16.4
		1600	11.8	16.1
		1800	11.9	16.3
	10℃	200	21.0	21.0
		400	20.3	21.0
		600	19.9	21.1
		800	20.1	20.9
		1000	19.5	20.7
		1200	19.5	20.7
		1400	17.2	20.5
		1600	17.6	21.2
		1800	17.7	20.6
	15℃	200	24.5	23.9
		400	24.0	23.6
		600	24.5	24.9
		800	24.5	25.4
		1200	24.6	25.6
	20℃	800	29.9	28.1
		1200	29.3	28.1

Table 4.2 Wall superheats at onset of nuclear boiling for 1.5 mm copper particles

Particle Diameter	Subcooling Degree	N_p	$(\Delta T_w)_{ONB}$(℃)	$(\Delta T_w)_{ONB}$(℃) for bare surface
$d_{p=}$1.5 (mm)	5℃	100	15.4	16.2
		200	14.7	16.2
		400	14.1	16.3
		600	13.5	16.1
		800	13.3	16.1
	10℃	200	19.3	20.9
		400	16.1	21.2
		600	18.1	20.5
		800	16.6	20.6
	15℃	200	24.5	25.5
		400	23.4	24.6
		600	23.5	24.8
		800	24.0	24.9
	20℃	200	28.2	28.0
		400	30.0	27.9
		600	29.1	28.8
		800	29.0	28.1

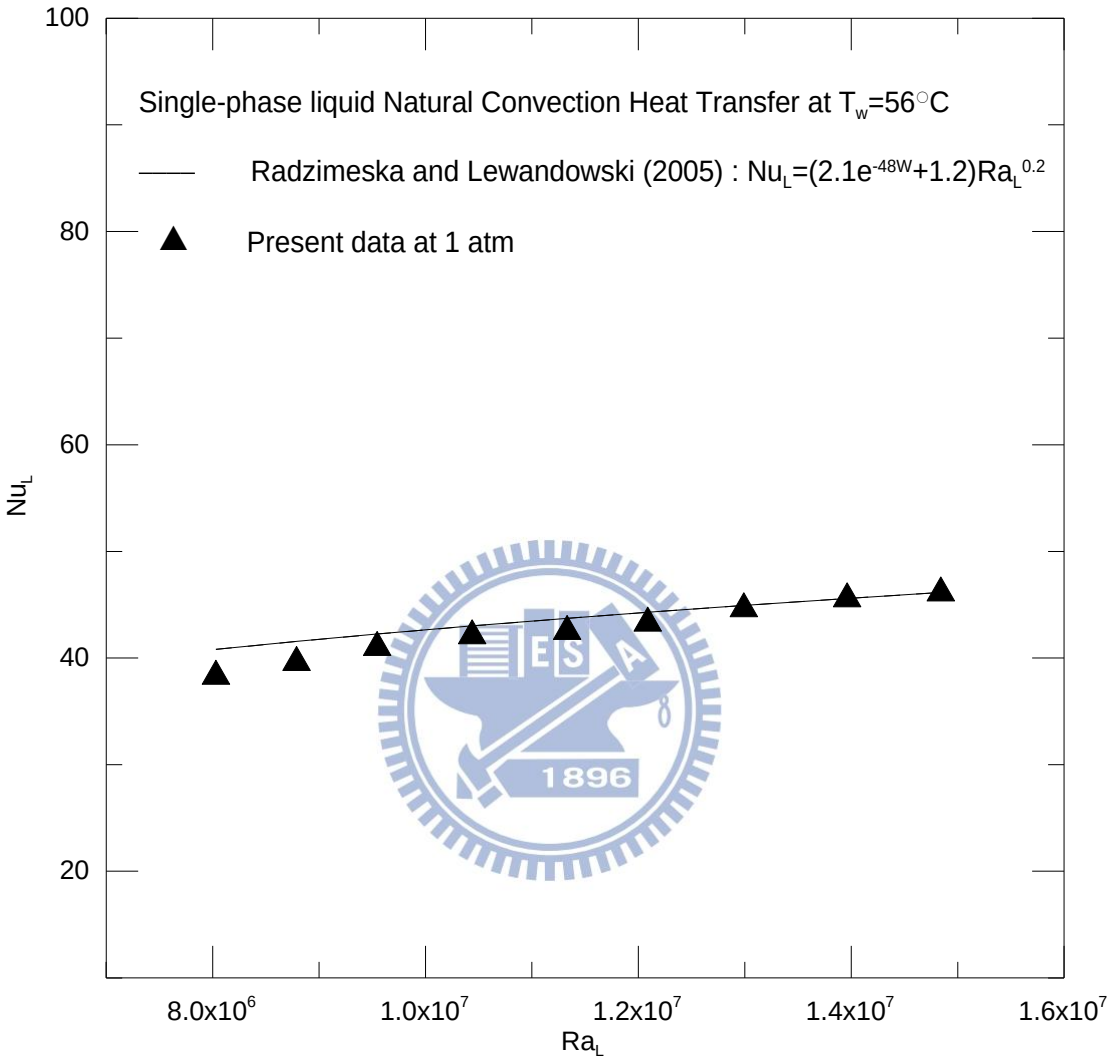

Fig. 4.1 Comparison of the present single-phase natural convection data with the empirical correlation of Radziemska and Lewandowski (2005).

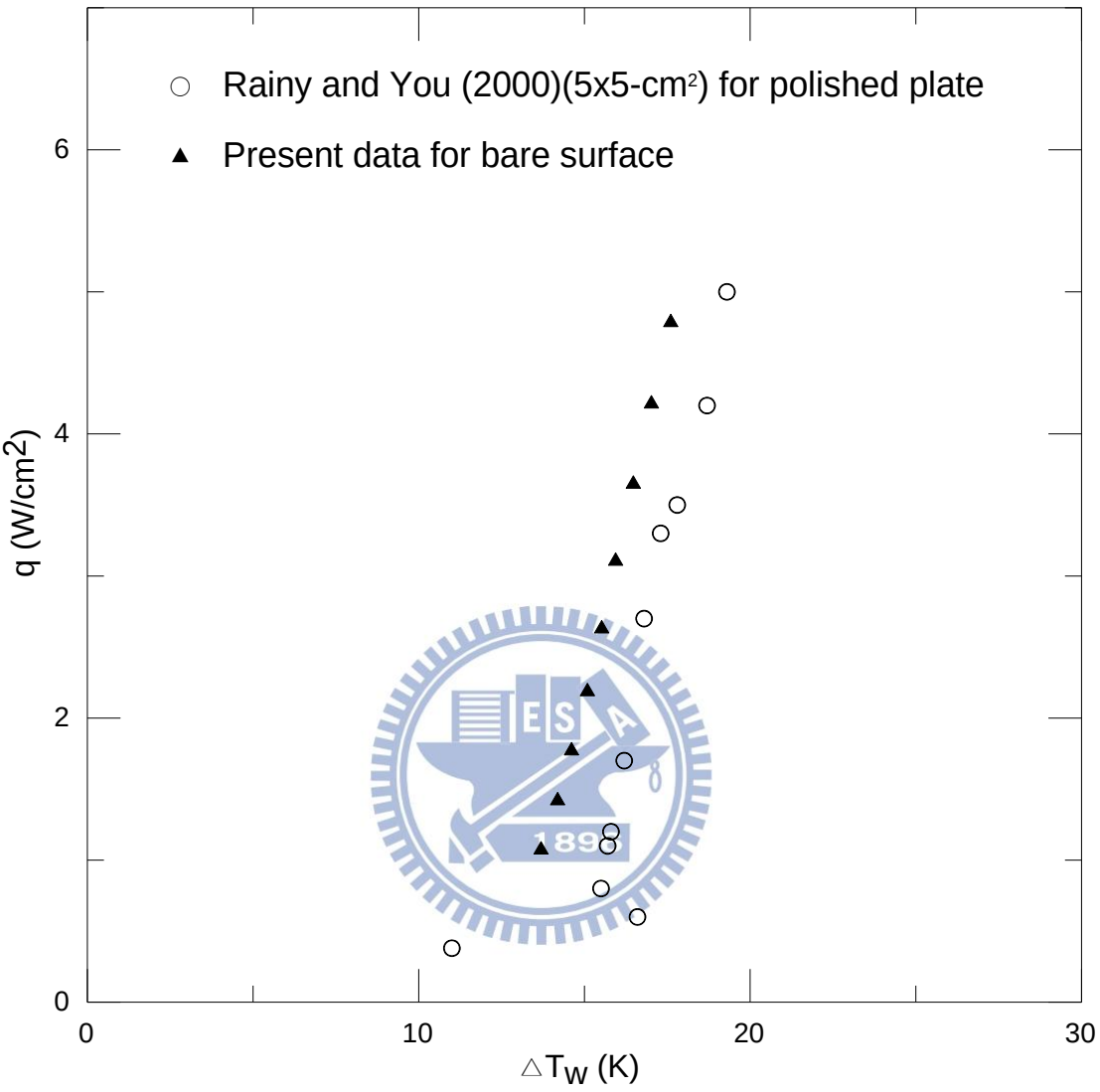

Fig. 4.2 Comparison of the present apparatus of saturated nucleate boiling heat transfer data for bare surface with Rainy and You (2000).

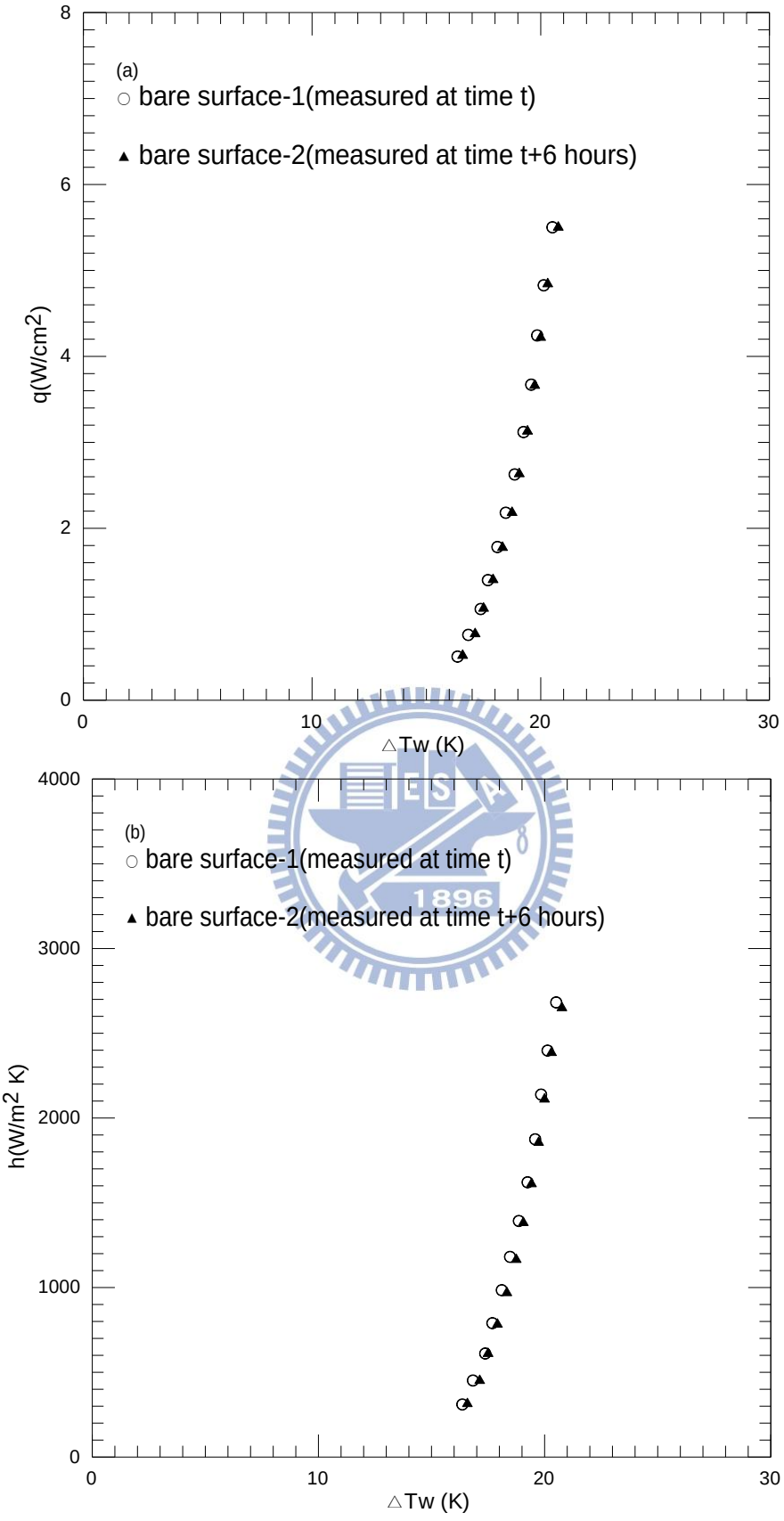

Fig. 4.3 Effects of surface aging on subcooled pool boiling curves (a) and boiling heat transfer coefficients (b) for ΔT_{sub}= 5℃ for the bare surface.

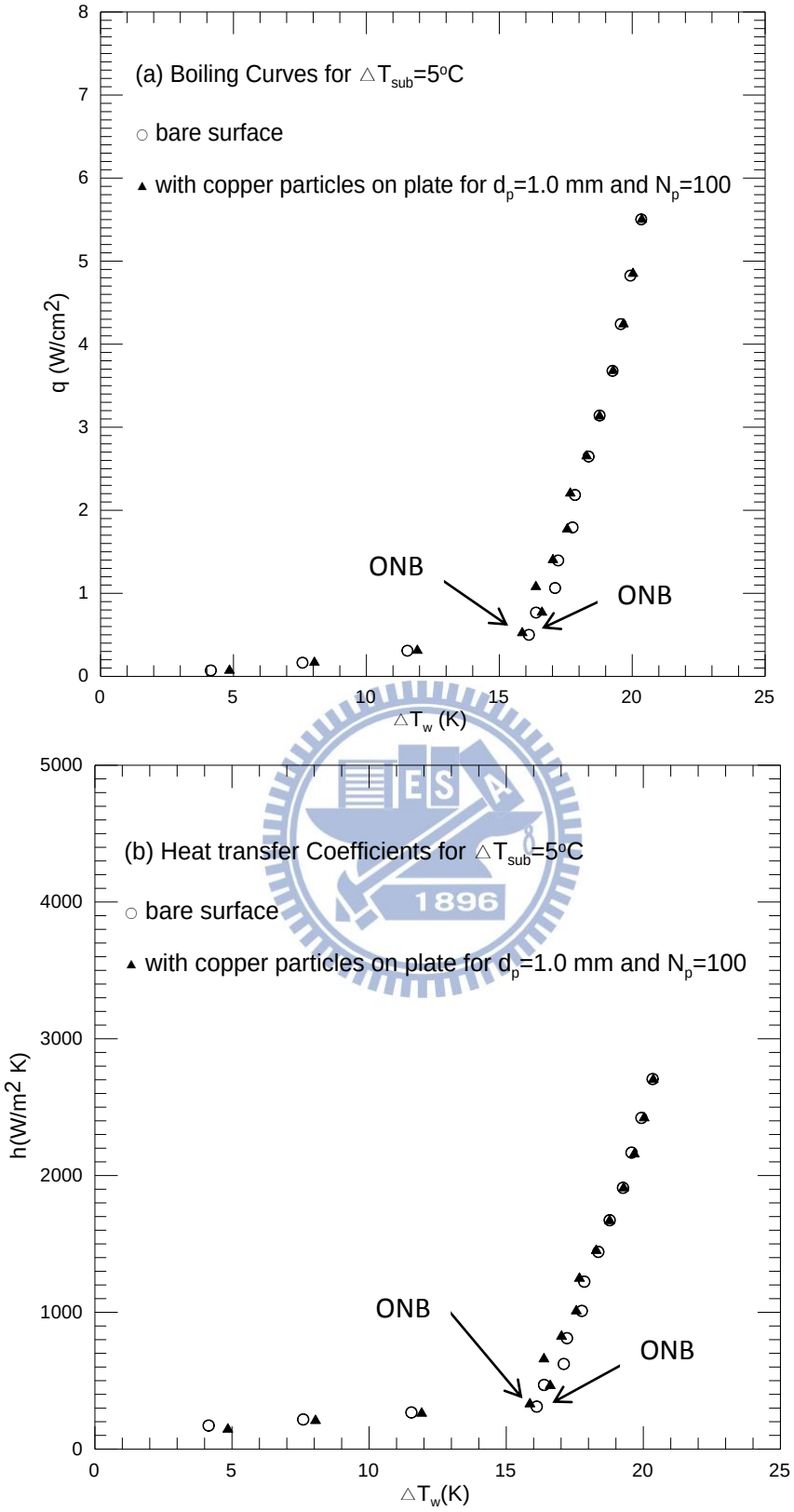

Fig. 4.4 Effects of copper particle diameter and number on subcooled pool boiling curves (a) and boiling heat transfer coefficients (b) for ΔT_{sub}= 5℃ at d_p=1.0 mm and $N_p = 100$.

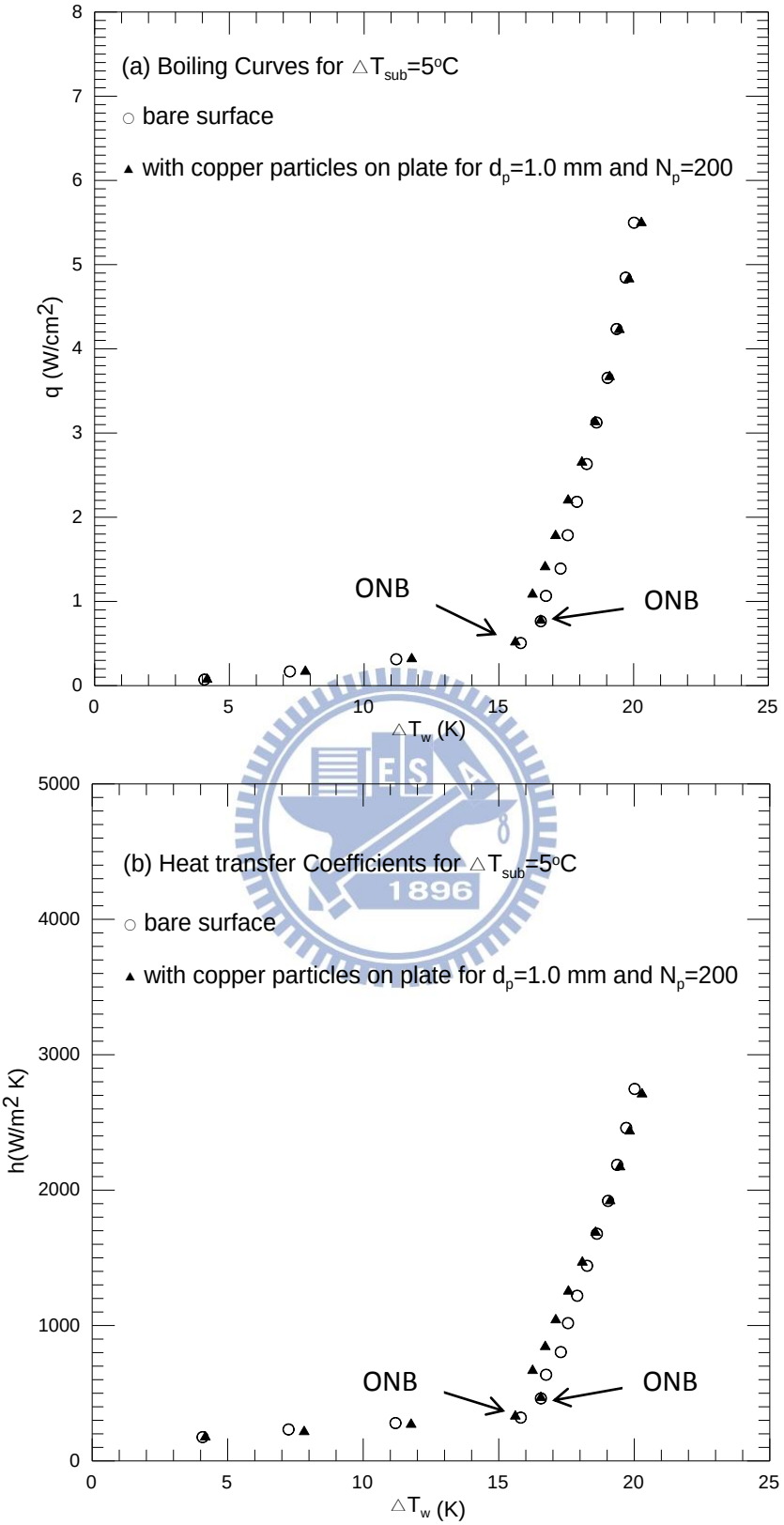

Fig. 4.5 Effects of copper particle diameter and number on subcooled pool boiling curves (a) and boiling heat transfer coefficients (b) for ΔT_{sub}= 5℃ at d_p=1.0 mm and $N_p = 200$.

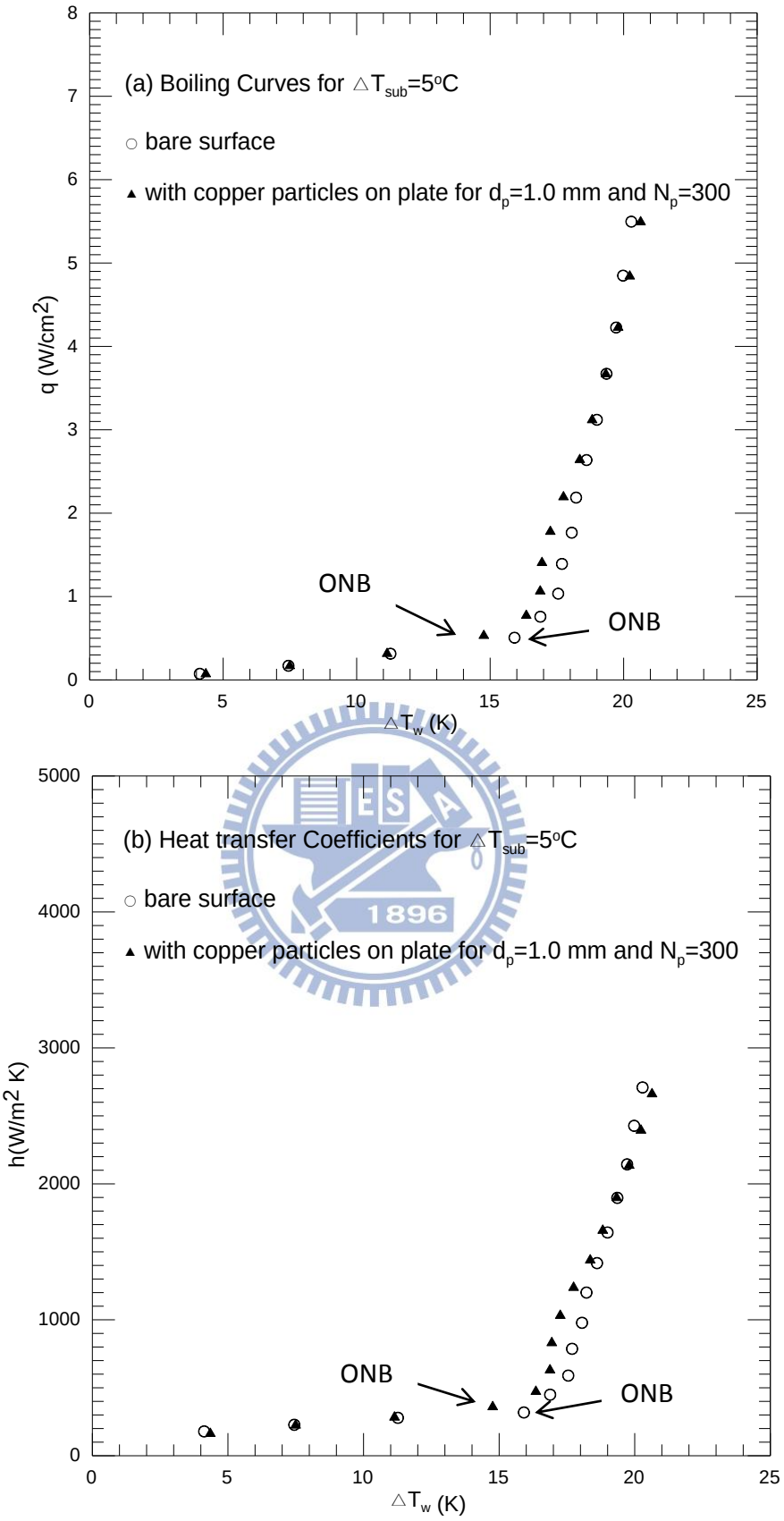

Fig. 4.6 Effects of copper particle diameter and number on subcooled pool boiling curves (a) and boiling heat transfer coefficients (b) for ΔT_{sub}= 5℃ at d_p=1.0 mm and $N_p = 300$.

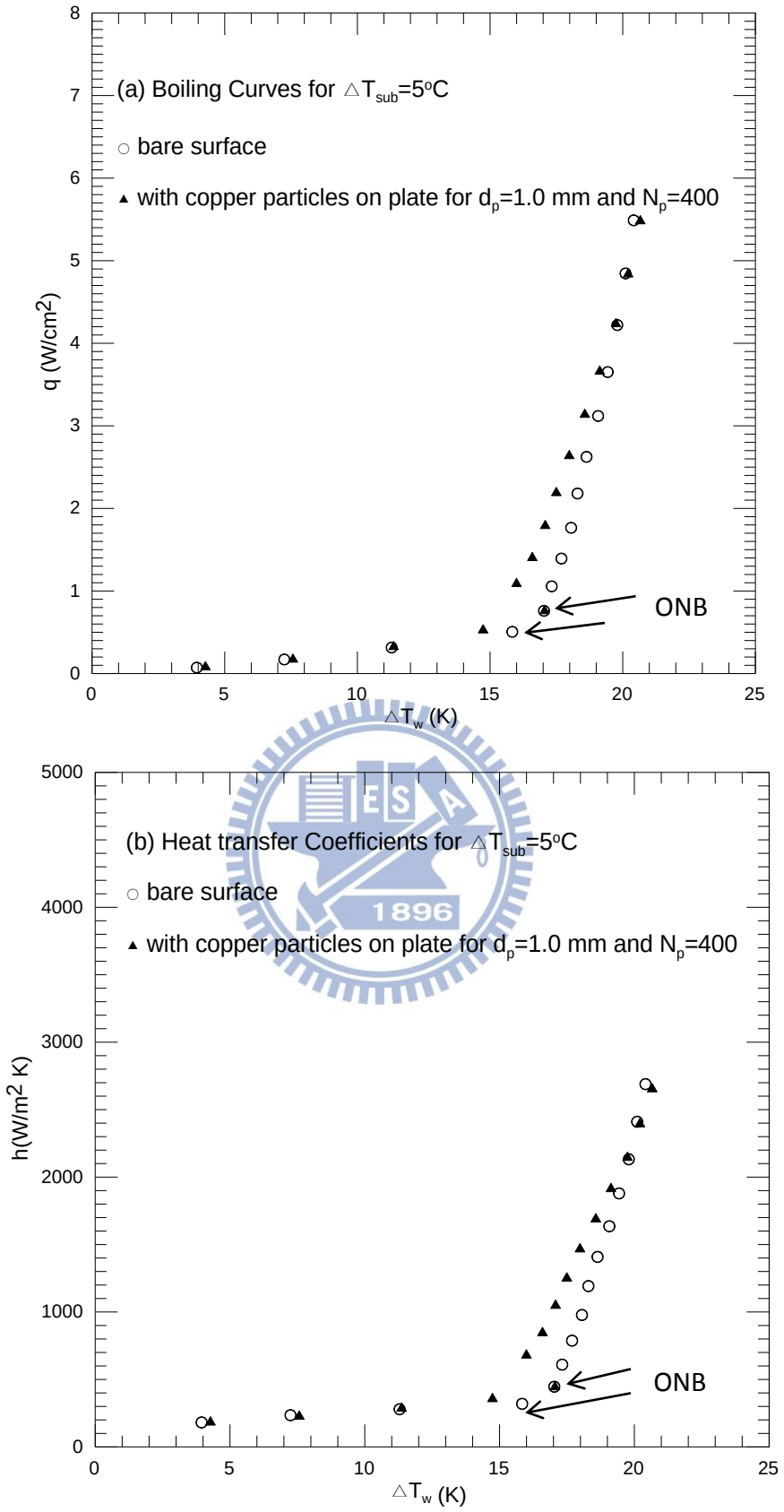

Fig. 4.7 Effects of copper particle diameter and number on subcooled pool boiling curves (a) and boiling heat transfer coefficients (b) for ΔT_{sub}= 5℃ at d_p=1.0 mm and $N_p = 400$.

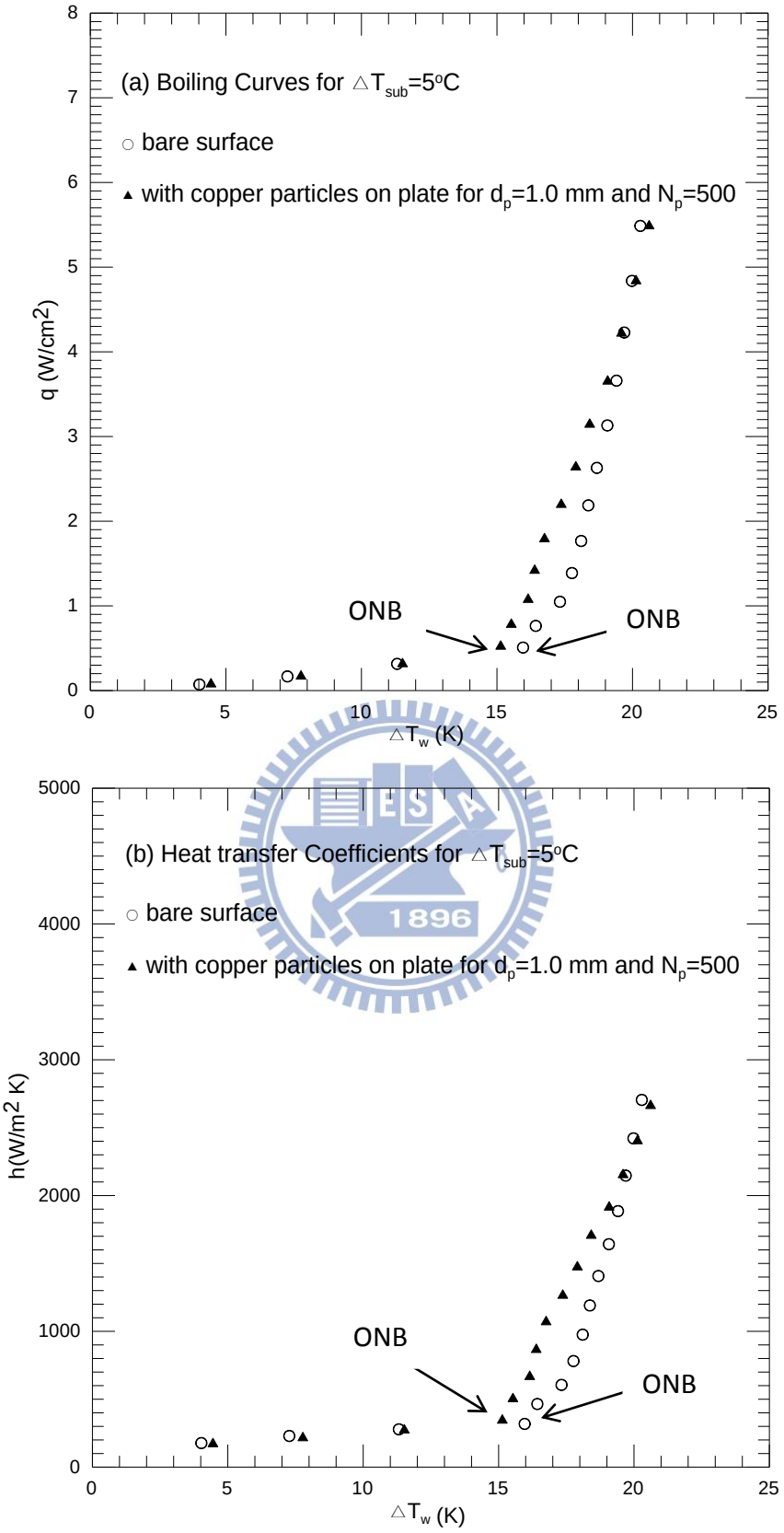

Fig. 4.8 Effects of copper particle diameter and number on subcooled pool boiling curves (a) and boiling heat transfer coefficients (b) for ΔT_{sub}= 5℃ at d_p=1.0 mm and $N_p = 500$.

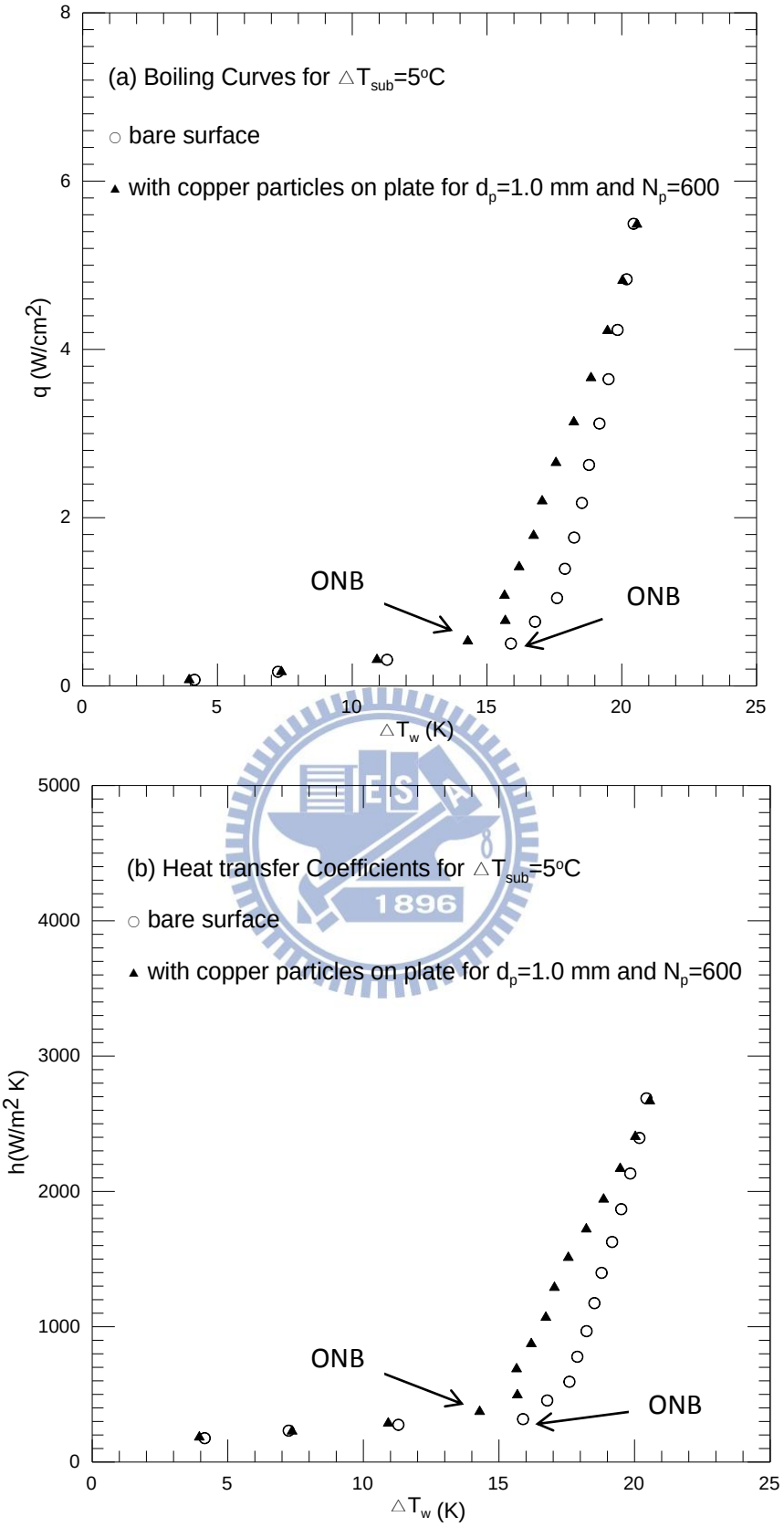

Fig. 4.9 Effects of copper particle diameter and number on subcooled pool boiling curves (a) and boiling heat transfer coefficients (b) for ΔT_{sub}= 5℃ at d_p=1.0 mm and $N_p = 600$.

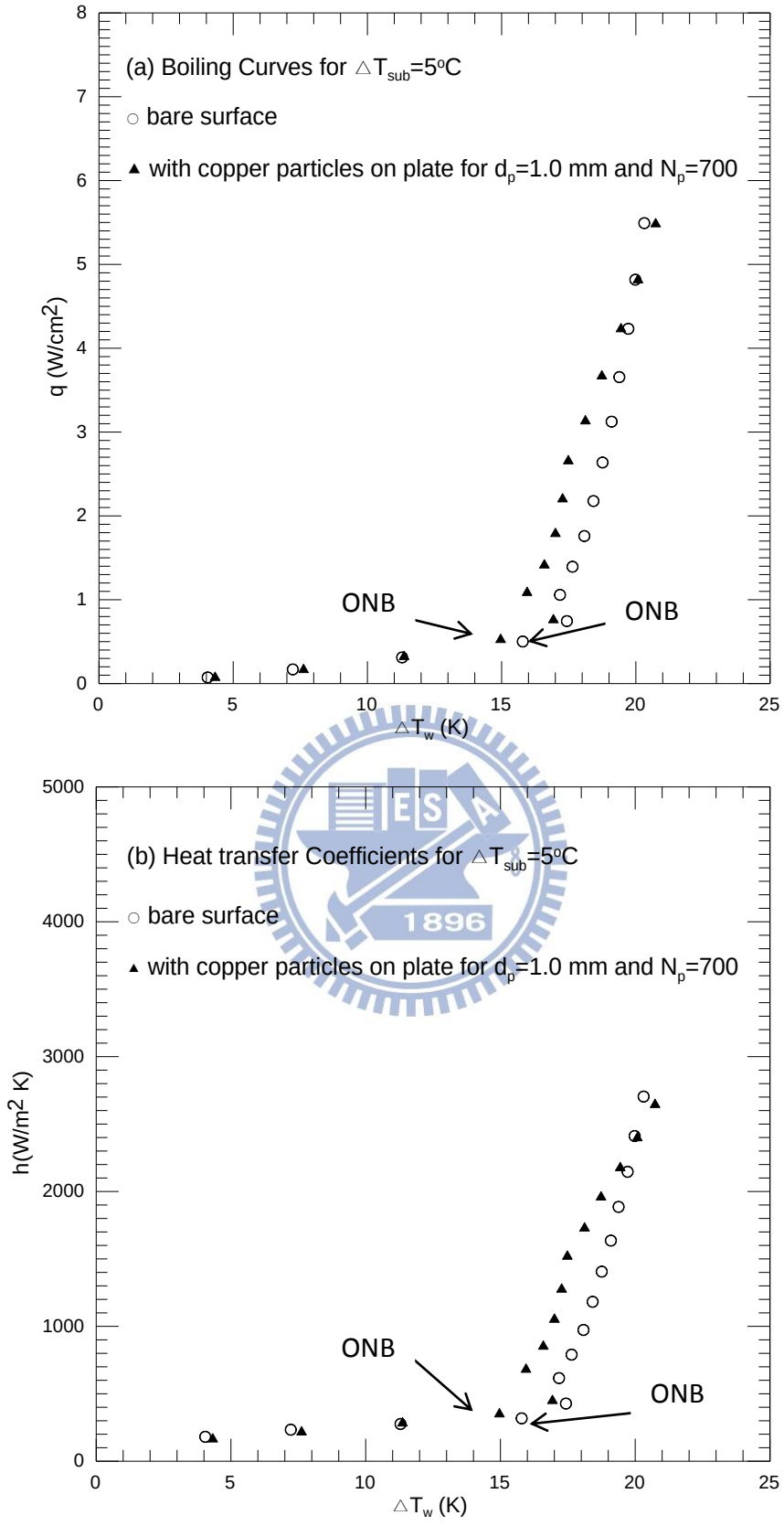

Fig. 4.10 Effects of copper particle diameter and number on subcooled pool boiling curves (a) and boiling heat transfer coefficients (b) for ΔT_{sub}= 5℃ at d_p=1.0 mm and $N_p = 700$.

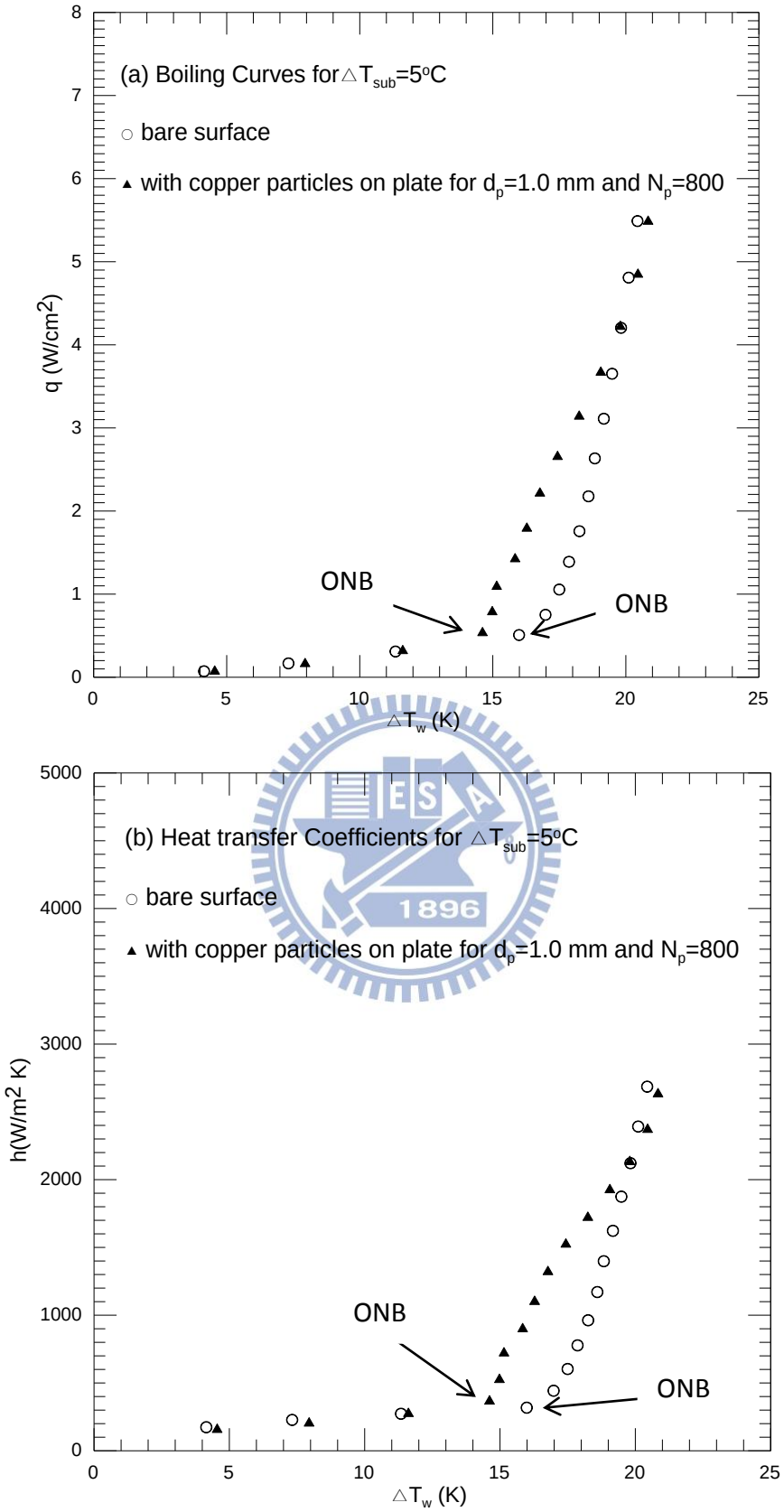

Fig. 4.11 Effects of copper particle diameter and number on subcooled pool boiling curves (a) and boiling heat transfer coefficients (b) for ΔT_{sub}= 5℃ at d_p=1.0 mm and $N_p = 800$.

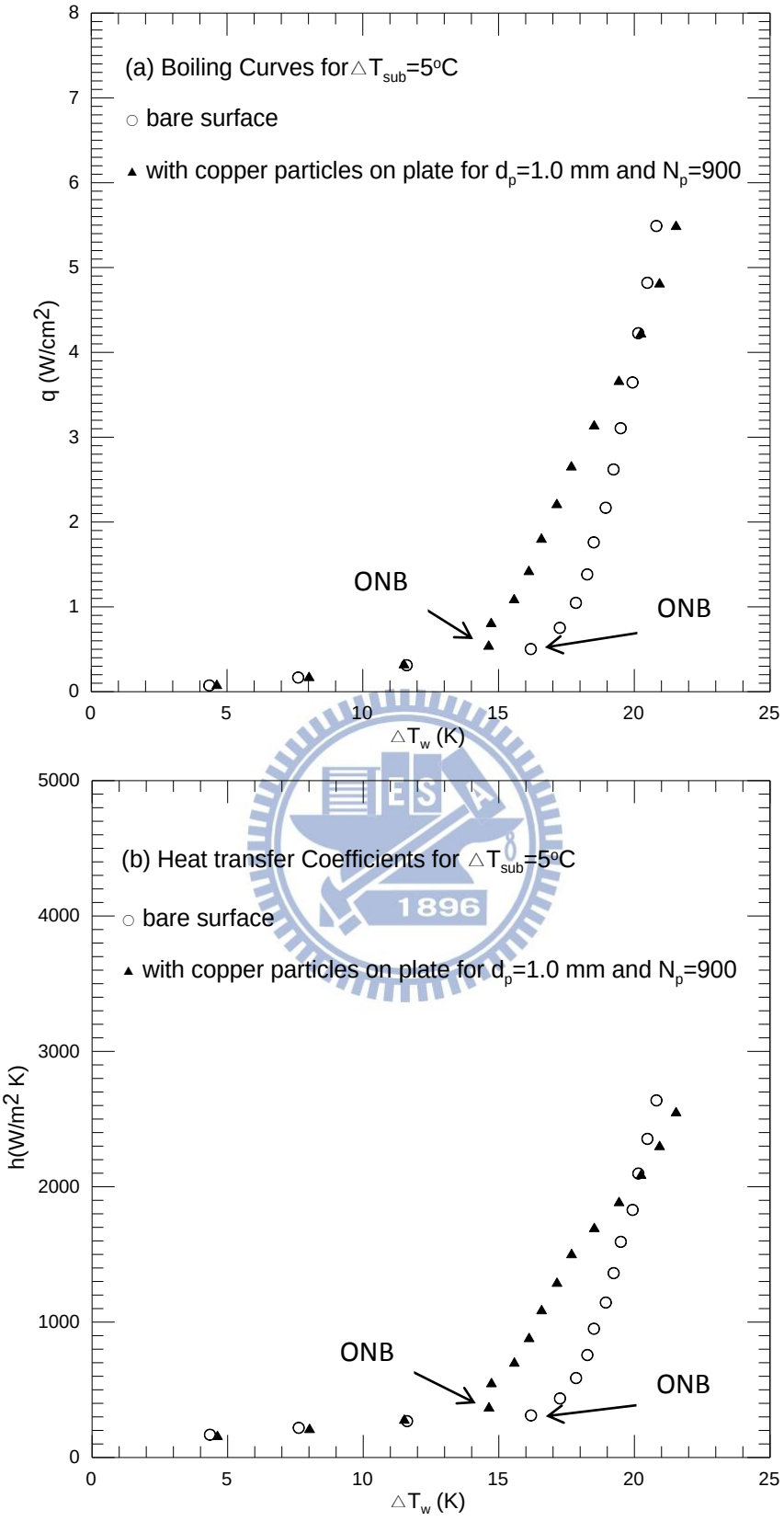

Fig. 4.12 Effects of copper particle diameter and number on subcooled pool boiling curves (a) and boiling heat transfer coefficients (b) for ΔT_{sub}= 5℃ at d_p=1.0 mm and $N_p = 900$.

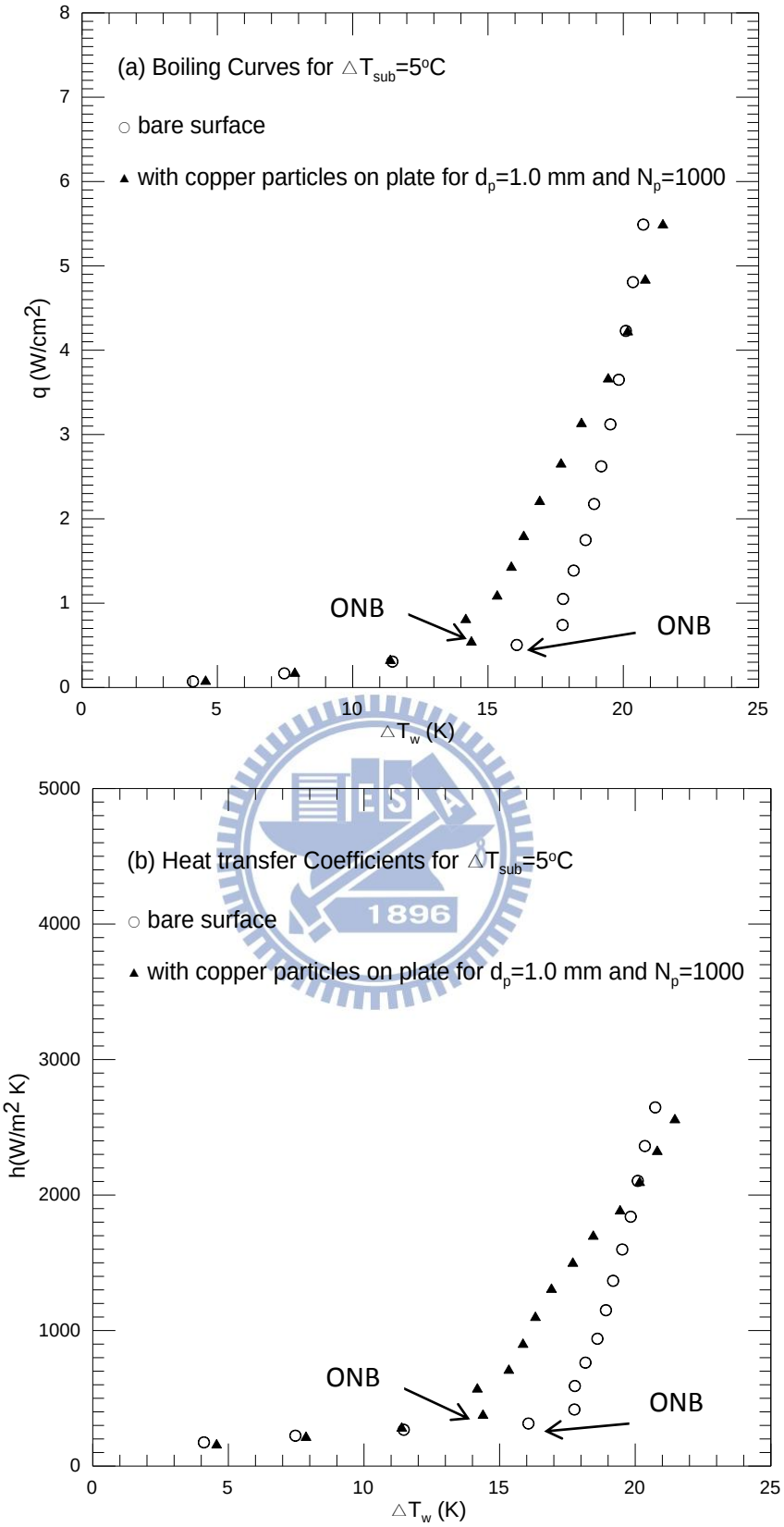

Fig. 4.13 Effects of copper particle diameter and number on subcooled pool boiling curves (a) and boiling heat transfer coefficients (b) for ΔT_{sub}= 5℃ at d_p=1.0 mm and $N_p = 1000$.

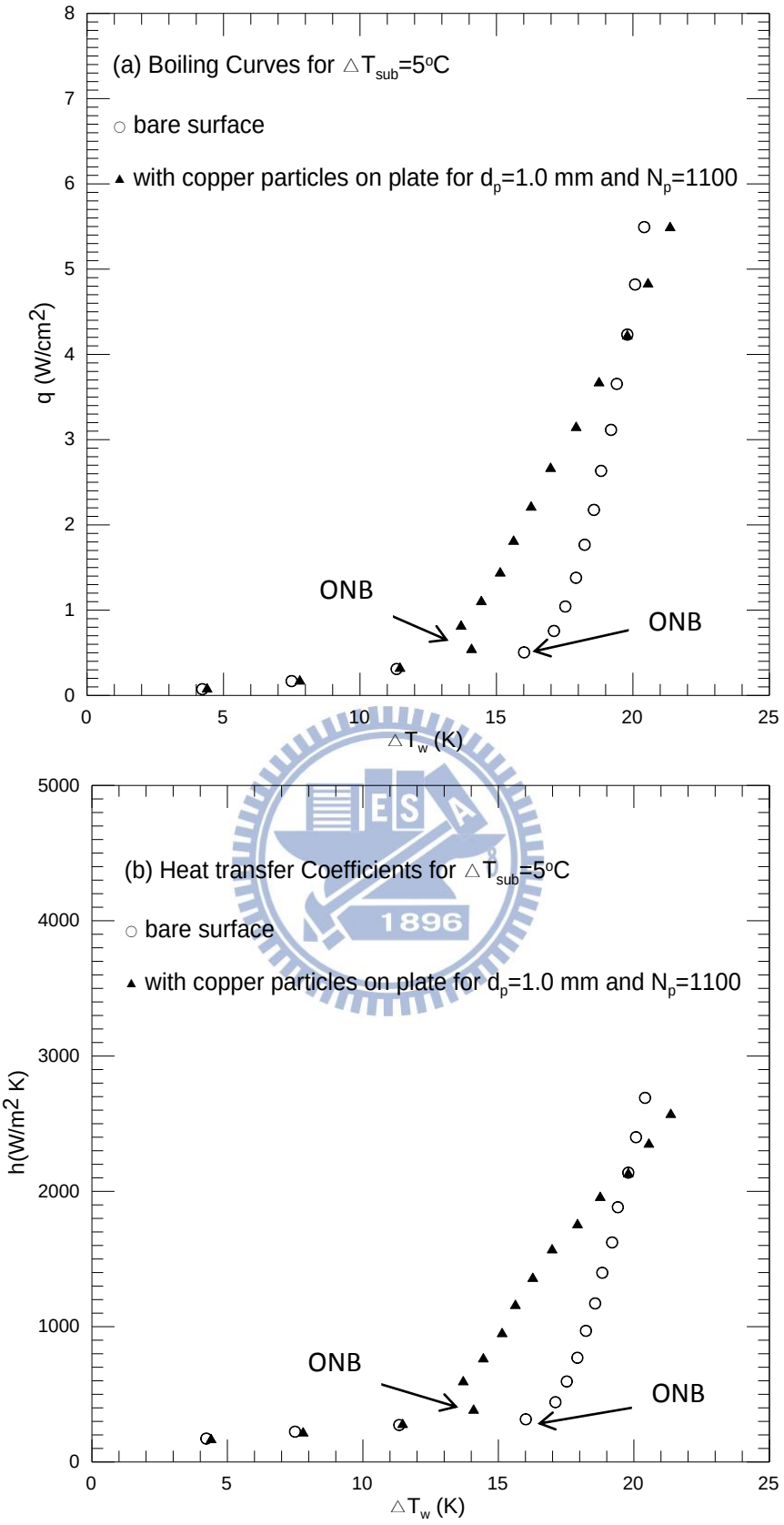

Fig. 4.14 Effects of copper particle diameter and number on subcooled pool boiling curves (a) and boiling heat transfer coefficients (b) for ΔT_{sub}= 5℃ at d_p=1.0 mm and $N_p = 1100$.

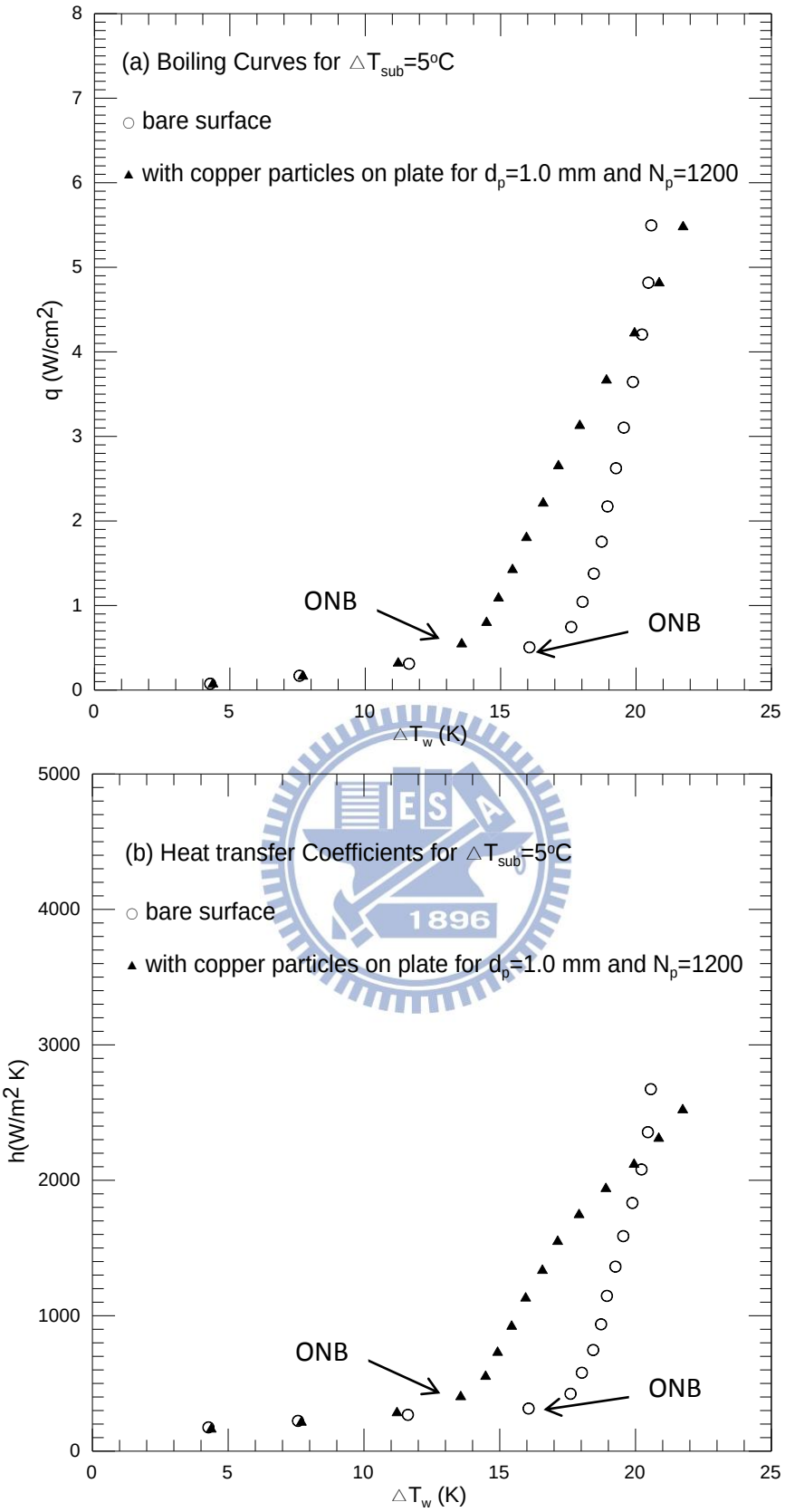

Fig. 4.15 Effects of copper particle diameter and number on subcooled pool boiling curves (a) and boiling heat transfer coefficients (b) for ΔT_{sub}= 5℃ at d_p=1.0 mm and $N_p = 1200$.

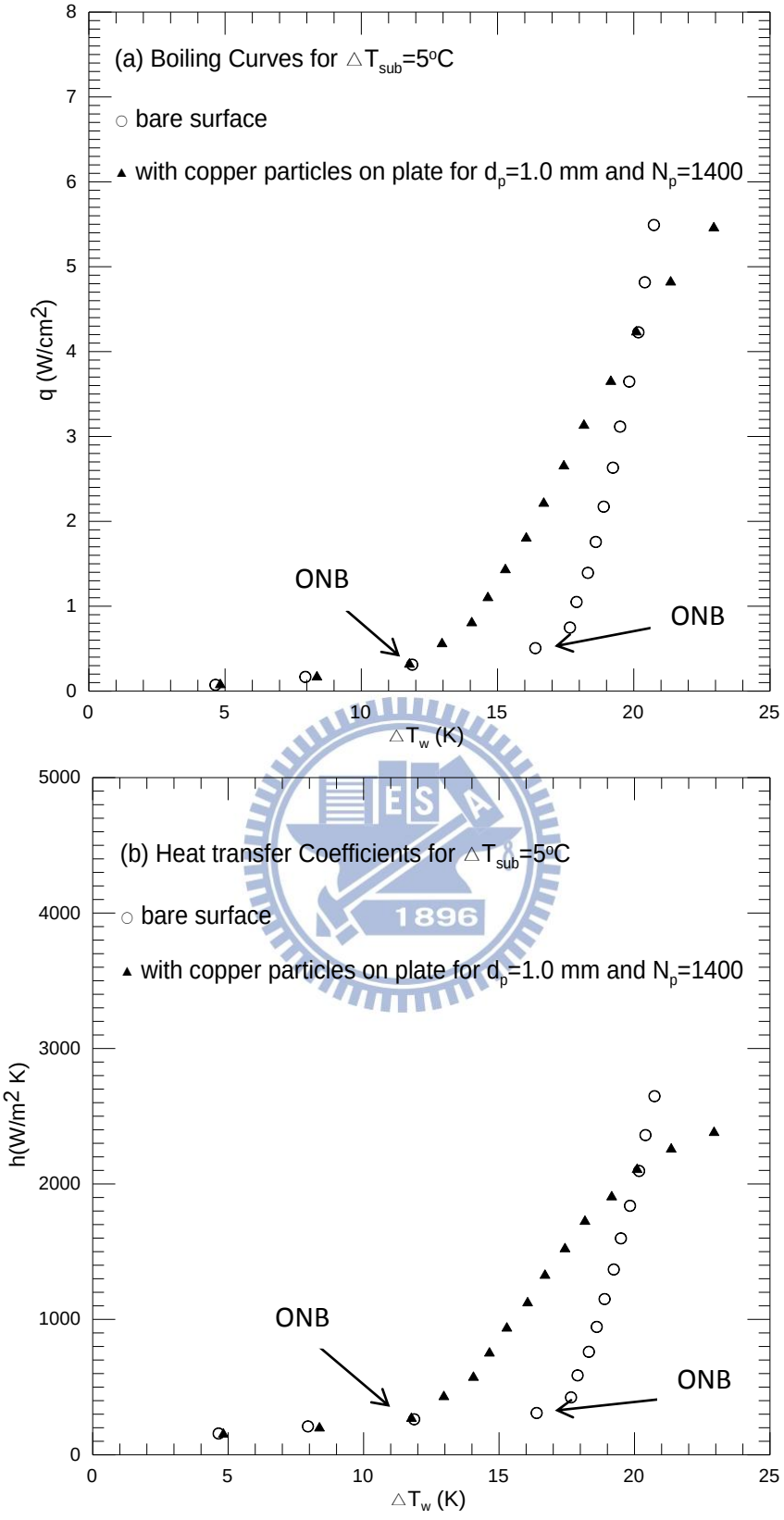

Fig. 4.16 Effects of copper particle diameter and number on subcooled pool boiling curves (a) and boiling heat transfer coefficients (b) for ΔT_{sub}= 5℃ at d_p=1.0 mm and $N_p = 1400$.

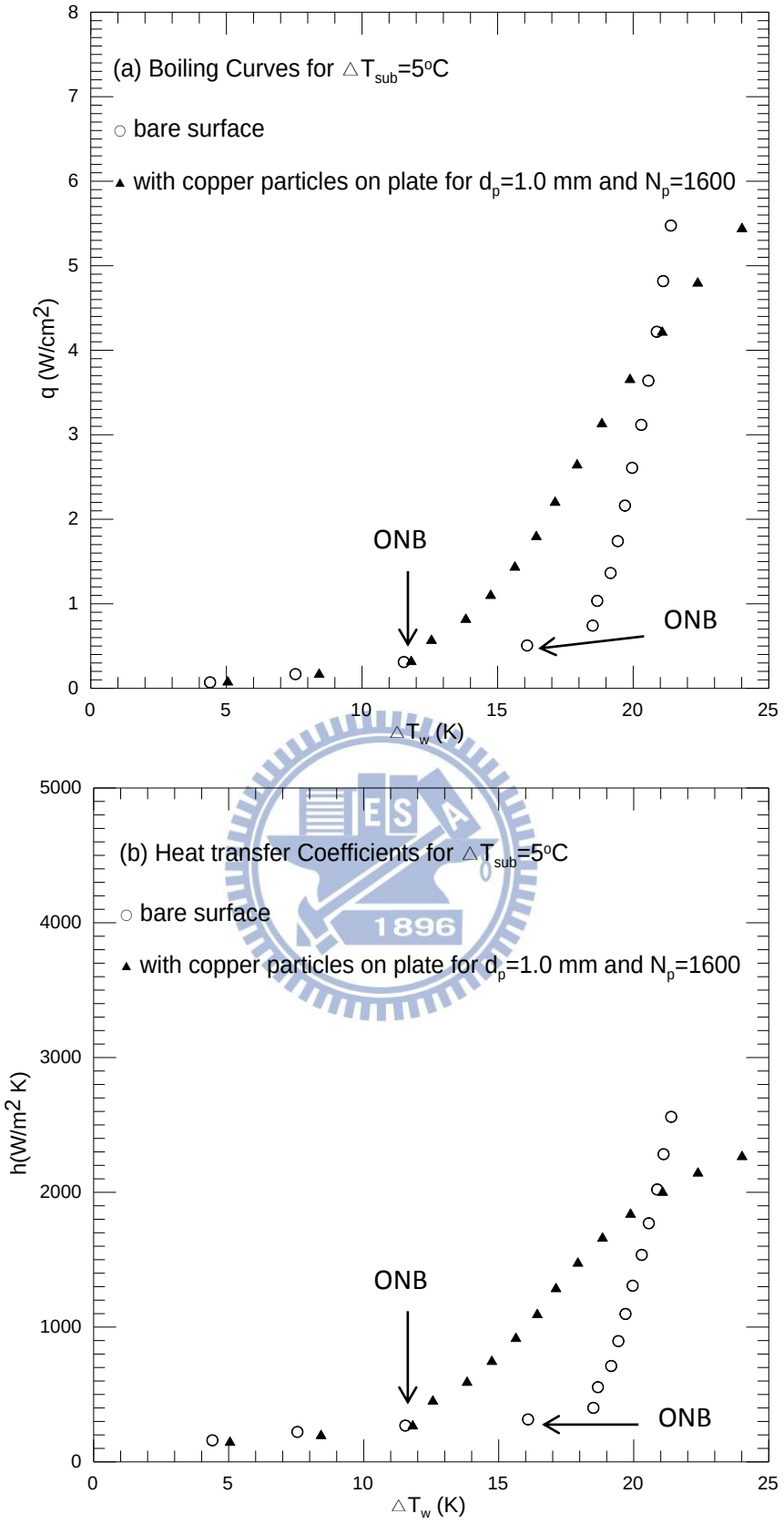

Fig. 4.17 Effects of copper particle diameter and number on subcooled pool boiling curves (a) and boiling heat transfer coefficients (b) for ΔT_{sub}= 5℃ at d_p=1.0 mm and $N_p = 1600$.

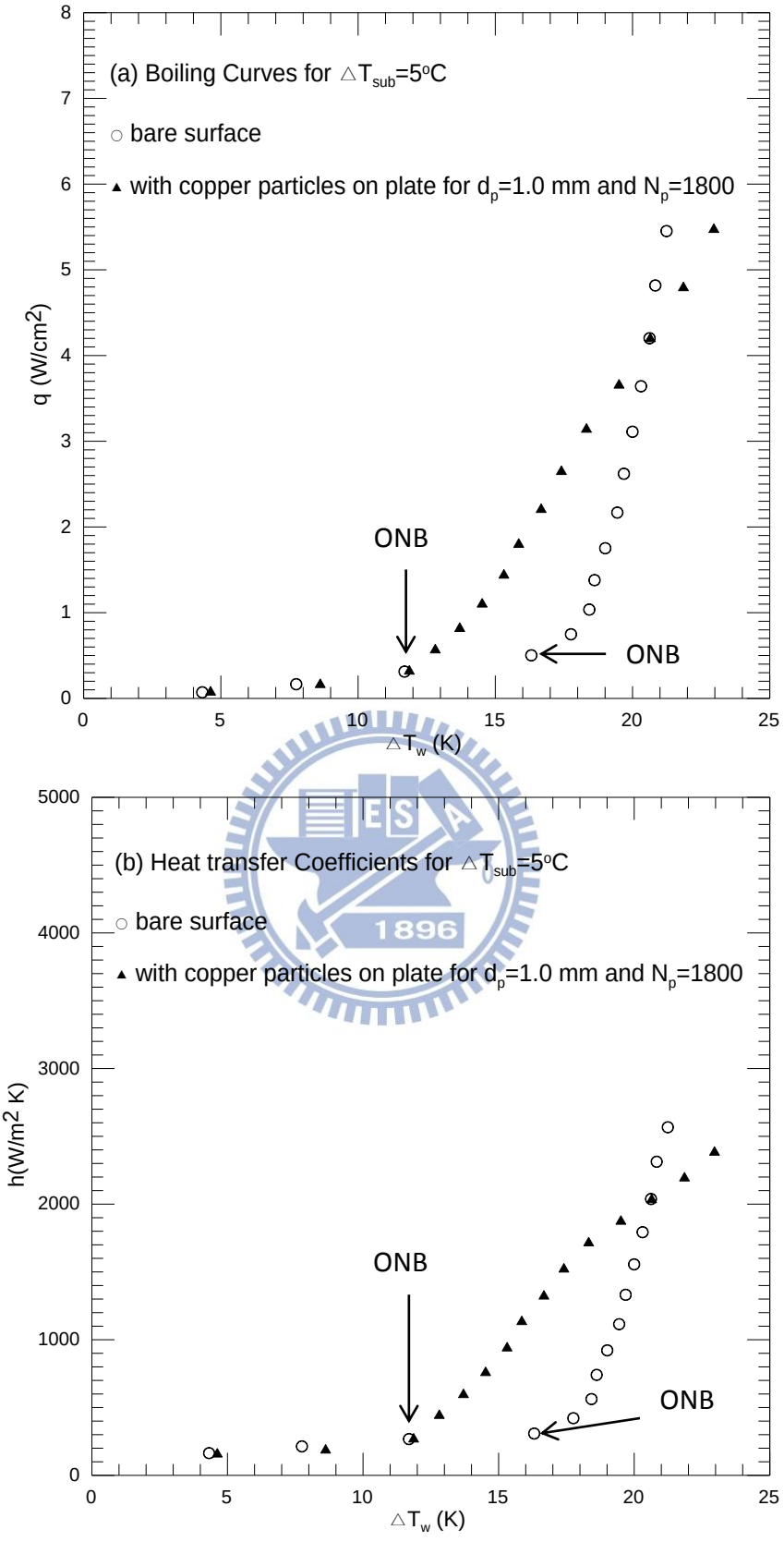

Fig. 4.18 Effects of copper particle diameter and number on subcooled pool boiling curves (a) and boiling heat transfer coefficients (b) for ΔT_{sub}= 5℃ at d_p=1.0 mm and $N_p = 1800$.

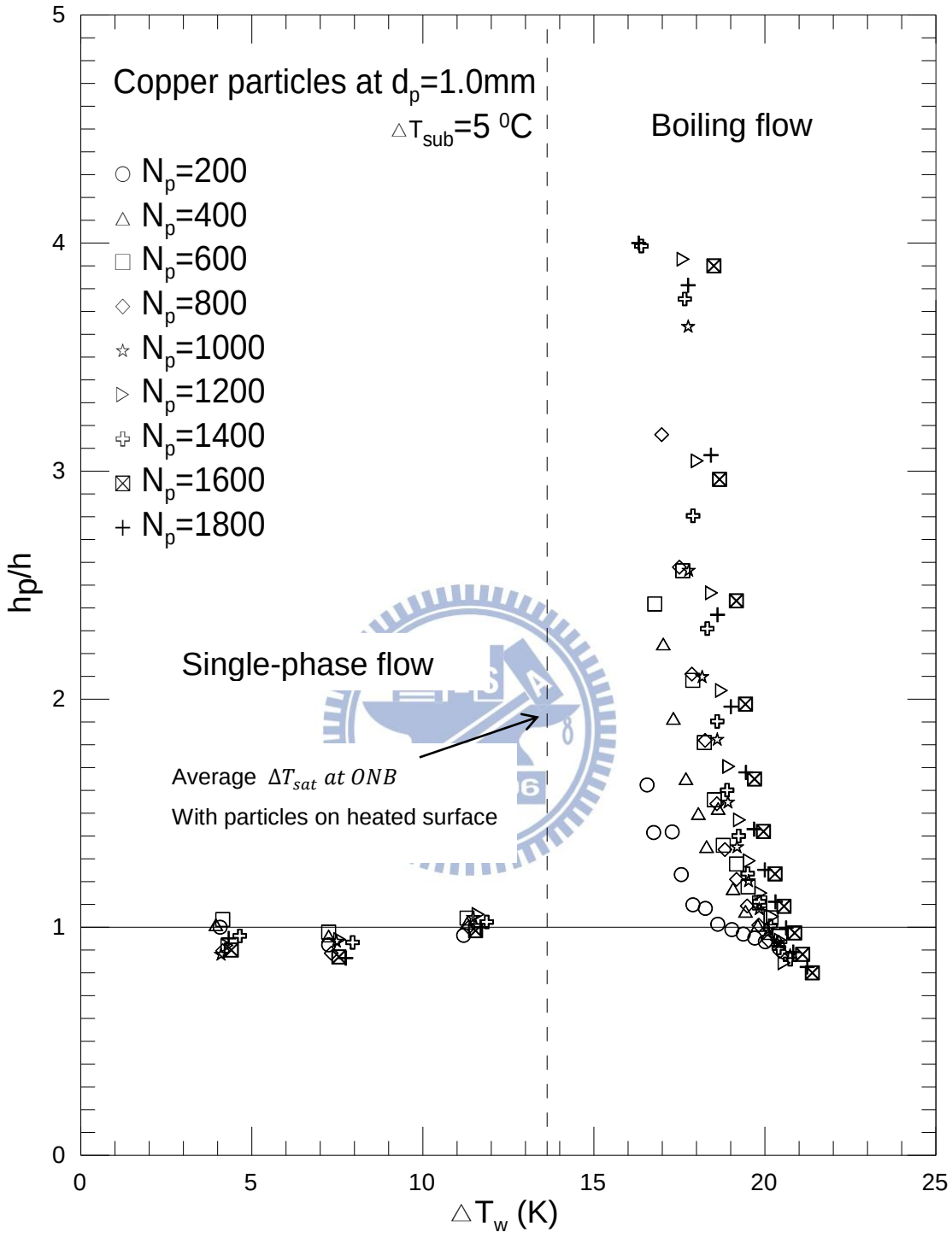

Fig. 4.19 Variations of h_p/h with wall superheat for various total copper particle numbers at d_p=1.0 mm and ΔT_{sub}=5℃.

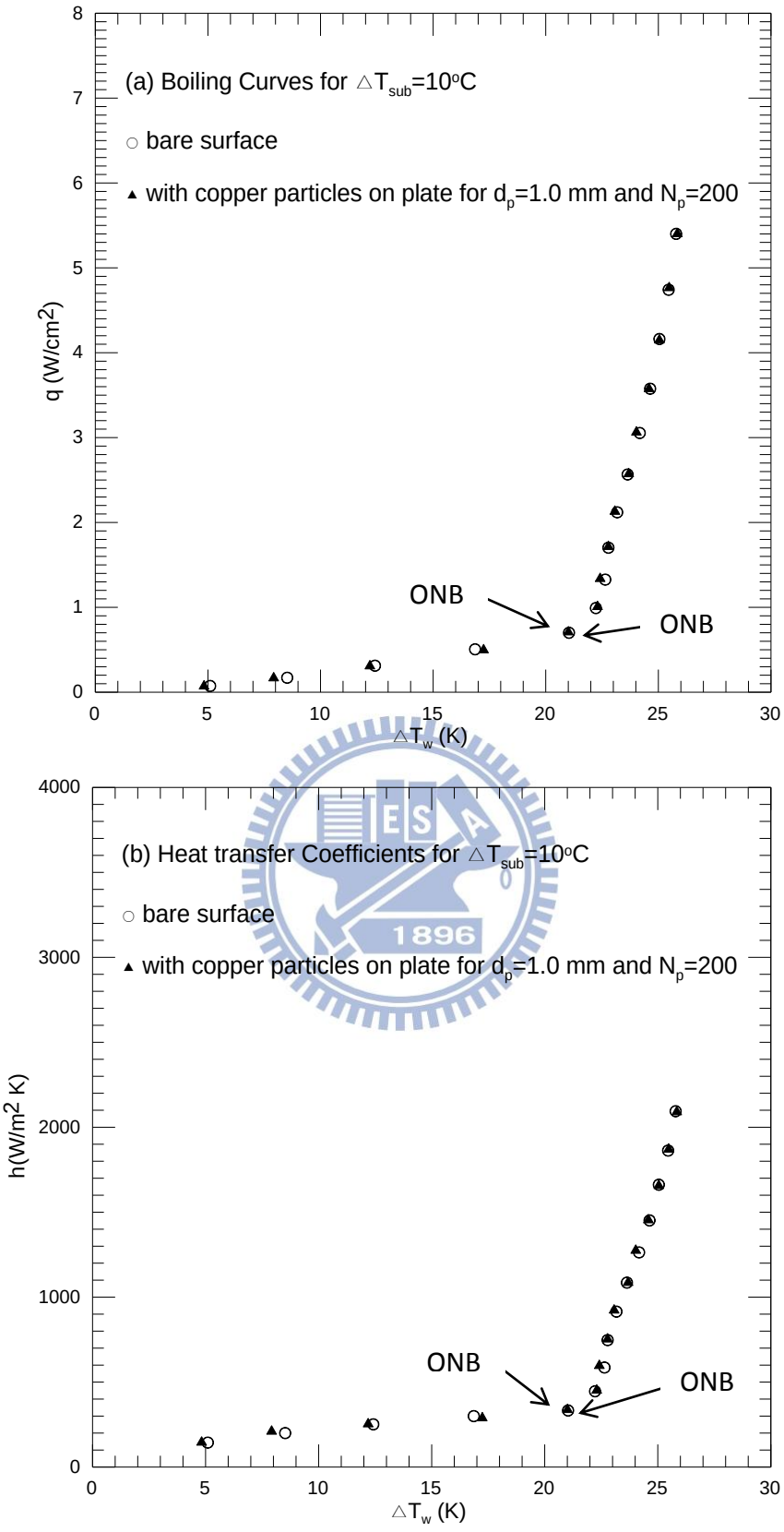

Fig. 4.20 Effects of copper particle diameter and number on subcooled pool boiling curves (a) and boiling heat transfer coefficients (b) for ΔT_{sub}= 10℃ at d_p=1.0 mm and $N_p = 200$.

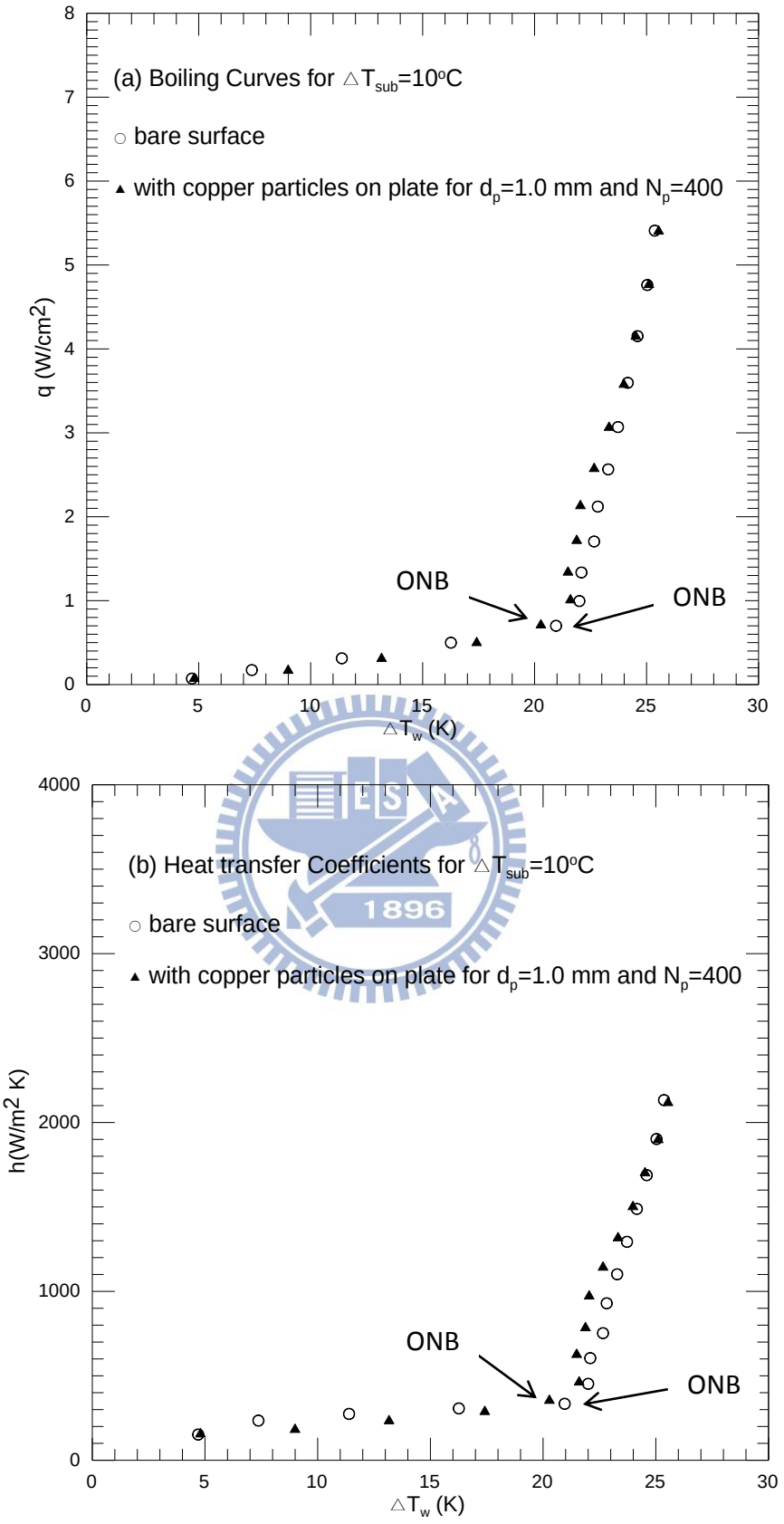

Fig. 4.21 Effects of copper particle diameter and number on subcooled pool boiling curves (a) and boiling heat transfer coefficients (b) for ΔT_{sub}= 10℃ at d_p=1.0 mm and $N_p = 400$.

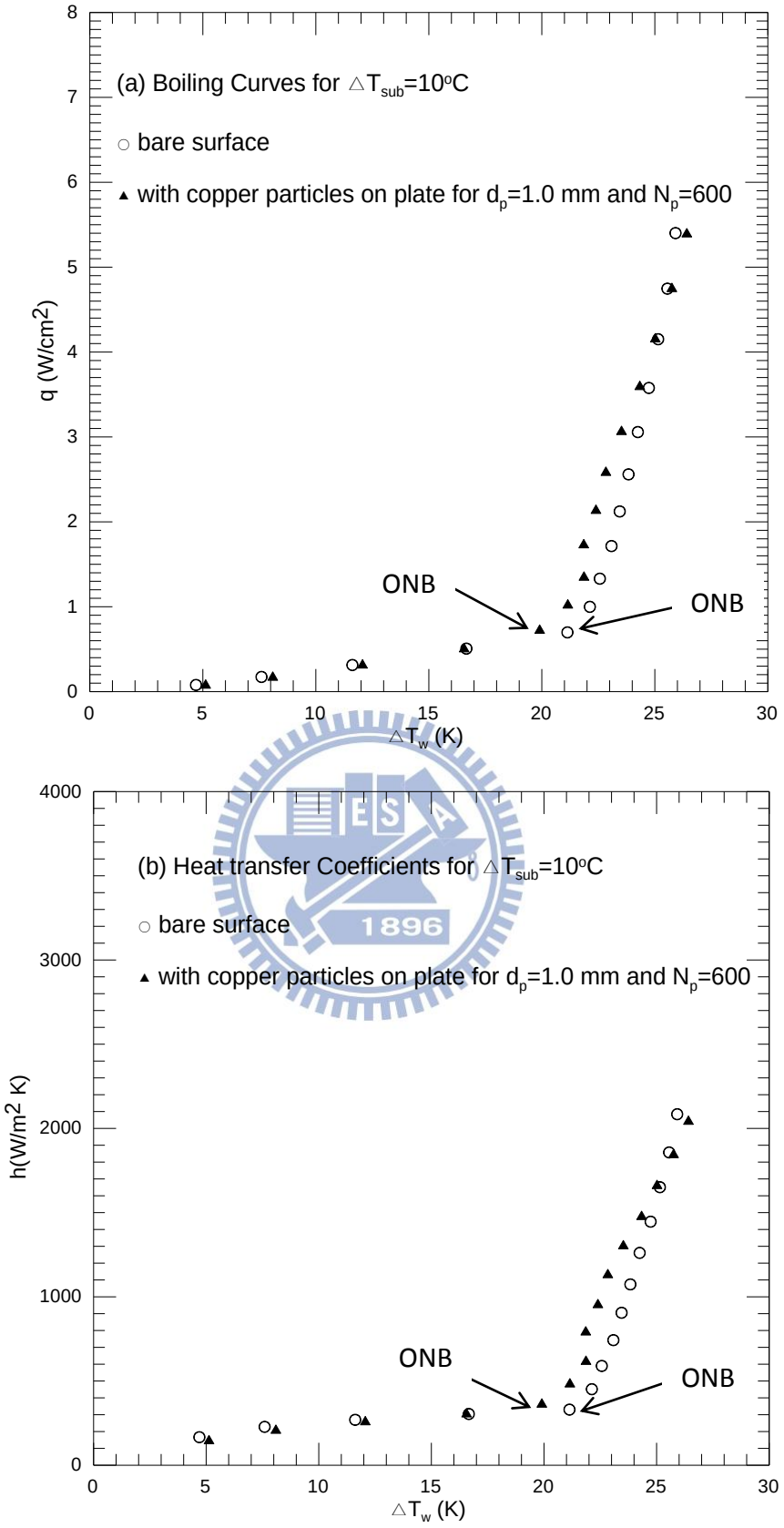

Fig. 4.22 Effects of copper particle diameter and number on subcooled pool boiling curves (a) and boiling heat transfer coefficients (b) for ΔT_{sub}= 10℃ at d_p=1.0 mm and $N_p = 600$.

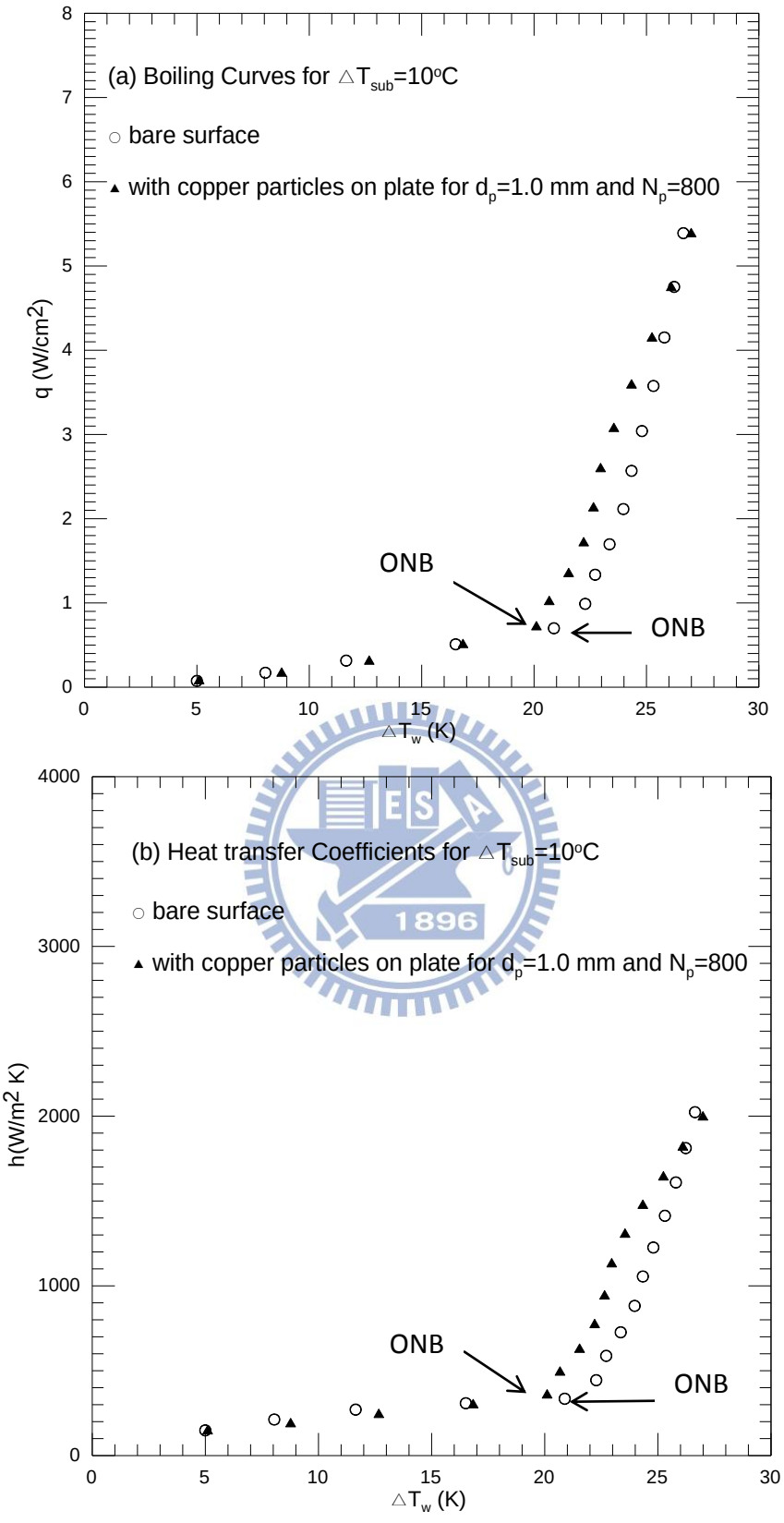

Fig. 4.23 Effects of copper particle diameter and number on subcooled pool boiling curves (a) and boiling heat transfer coefficients (b) for ΔT_{sub}= 10℃ at d_p=1.0 mm and $N_p = 800$.

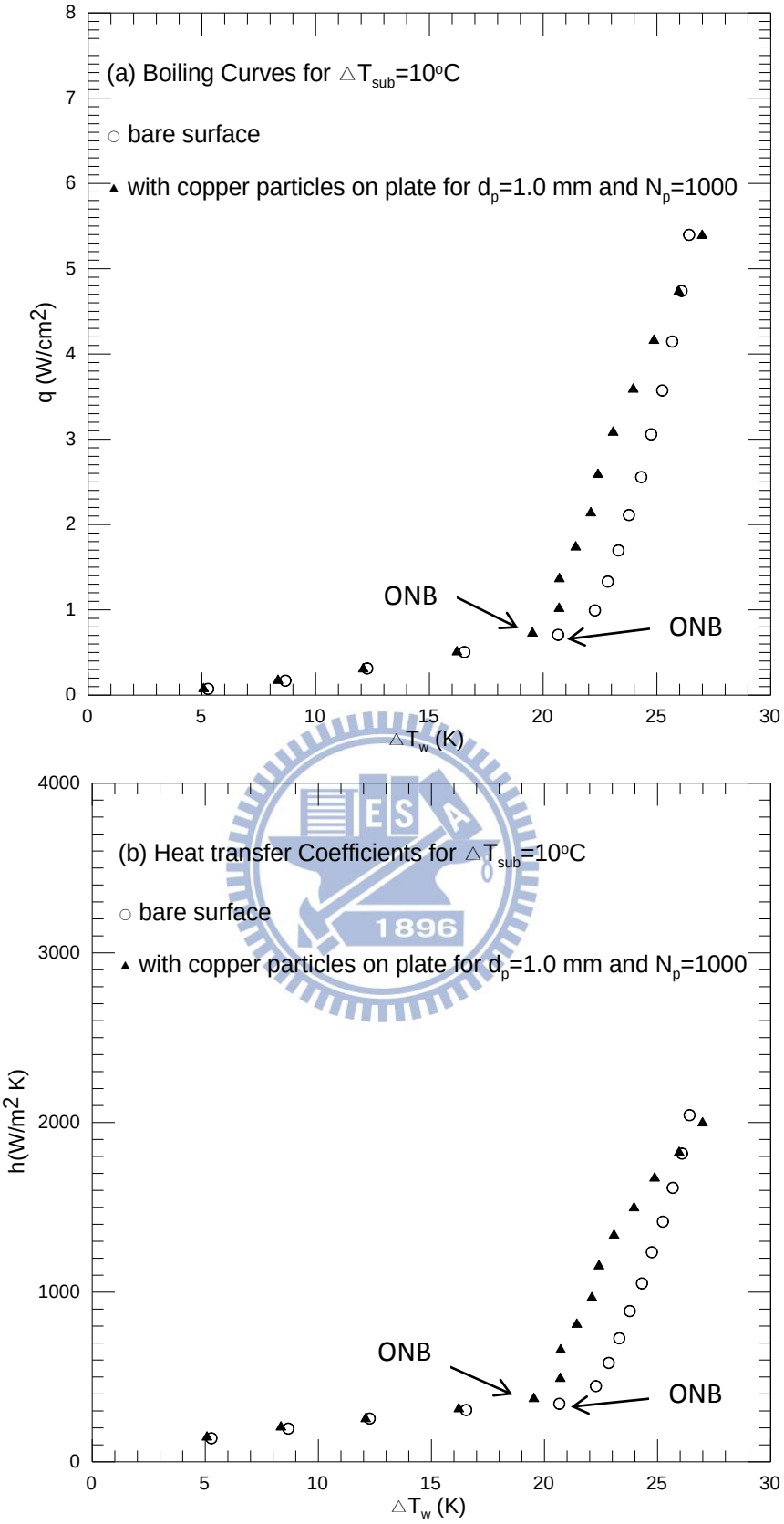

Fig. 4.24 Effects of copper particle diameter and number on subcooled pool boiling curves (a) and boiling heat transfer coefficients (b) for ΔT_{sub}= 10℃ at d_p=1.0 mm and $N_p = 1000$.

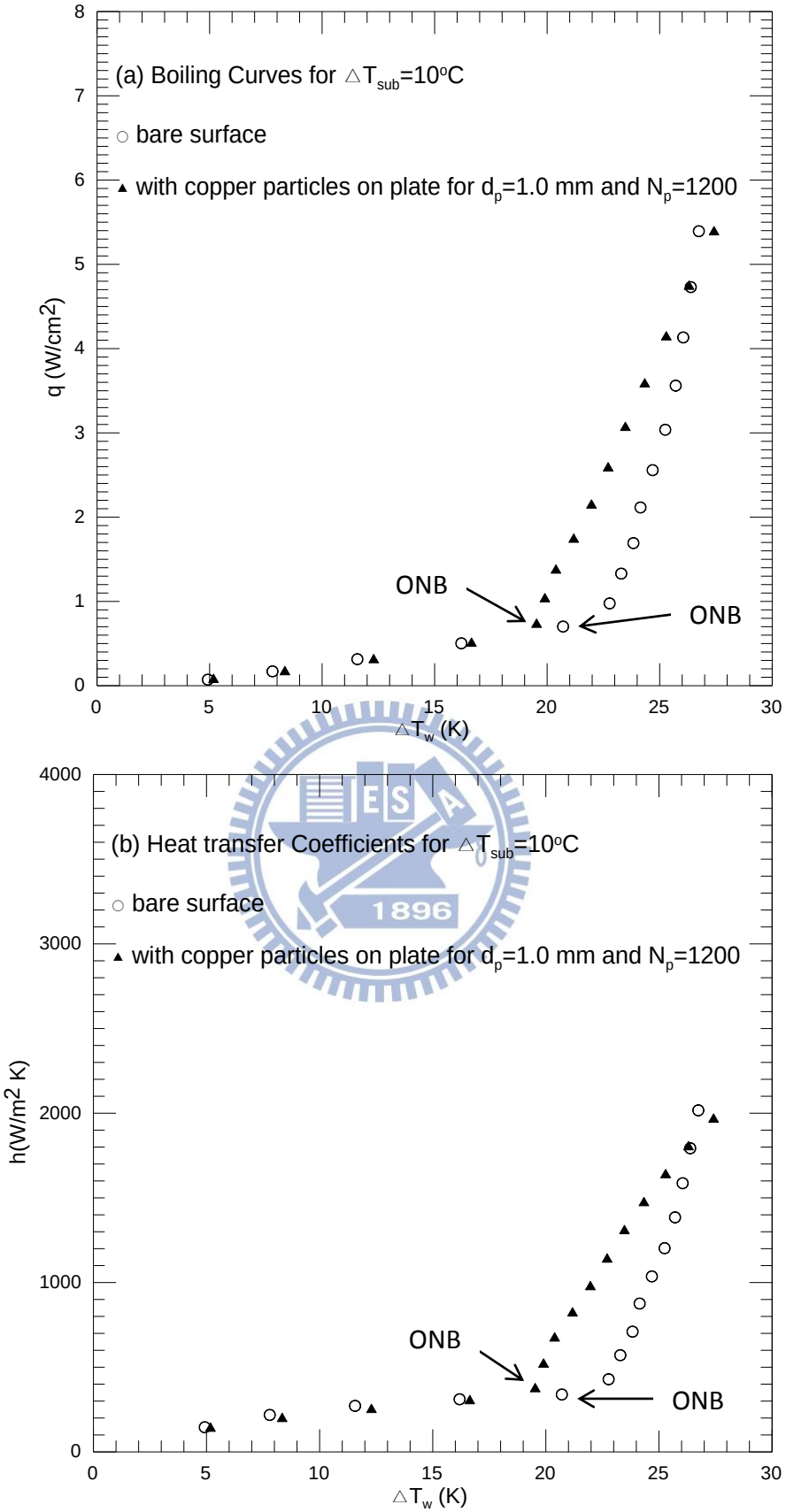

Fig. 4.25 Effects of copper particle diameter and number on subcooled pool boiling curves (a) and boiling heat transfer coefficients (b) for ΔT_{sub}= 10℃ at d_p=1.0 mm and $N_p = 1200$..

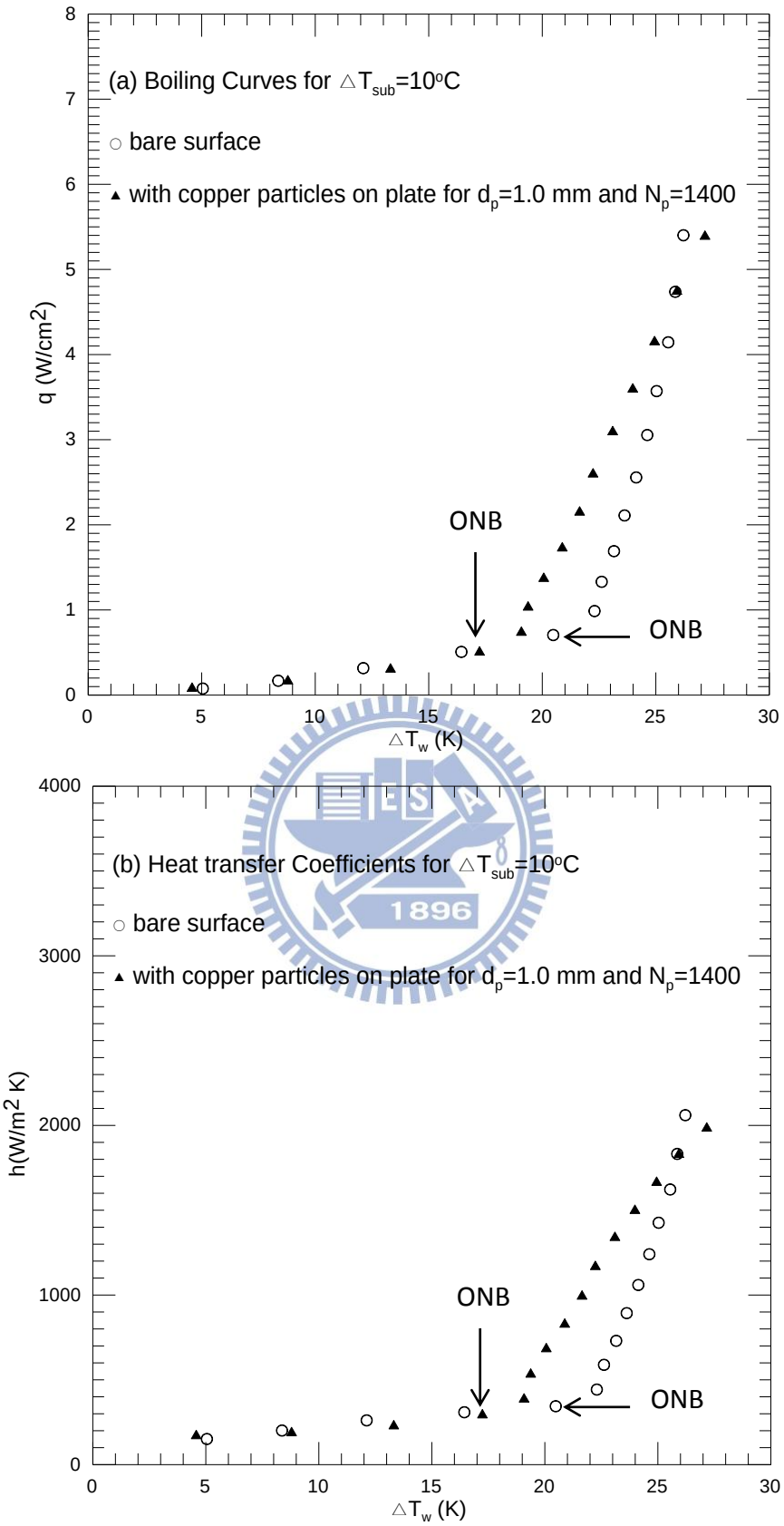

Fig. 4.26 Effects of copper particle diameter and number on subcooled pool boiling curves (a) and boiling heat transfer coefficients (b) for ΔT_{sub}= 10℃ at d_p=1.0 mm and $N_p = 1400$.

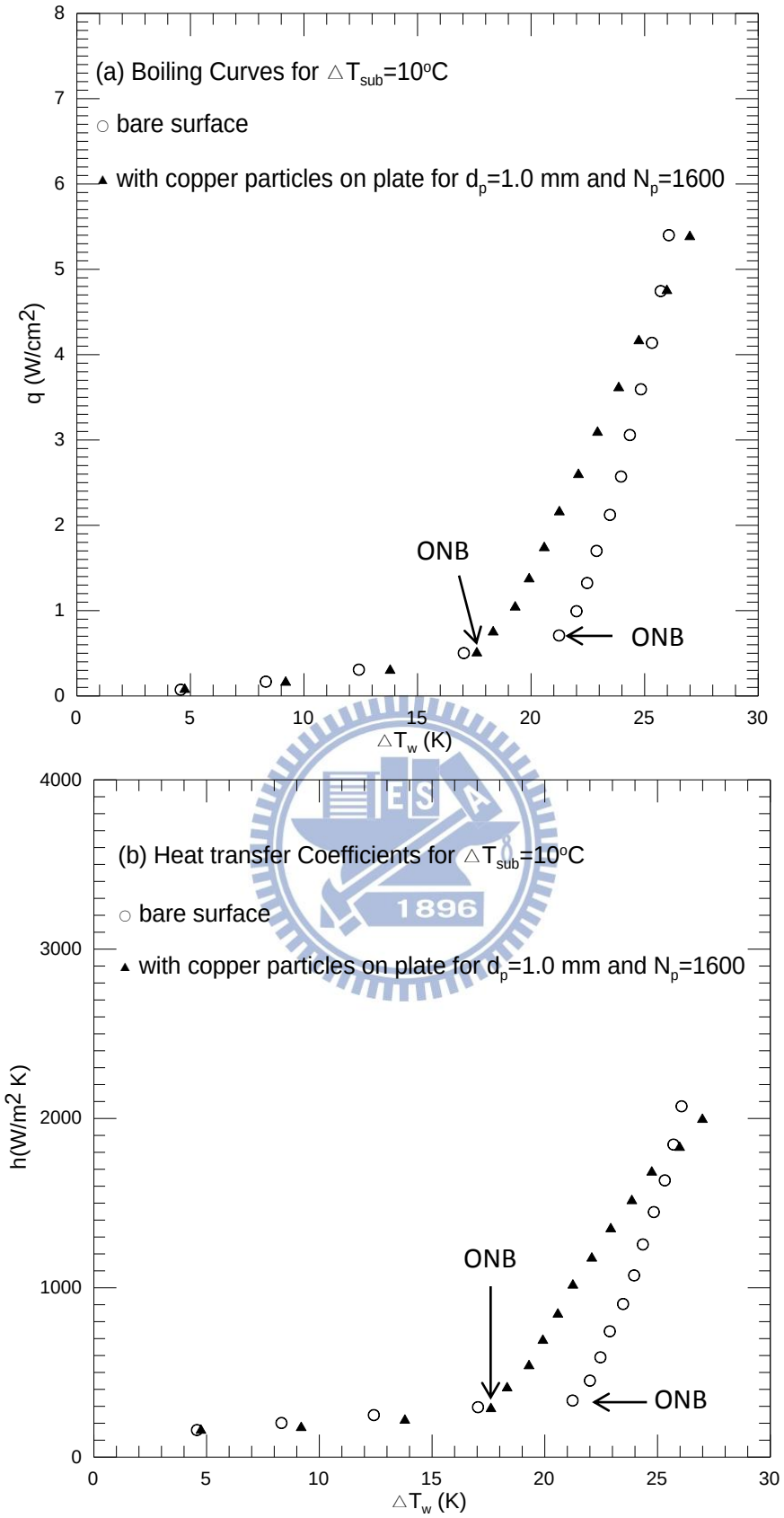

Fig. 4.27 Effects of copper particle diameter and number on subcooled pool boiling curves (a) and boiling heat transfer coefficients (b) for ΔT_{sub}= 10℃ at d_p=1.0 mm and $N_p = 1600$.

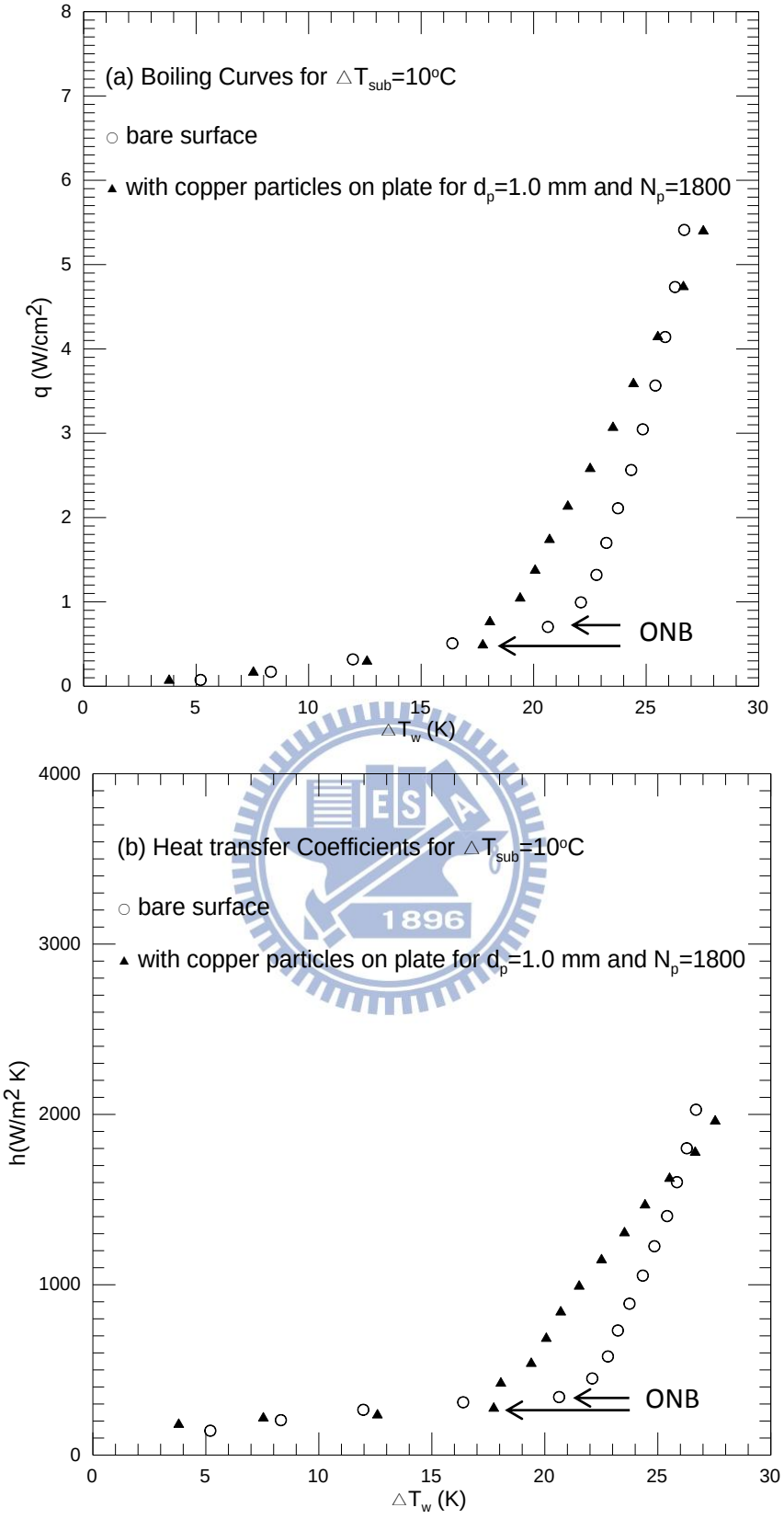

Fig. 4.28 Effects of copper particle diameter and number on subcooled pool boiling curves (a) and boiling heat transfer coefficients (b) for ΔT_{sub}= 10℃ at d_p=1.0 mm and $N_p = 1800$.

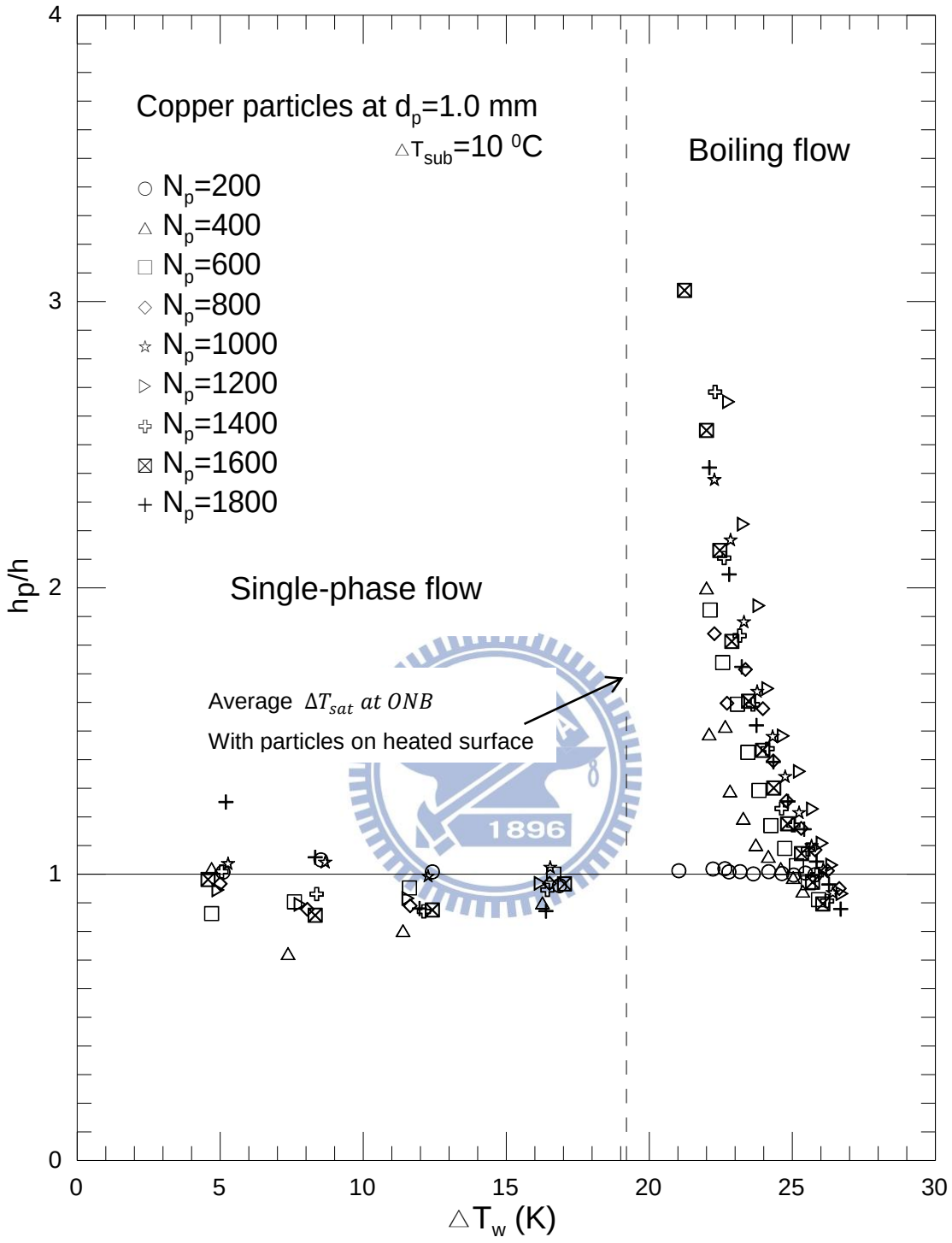

Fig. 4.29 Variations of h_p/h with wall superheat for various total copper particle numbers at d_p=1.0 mm and ΔT_{sub}=10℃.

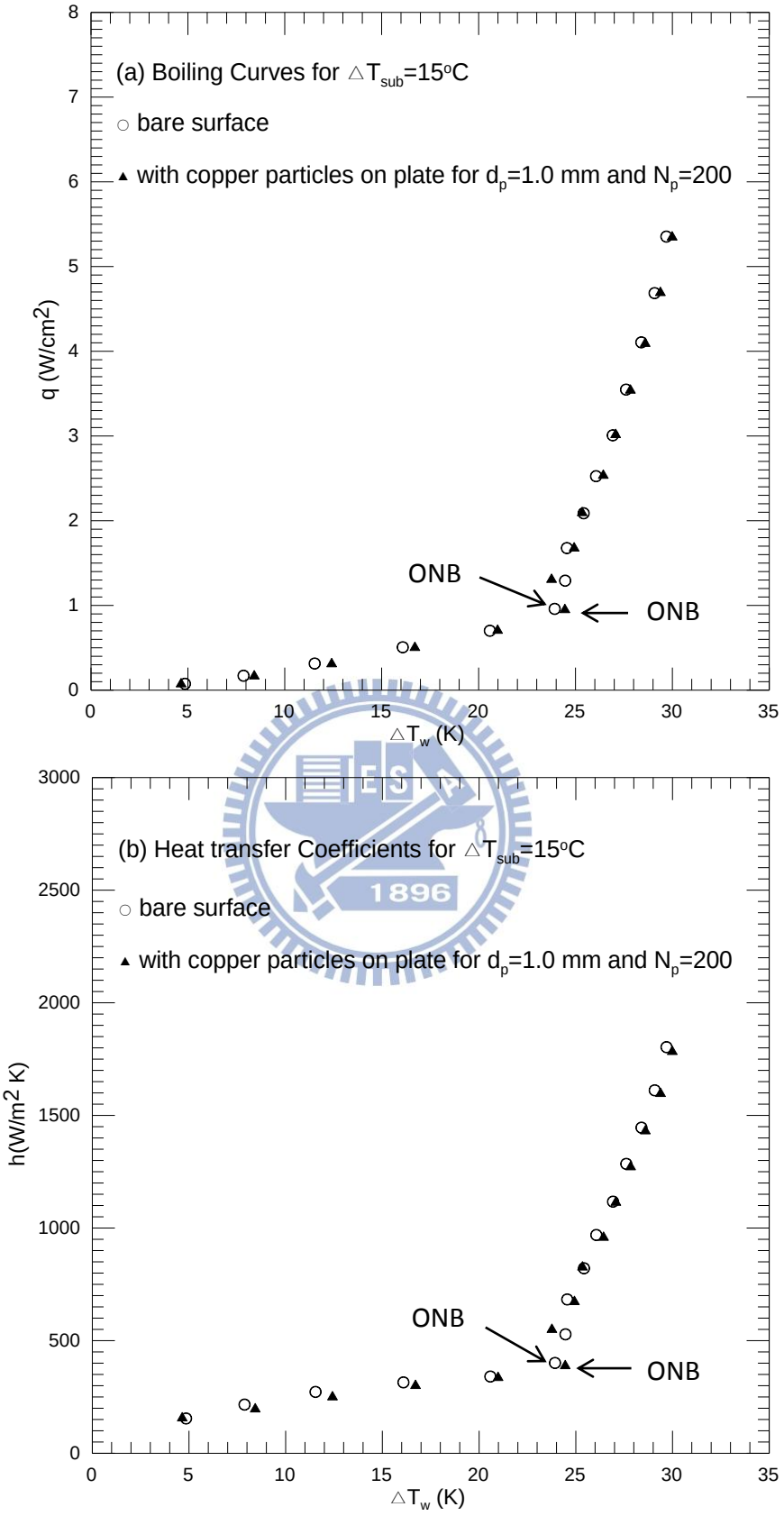

Fig. 4.30 Effects of copper particle diameter and number on subcooled pool boiling curves (a) and boiling heat transfer coefficients (b) for ΔT_{sub}= 15℃ at d_p=1.0 mm and $N_p = 200$.

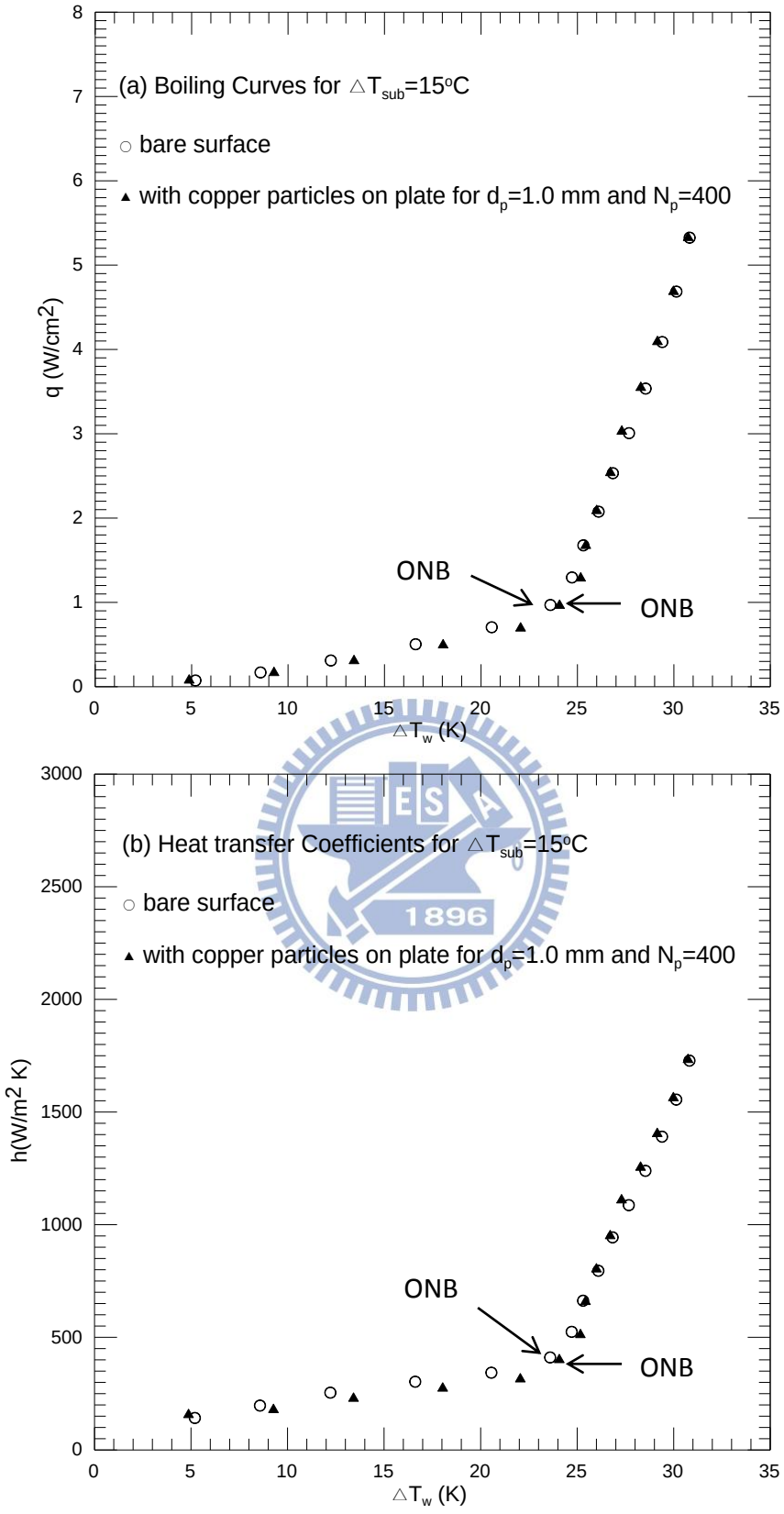

Fig. 4.31 Effects of copper particle diameter and number on subcooled pool boiling curves (a) and boiling heat transfer coefficients (b) for ΔT_{sub}= 15℃ at d_p=1.0 mm and $N_p = 400$.

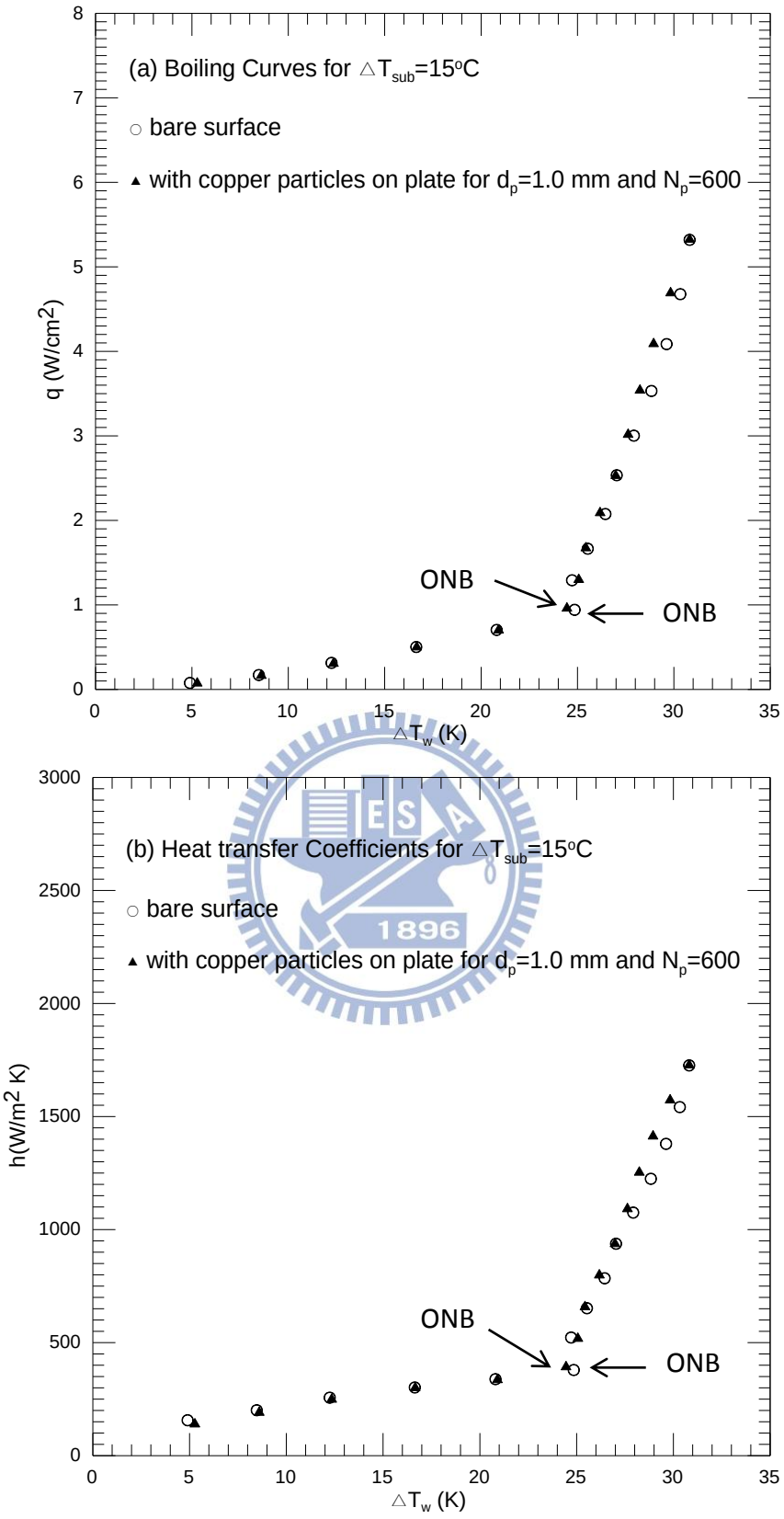

Fig. 4.32 Effects of copper particle diameter and number on subcooled pool boiling curves (a) and boiling heat transfer coefficients (b) for ΔT_{sub}= 15℃ at d_p=1.0 mm and $N_p = 600$.

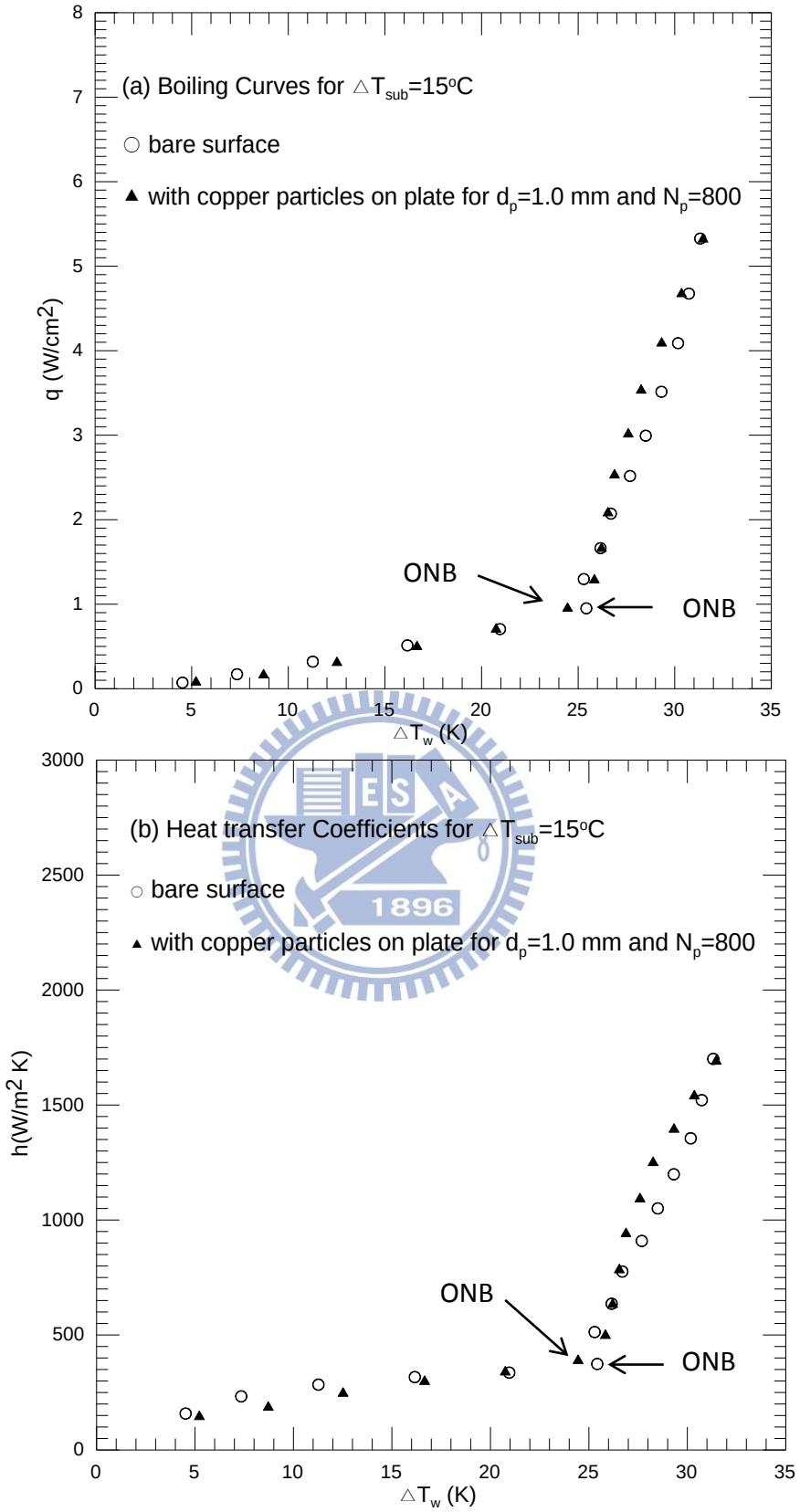

Fig. 4.33 Effects of copper particle diameter and number on subcooled pool boiling curves (a) and boiling heat transfer coefficients (b) for ΔT_{sub}= 15℃ at d_p=1.0 mm and $N_p = 800$.

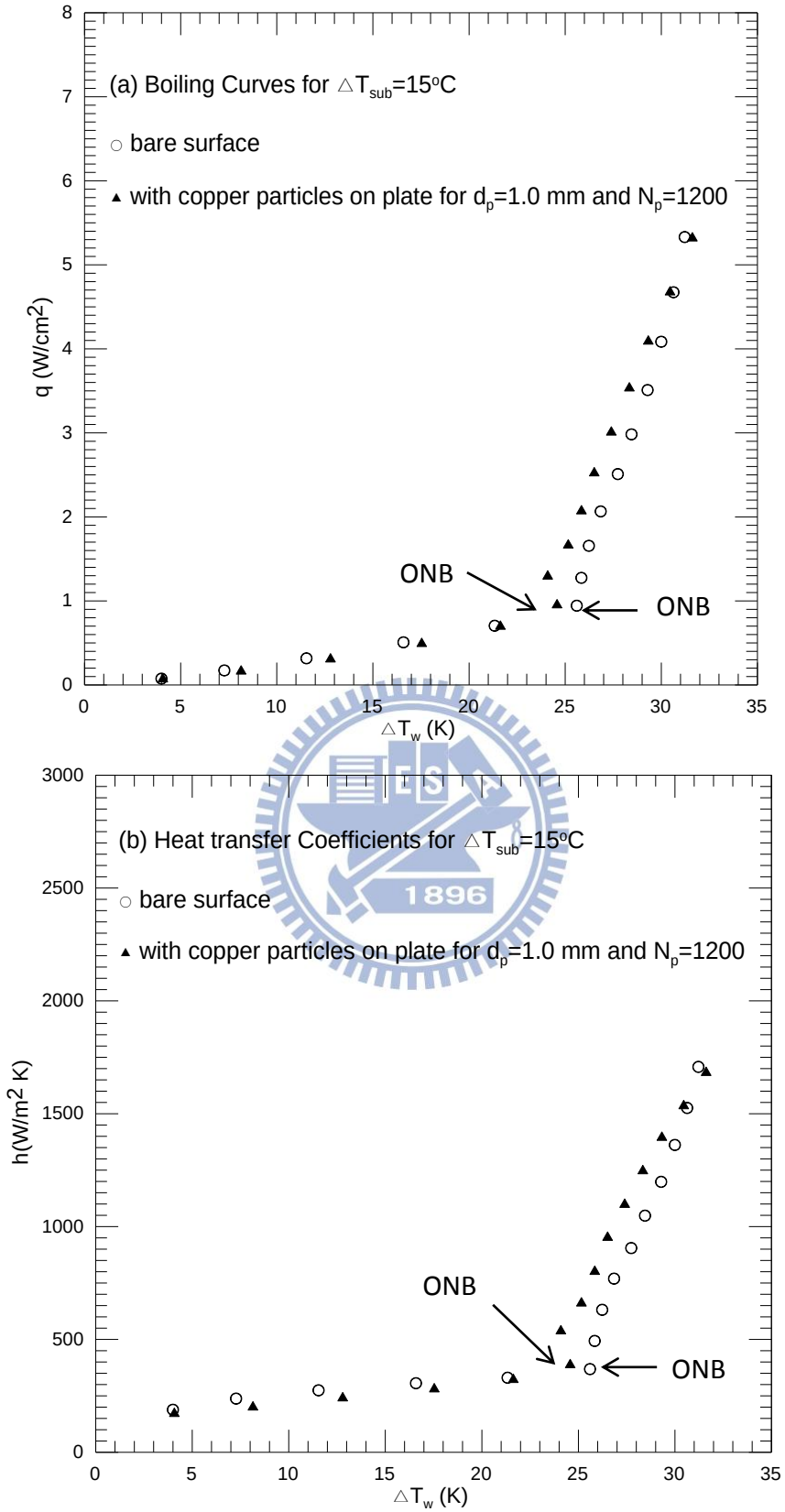

Fig. 4.34 Effects of copper particle diameter and number on subcooled pool boiling curves (a) and boiling heat transfer coefficients (b) for ΔT_{sub}= 15℃ at d_p=1.0 mm and $N_p = 1200$.

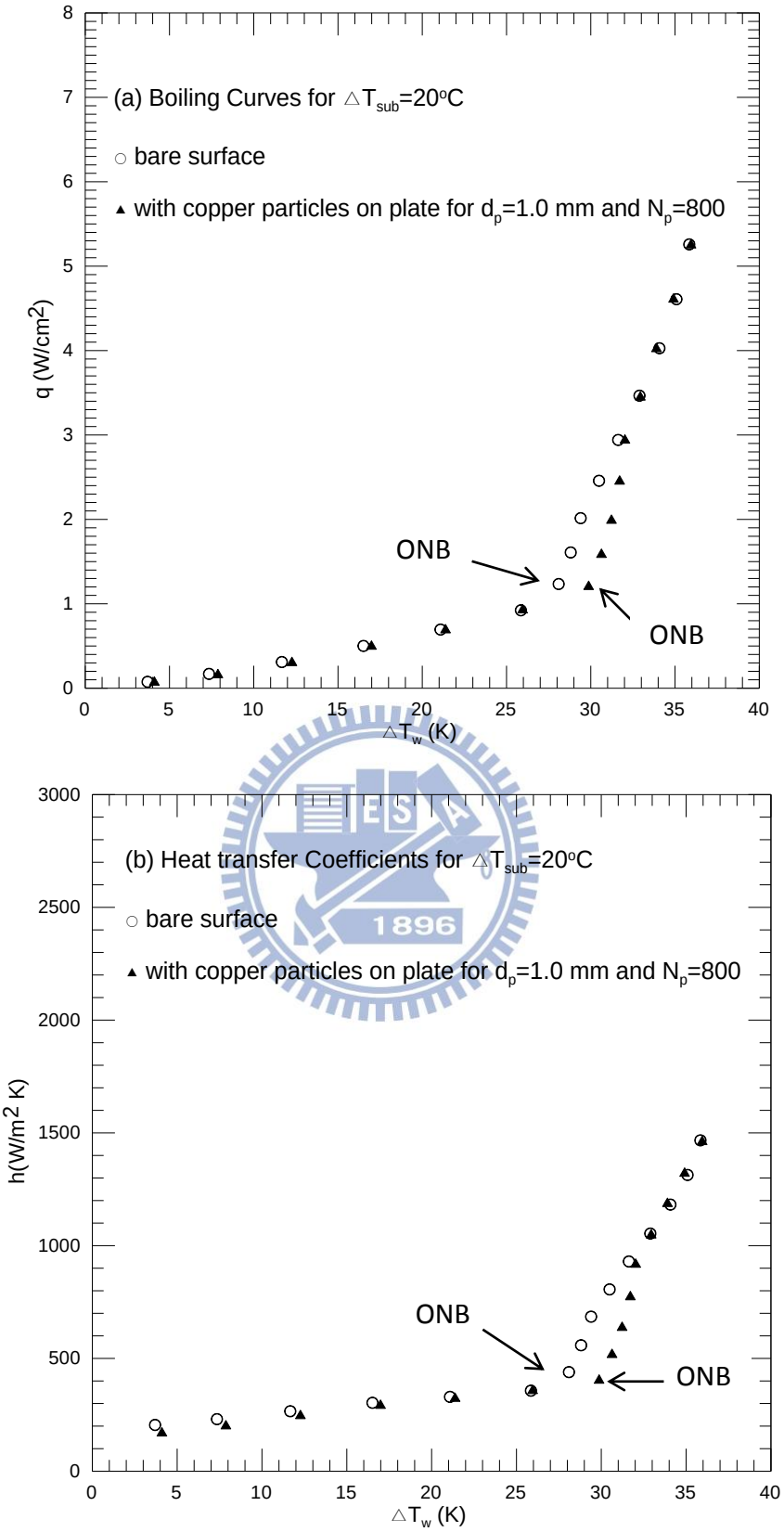

Fig. 4.35 Effects of copper particle diameter and number on subcooled pool boiling curves (a) and boiling heat transfer coefficients (b) for ΔT_{sub}= 20℃ at d_p=1.0 mm and $N_p = 800$.

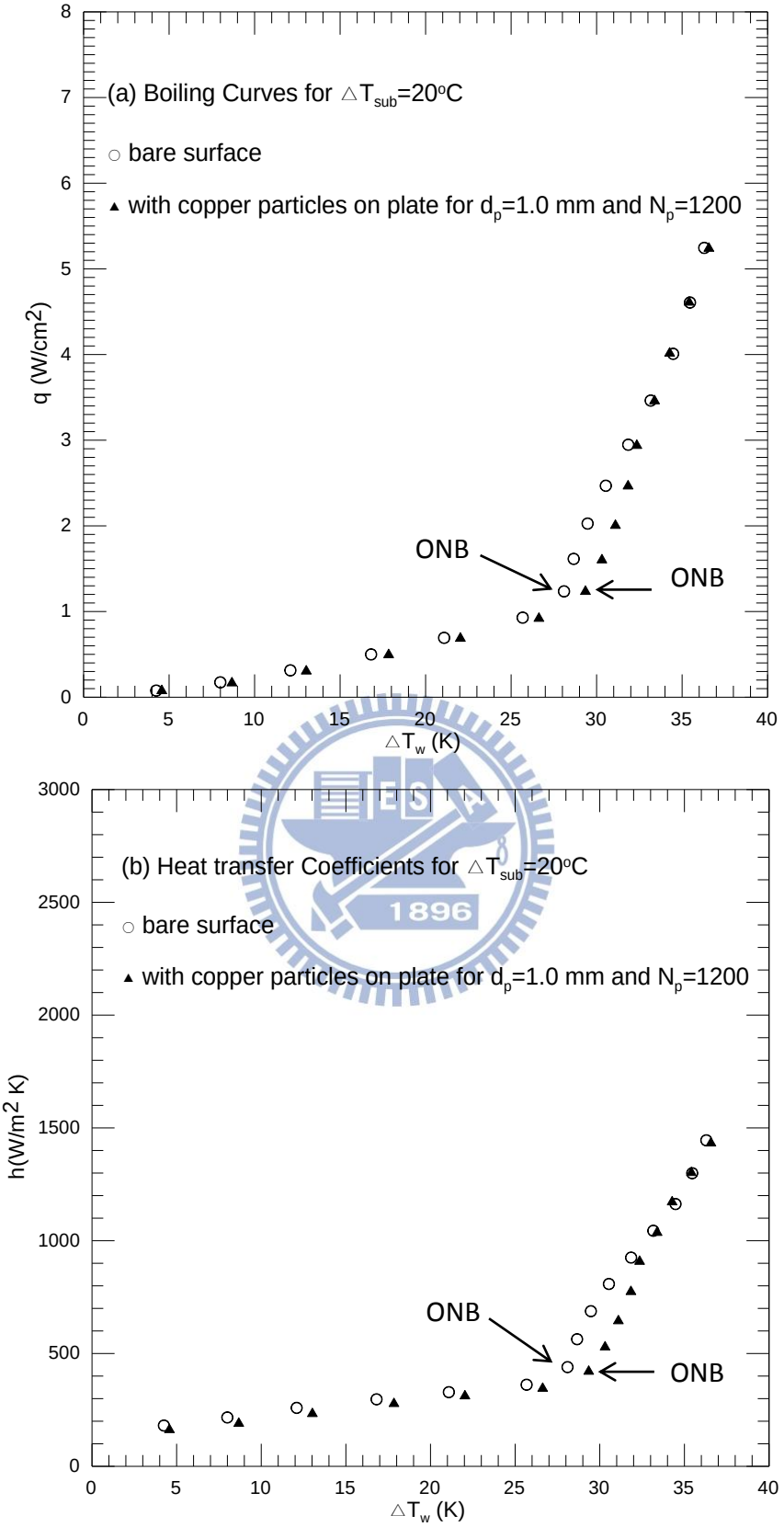

Fig. 4.36 Effects of copper particle diameter and number on subcooled pool boiling curves (a) and boiling heat transfer coefficients (b) for ΔT_{sub}= 20℃ at d_p=1.0 mm and $N_p = 1200$.

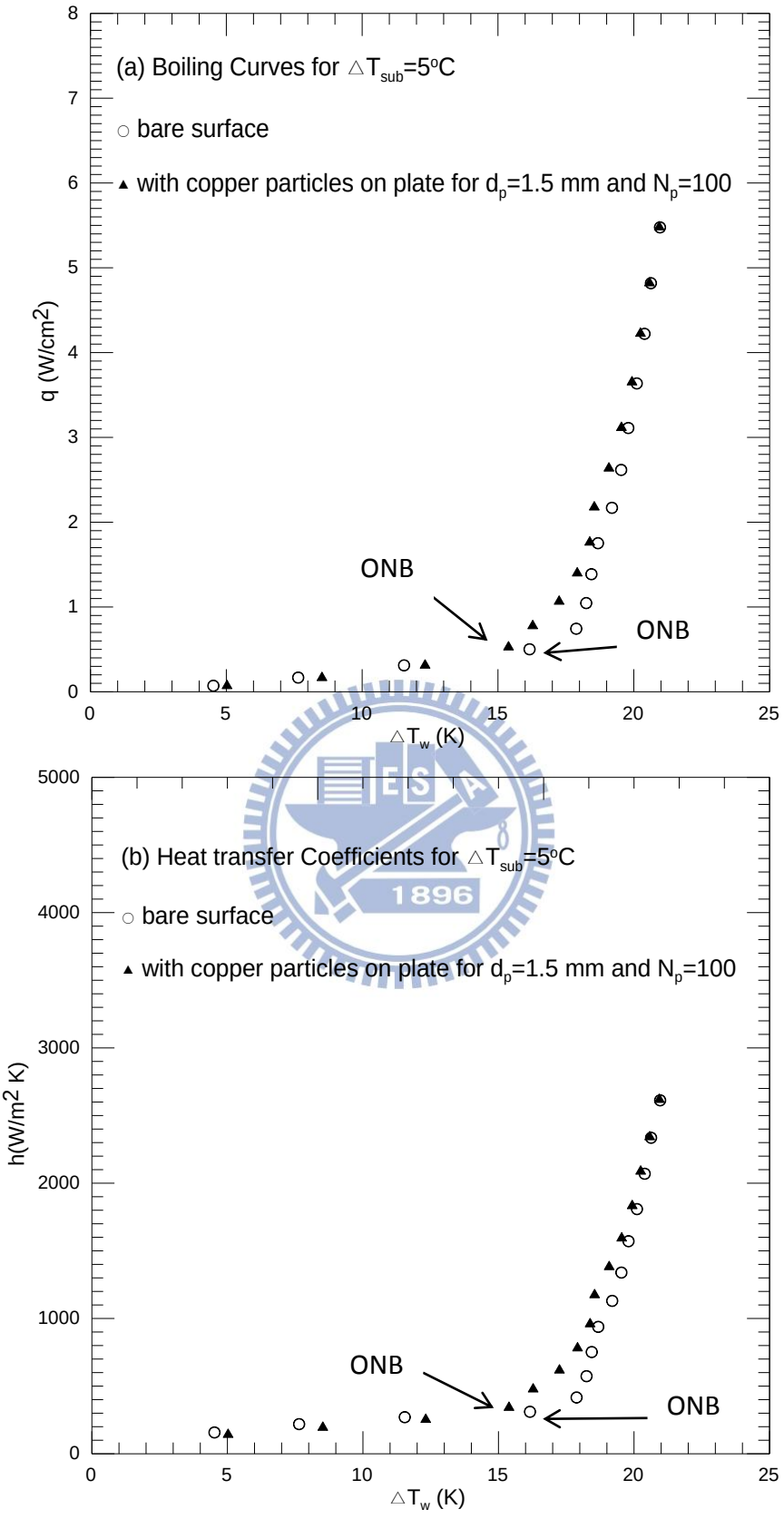

Fig. 4.37 Effects of copper particle diameter and number on subcooled pool boiling curves (a) and boiling heat transfer coefficients (b) for ΔT_{sub}= 5℃ at d_p=1.5 mm and $N_p = 100$.

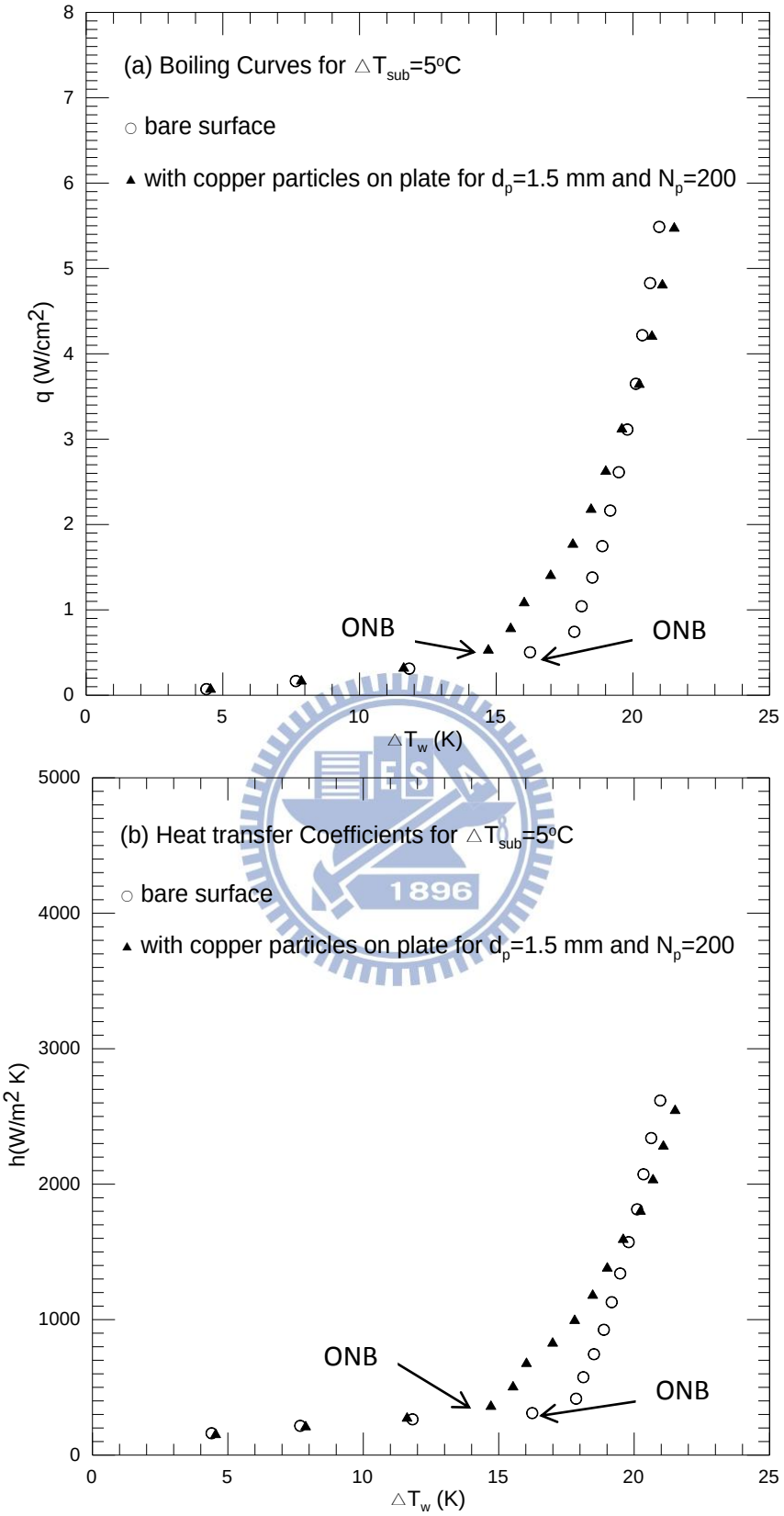

Fig. 4.38 Effects of copper particle diameter and number on subcooled pool boiling curves (a) and boiling heat transfer coefficients (b) for ΔT_{sub}= 5℃ at d_p=1.5 mm and $N_p = 200$.

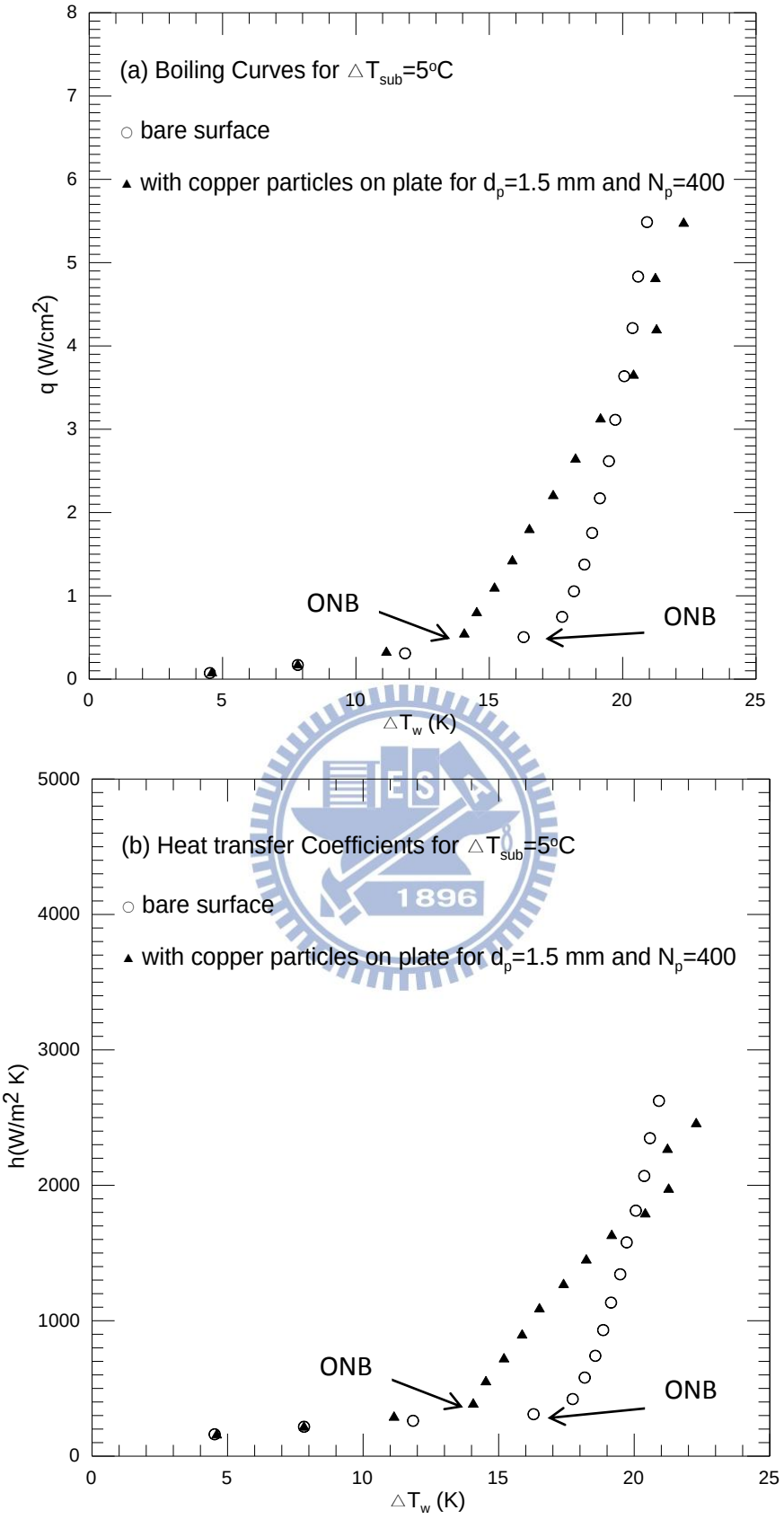

Fig. 4.39 Effects of copper particle diameter and number on subcooled pool boiling curves (a) and boiling heat transfer coefficients (b) for ΔT_{sub}= 5℃ at d_p=1.5 mm and $N_p = 400$.

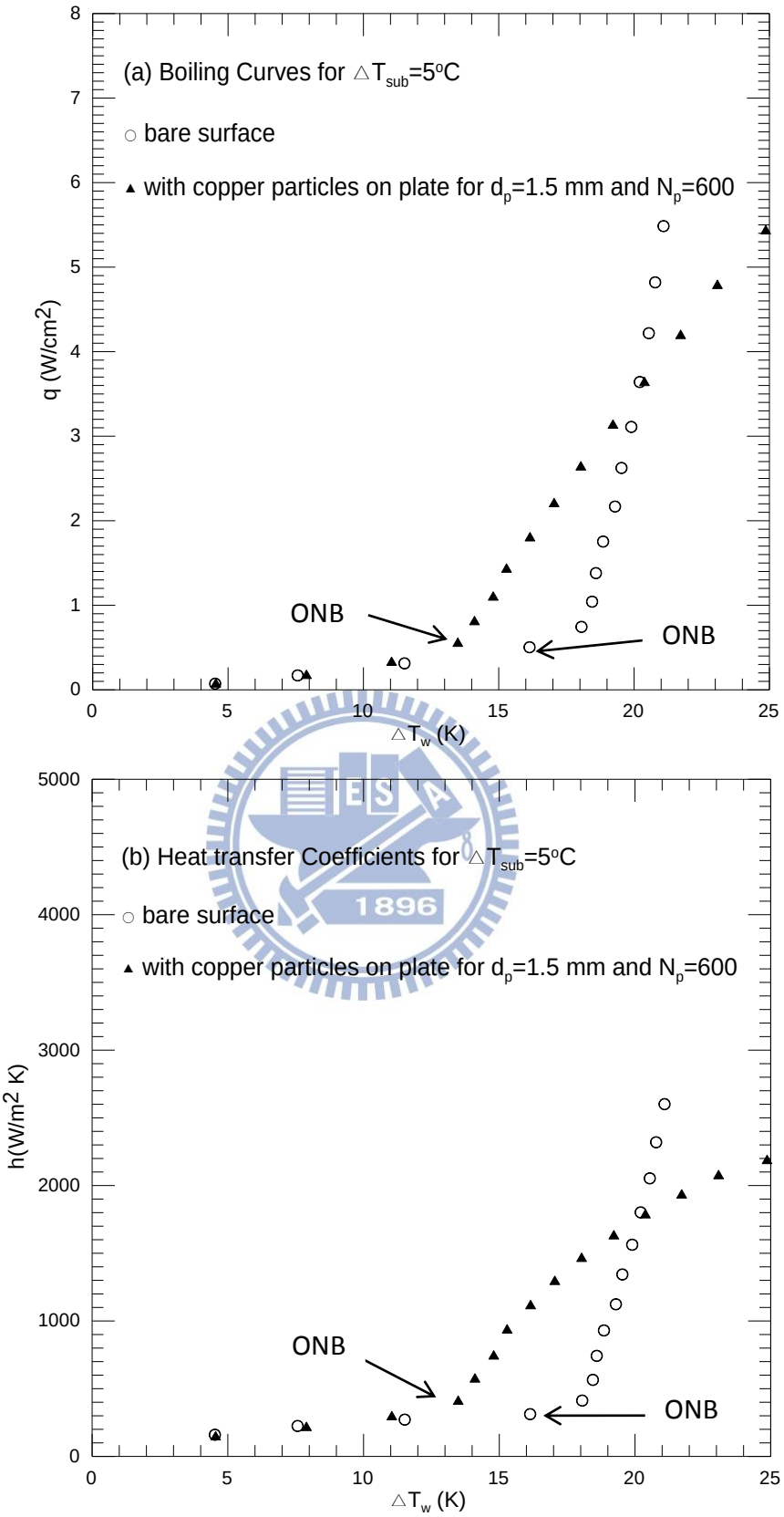

Fig. 4.40 Effects of copper particle diameter and number on subcooled pool boiling curves (a) and boiling heat transfer coefficients (b) for ΔT_{sub}= 5℃ at d_p=1.5 mm and $N_p = 600$.

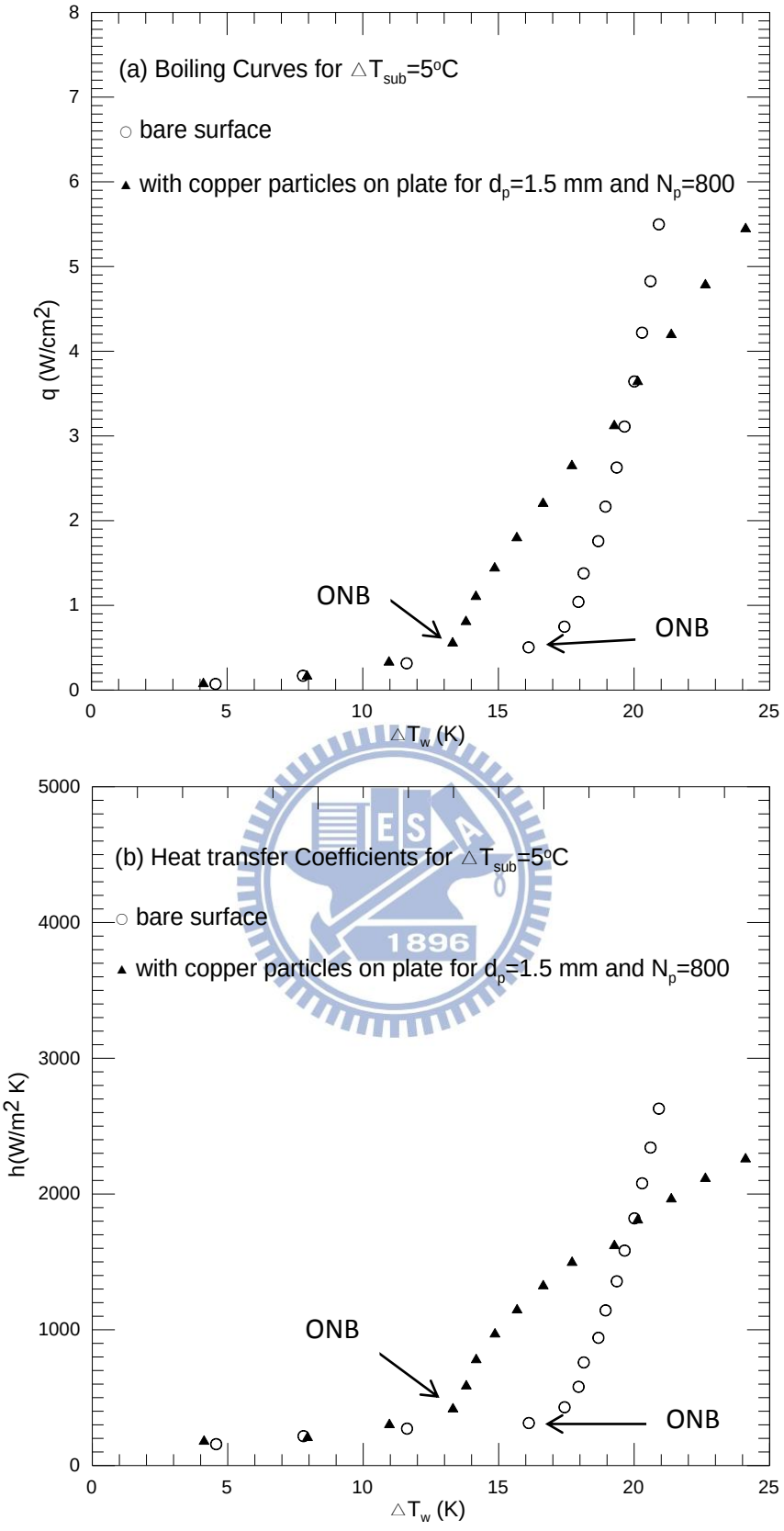

Fig. 4.41 Effects of copper particle diameter and number on subcooled pool boiling curves (a) and boiling heat transfer coefficients (b) for ΔT_{sub}= 5℃ at d_p=1.5 mm and $N_p = 800$.

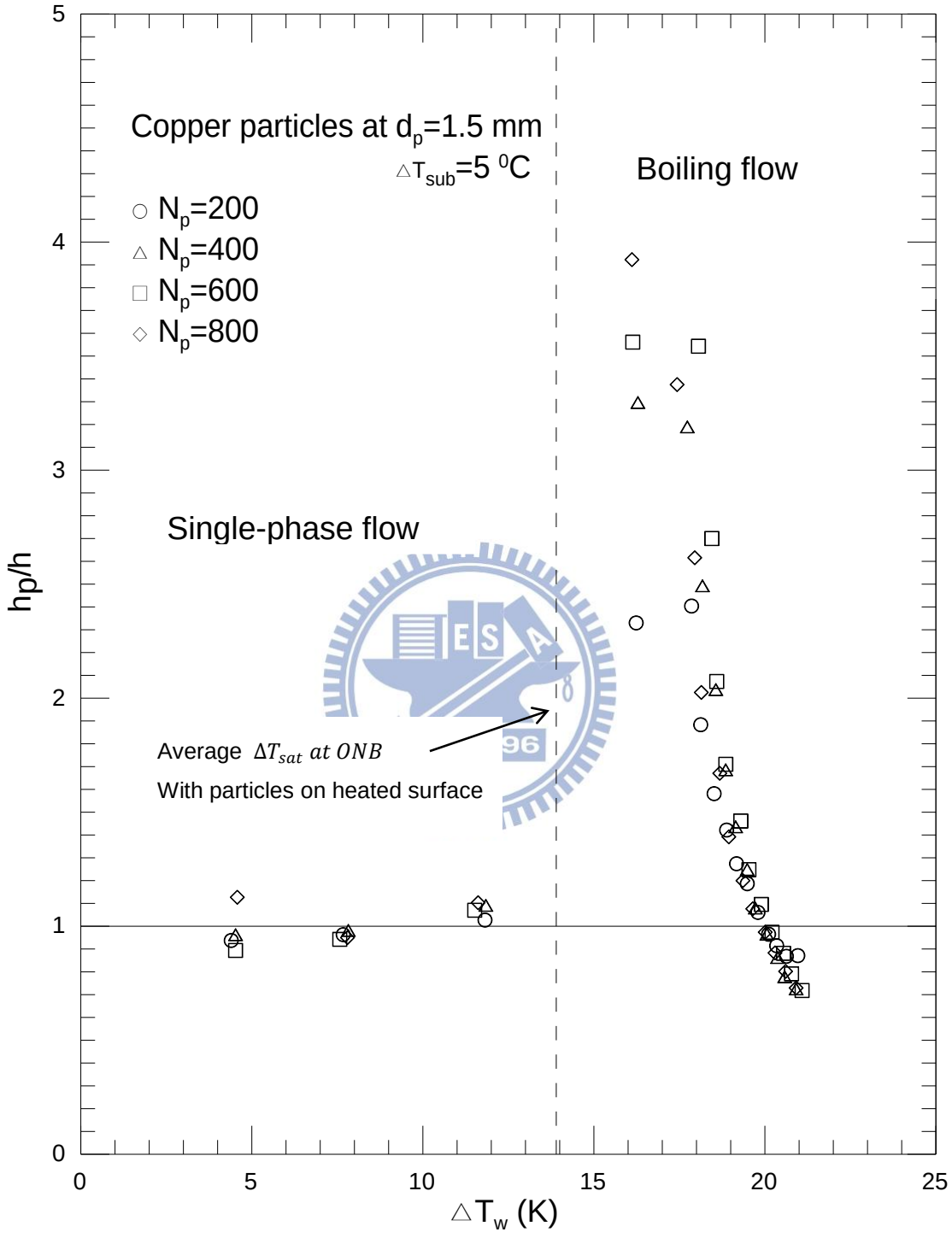

Fig. 4.42 Variations of h_p/h with wall superheat for total various copper particle numbers at d_p=1.5 mm and ΔT_{sub}=5℃.

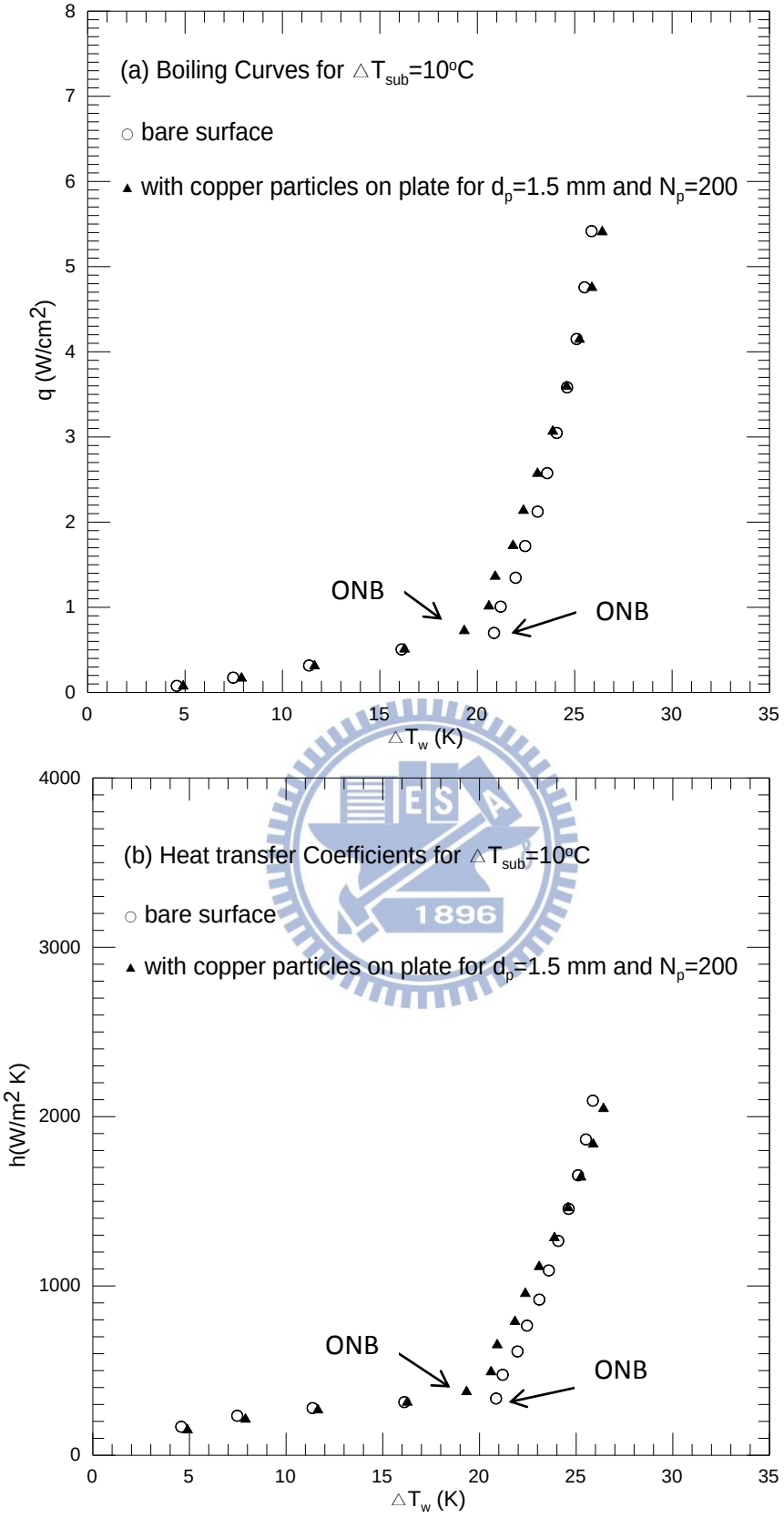

Fig. 4.43 Effects of copper particle diameter and number on subcooled pool boiling curves (a) and boiling heat transfer coefficients (b) for ΔT_{sub}= 10℃ at d_p=1.5 mm and $N_p = 200$.

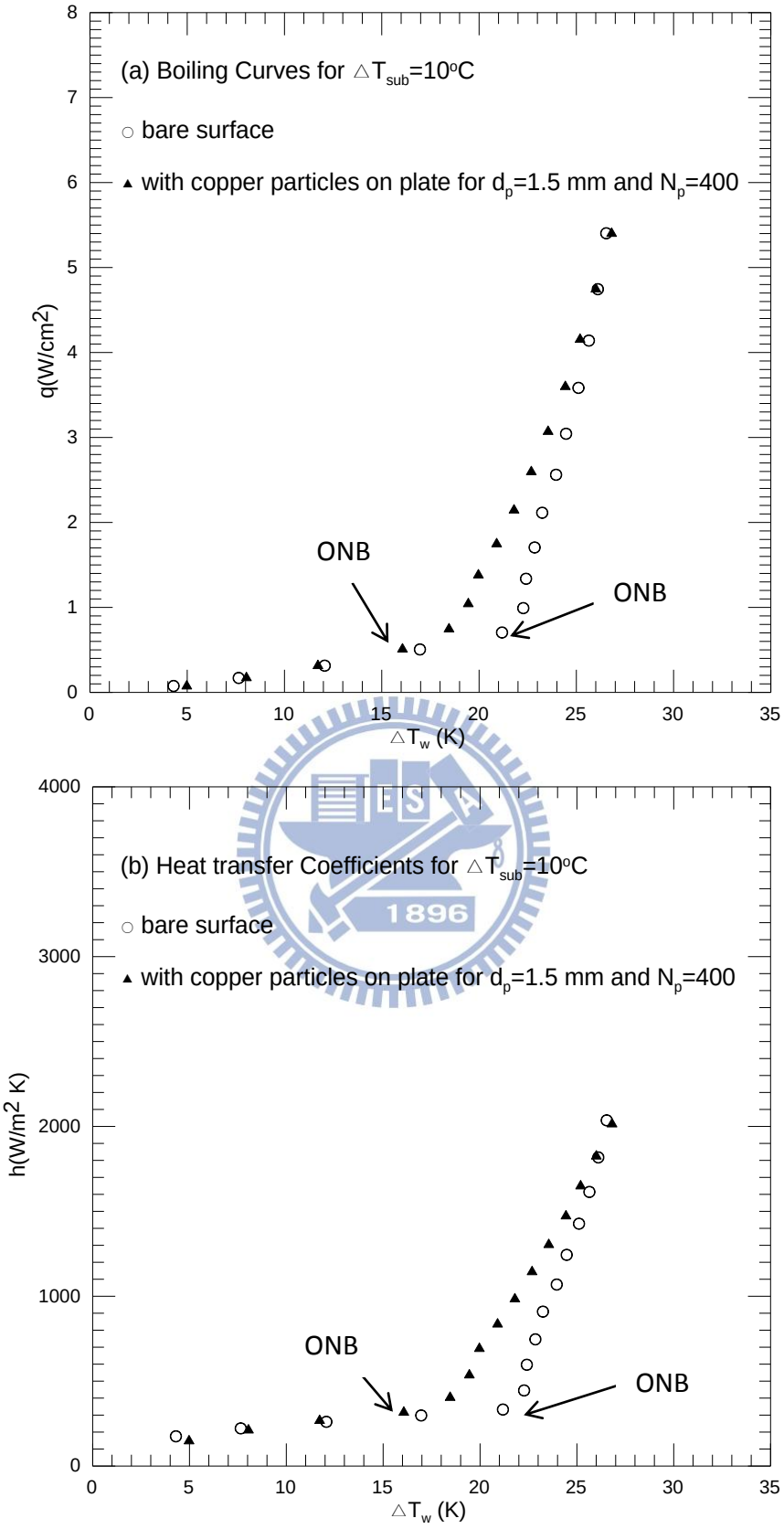

Fig. 4.44 Effects of copper particle diameter and number on subcooled pool boiling curves (a) and boiling heat transfer coefficients (b) for ΔT_{sub}= 10℃ at d_p=1.5 mm and $N_p = 400$.

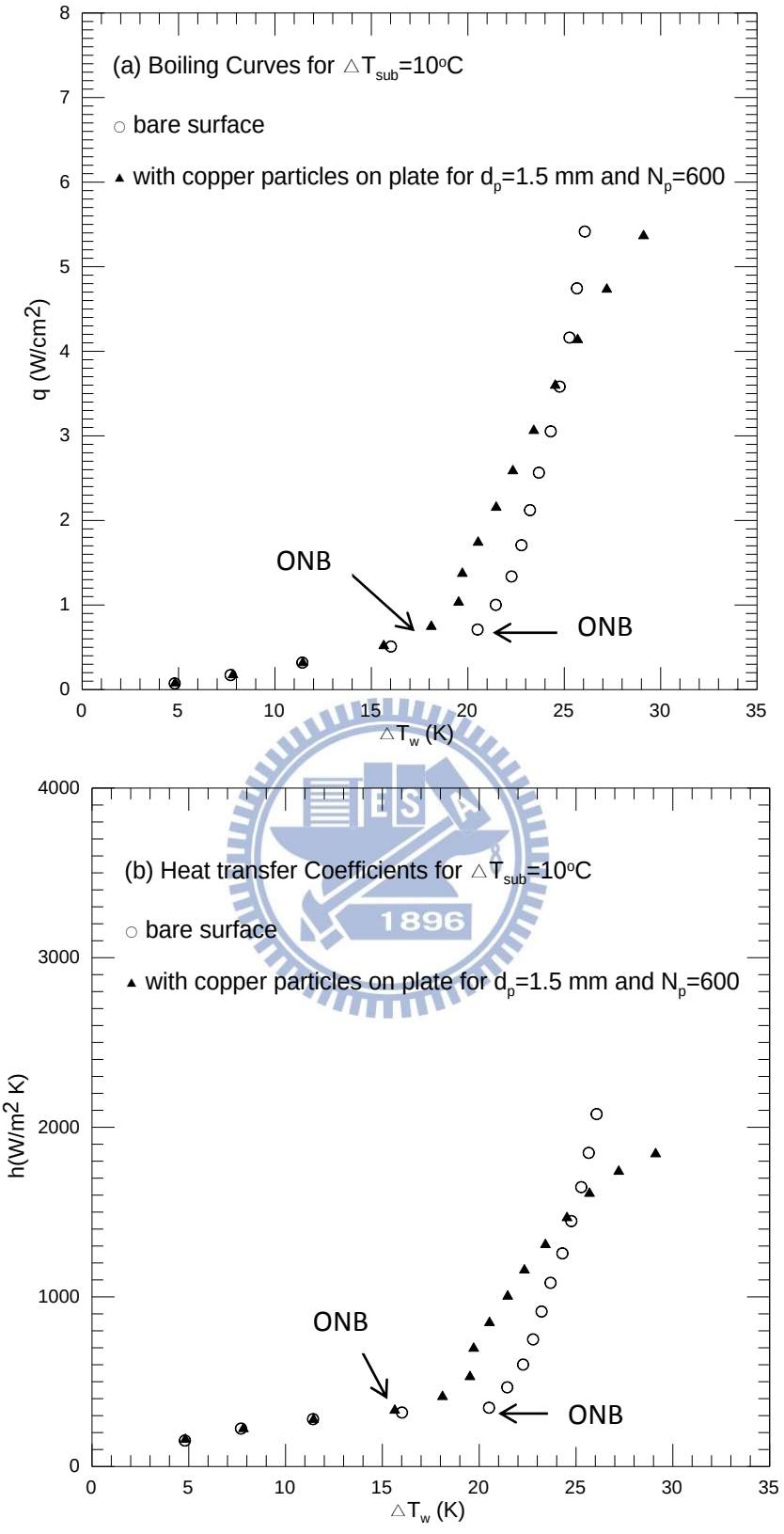

Fig. 4.45 Effects of copper particle diameter and number on subcooled pool boiling curves (a) and boiling heat transfer coefficients (b) for ΔT_{sub}= 10℃ at d_p=1.5 mm and $N_p = 600$.

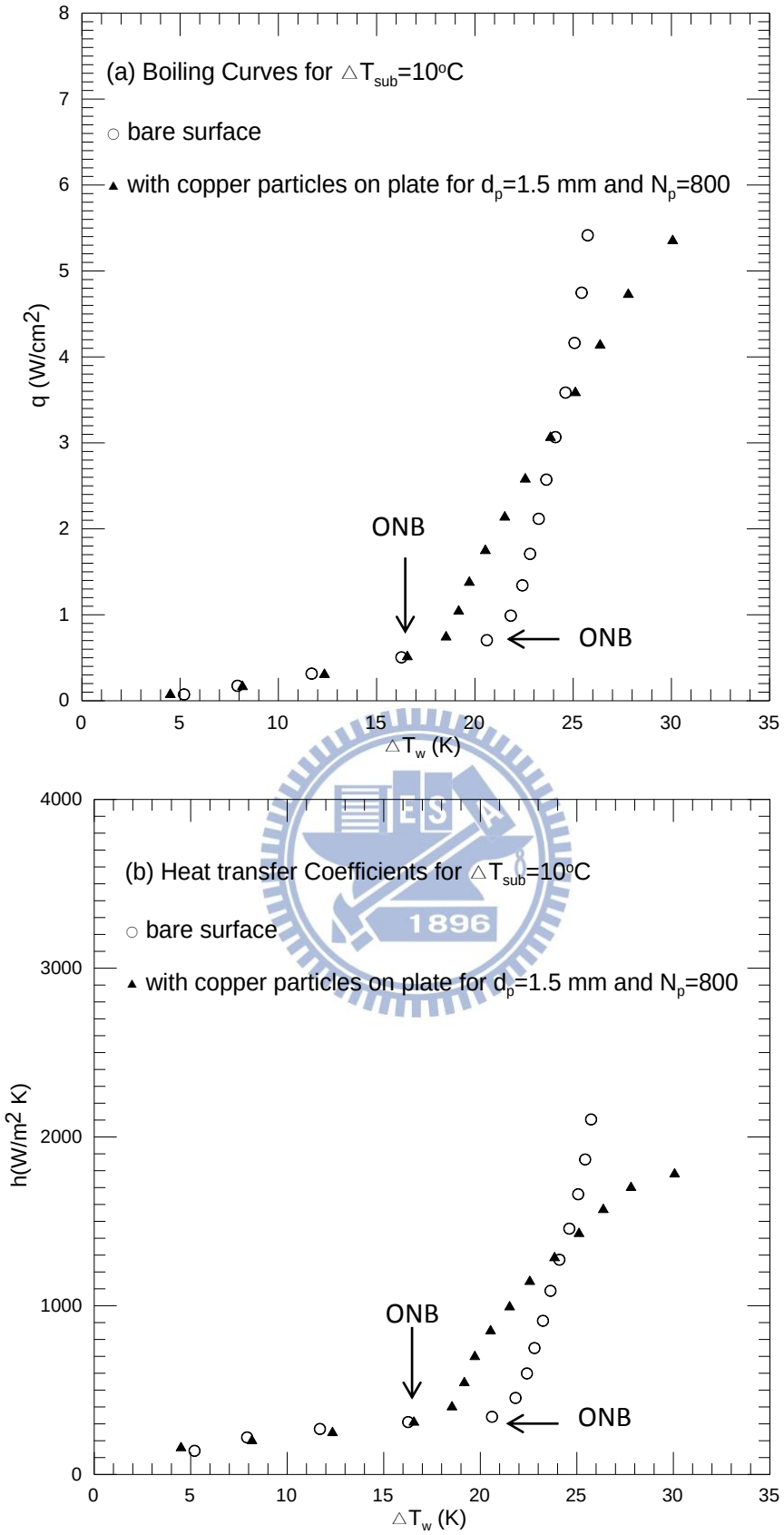

Fig. 4.46 Effects of copper particle diameter and number on subcooled pool boiling curves (a) and boiling heat transfer coefficients (b) for ΔT_{sub}= 10℃ at d_p=1.5 mm and $N_p = 800$.

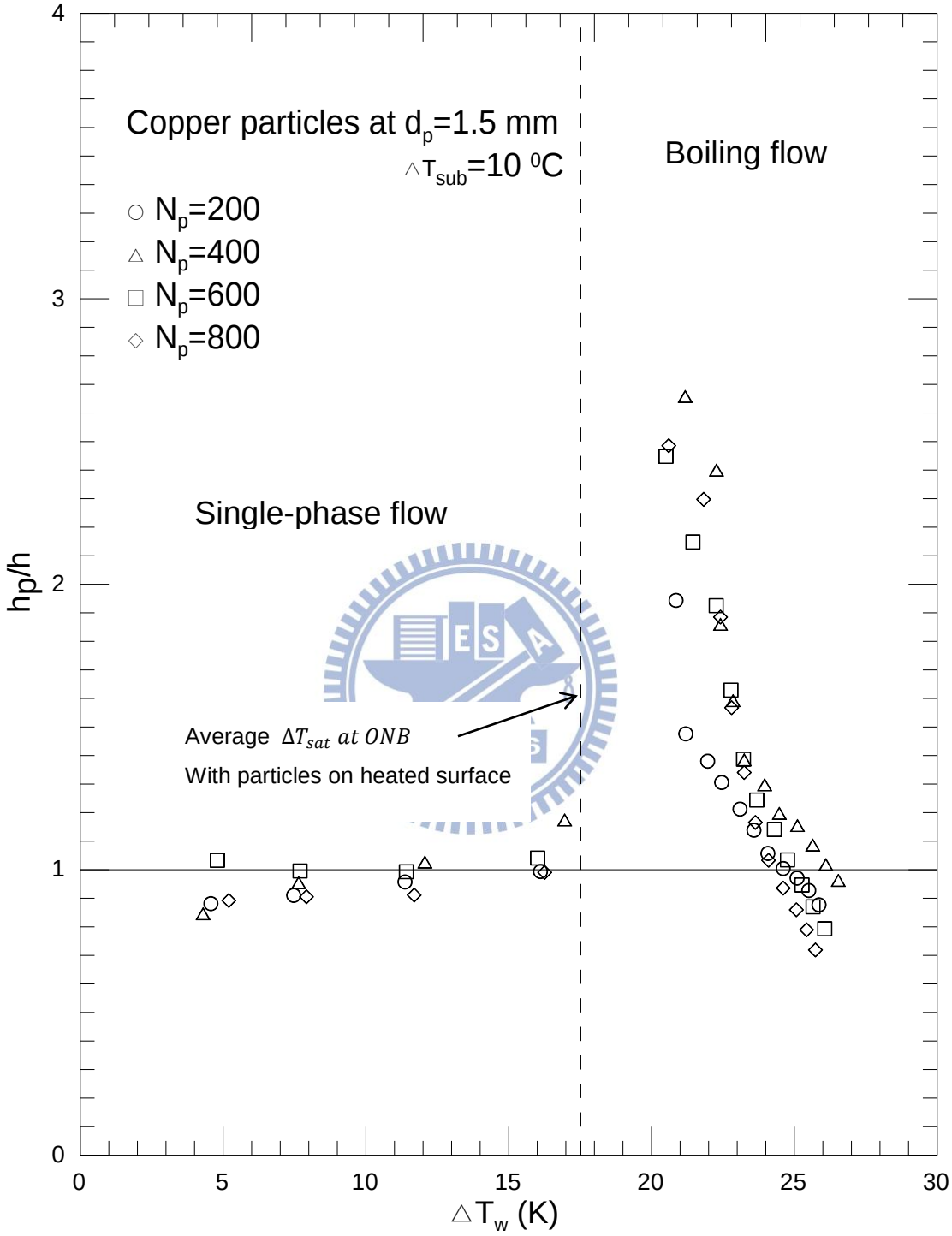

Fig. 4.47 Variations of h_p/h with wall superheat for various total copper particle numbers at d_p=1.5 mm and ΔT_{sub}=10℃.

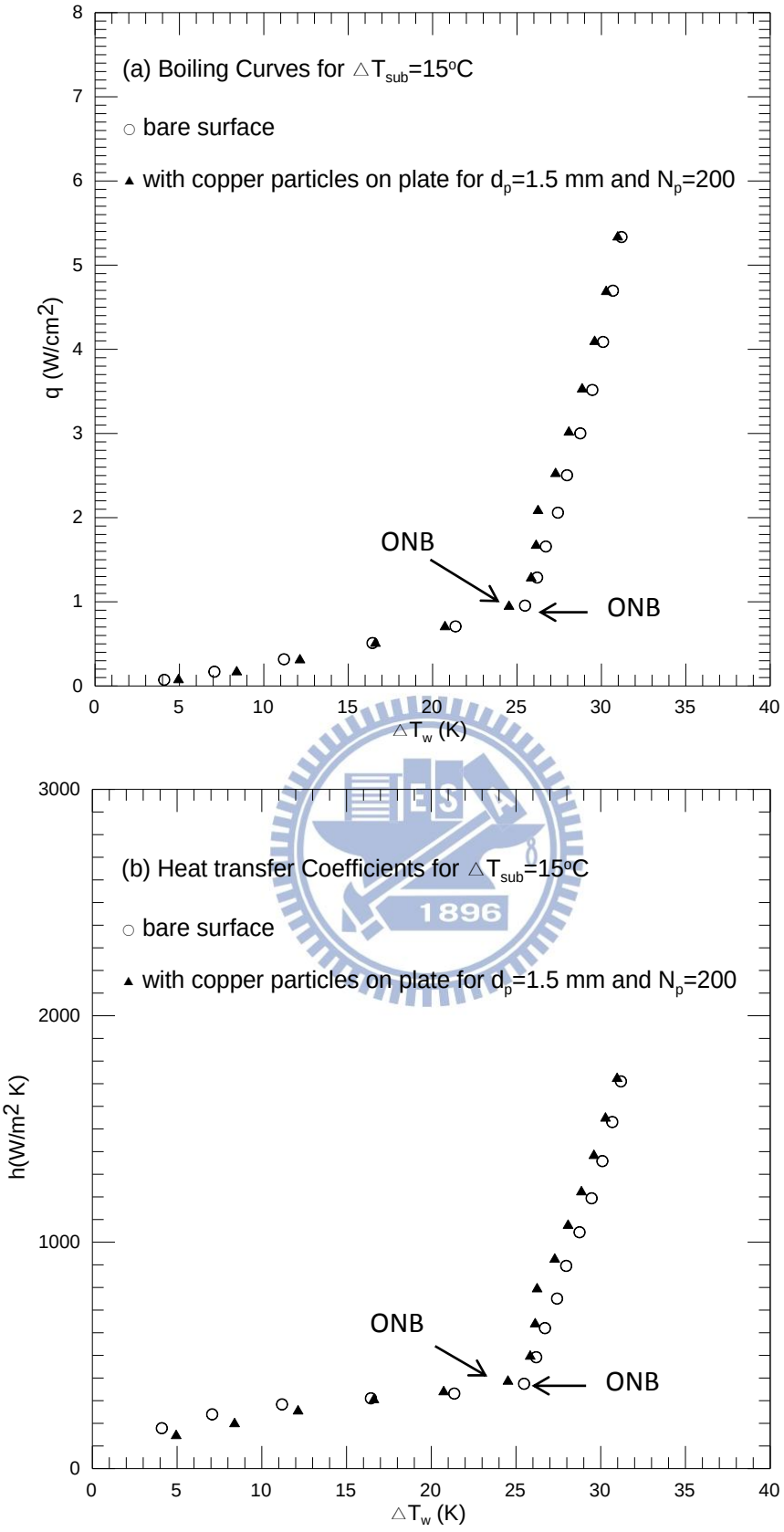

Fig. 4.48 Effects of copper particle diameter and number on subcooled pool boiling curves (a) and boiling heat transfer coefficients (b) for ΔT_{sub}= 15℃ at d_p=1.5 mm and $N_p = 200$.

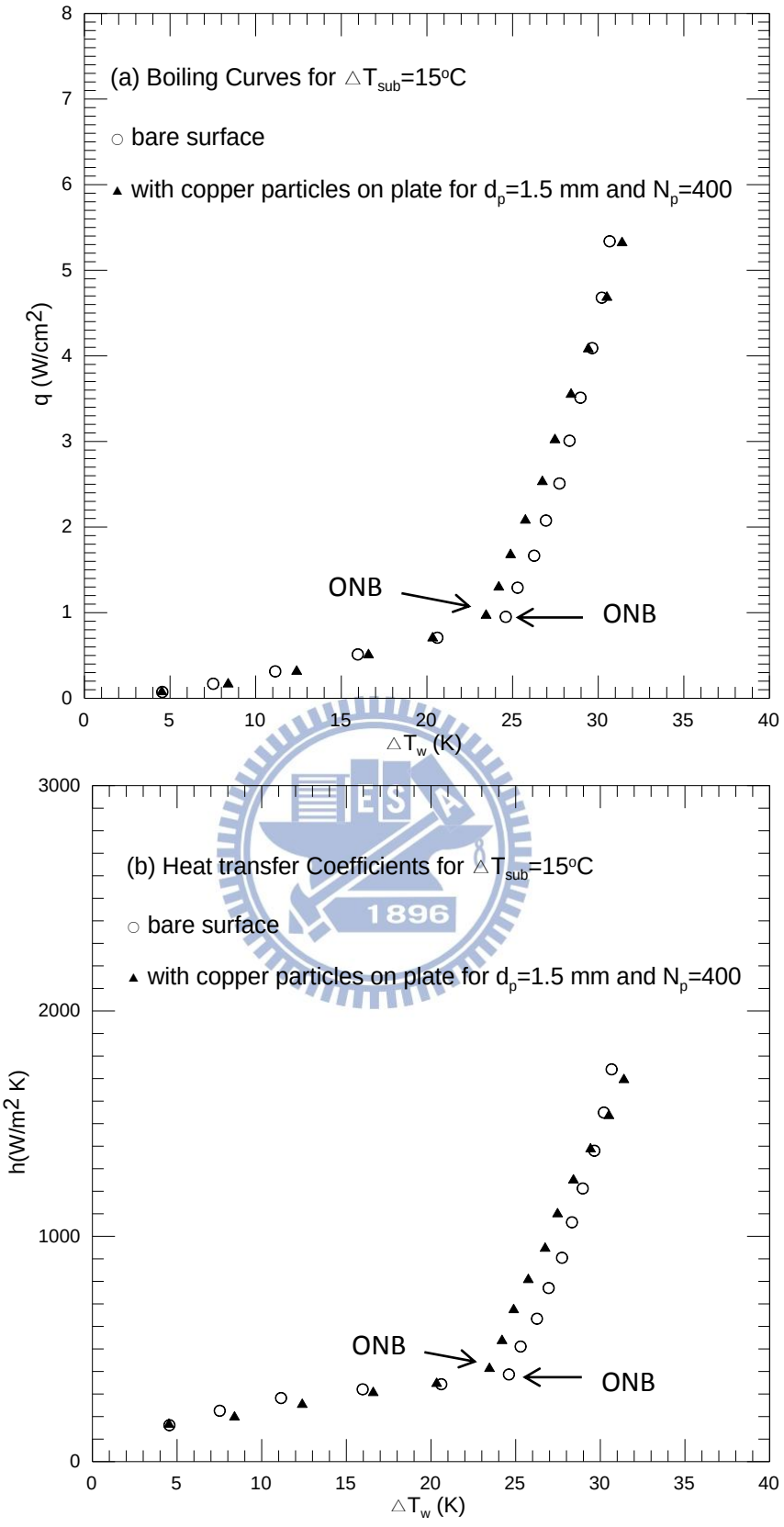

Fig. 4.49 Effects of copper particle diameter and number on subcooled pool boiling curves (a) and boiling heat transfer coefficients (b) for ΔT_{sub}= 15℃ at d_p=1.5 mm and $N_p = 400$.

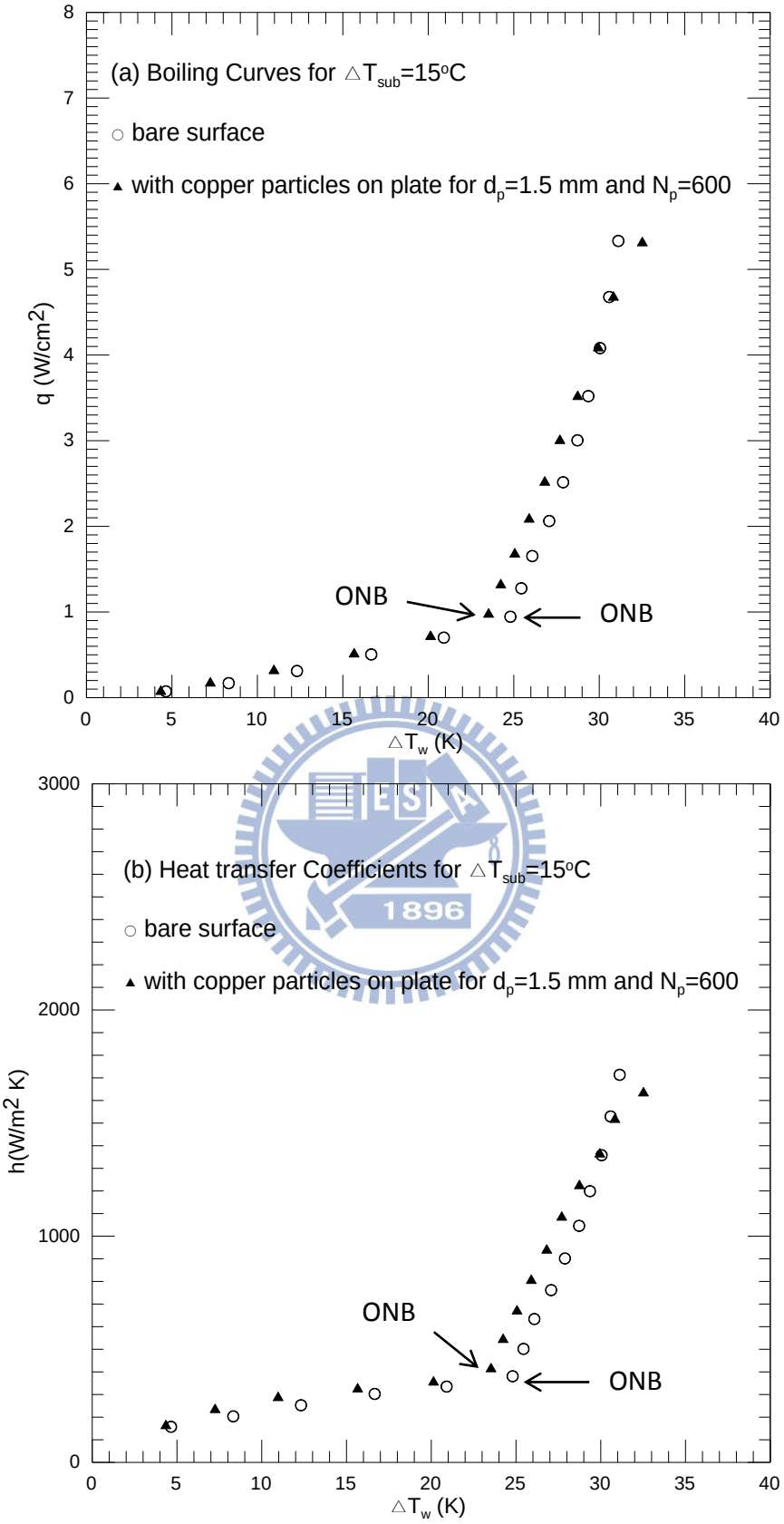

Fig. 4.50 Effects of copper particle diameter and number on subcooled pool boiling curves (a) and boiling heat transfer coefficients (b) for ΔT_{sub}= 15℃ at d_p=1.5 mm and $N_p = 600$.

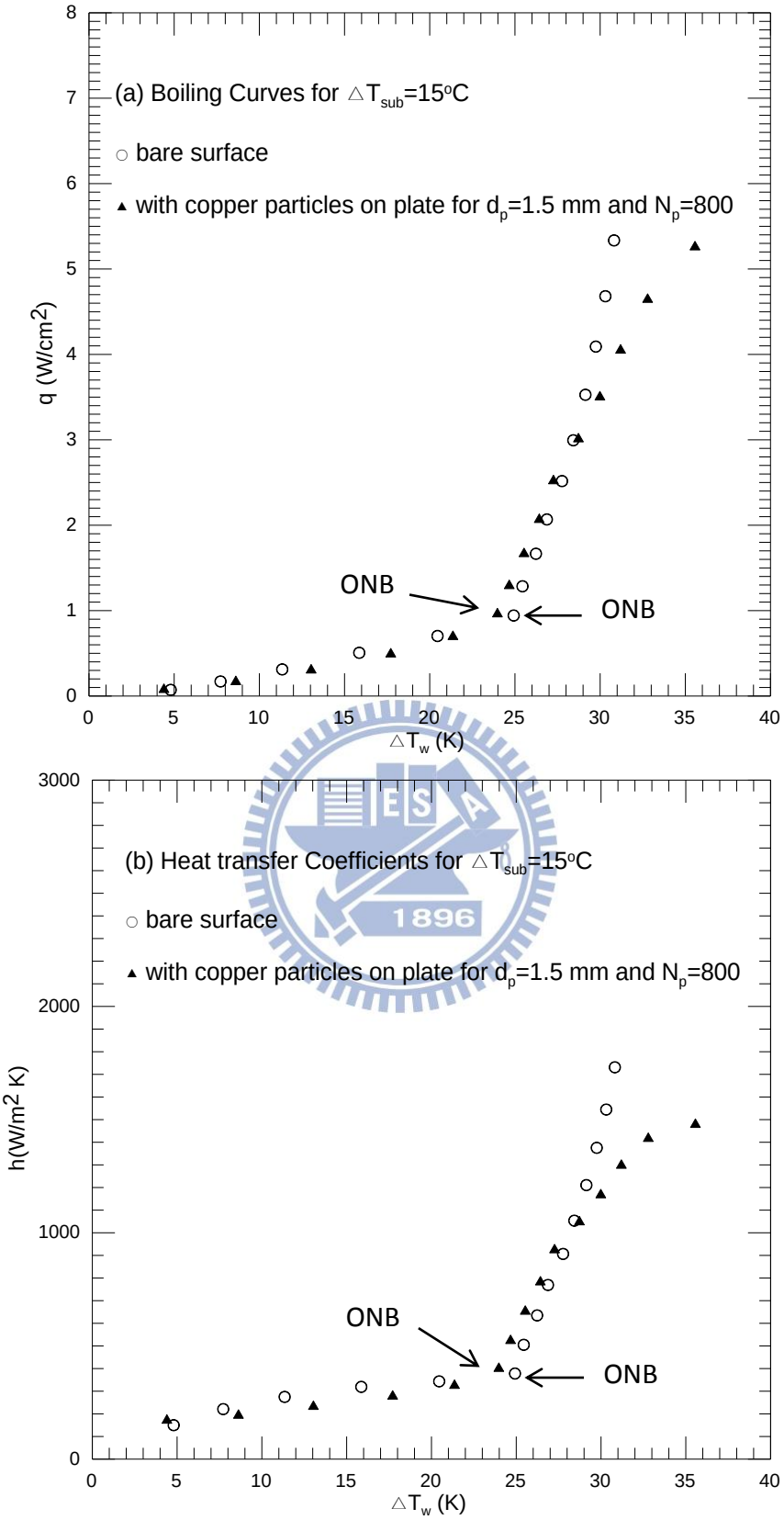

Fig. 4.51 Effects of copper particle diameter and number on subcooled pool boiling curves (a) and boiling heat transfer coefficients (b) for ΔT_{sub}= 15℃ at d_p=1.5 mm and $N_p = 800$.

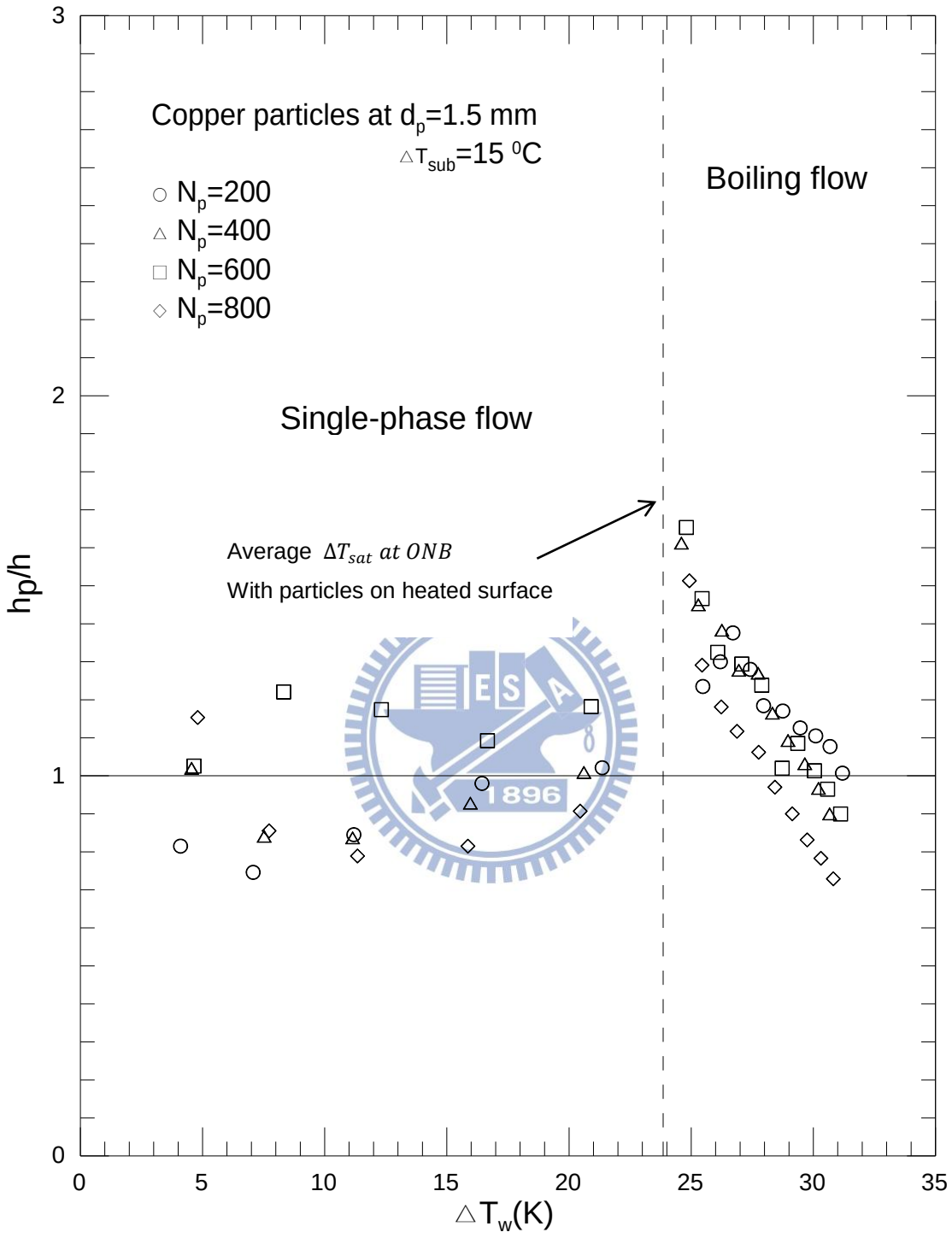

Fig. 4.52 Variations of h_p/h with wall superheat for various total copper particle numbers at d_p=1.5 mm and ΔT_{sub}=15℃.

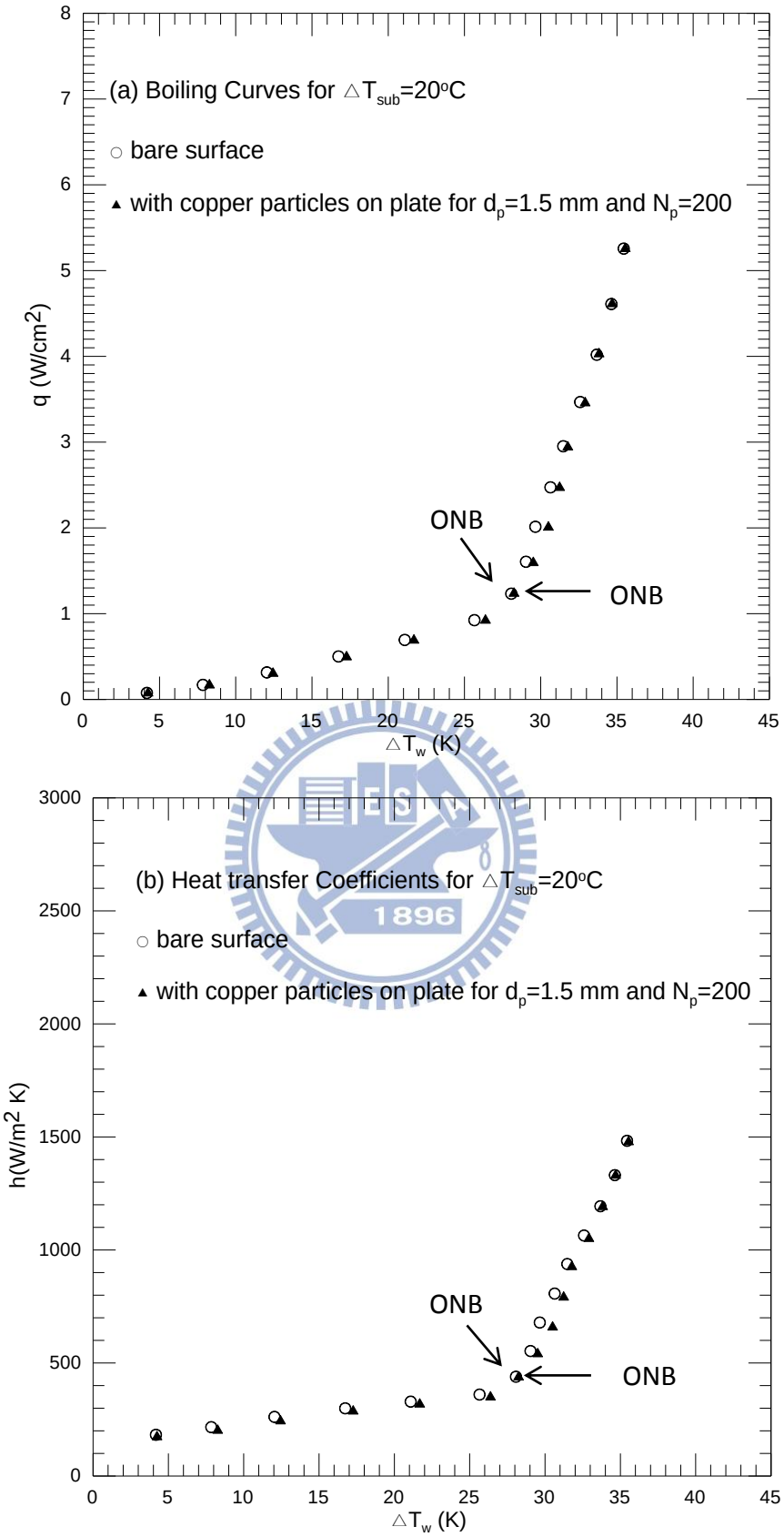

Fig. 4.53 Effects of copper particle diameter and number on subcooled pool boiling curves (a) and boiling heat transfer coefficients (b) for ΔT_{sub}= 20℃ at d_p=1.5 mm and $N_p = 200$.

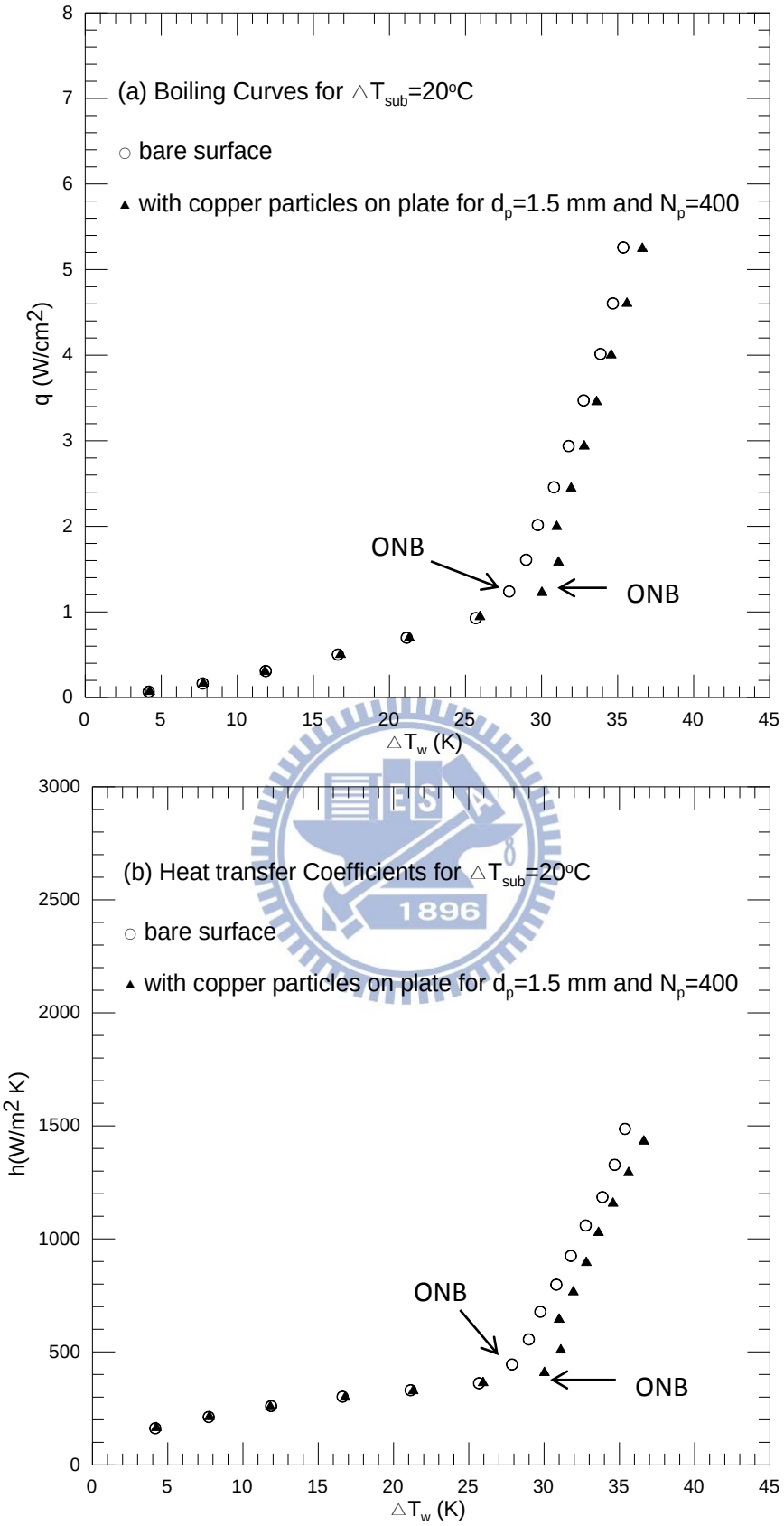

Fig. 4.54 Effects of copper particle diameter and number on subcooled pool boiling curves (a) and boiling heat transfer coefficients (b) for ΔT_{sub}= 20℃ at d_p=1.5 mm and $N_p = 400$.

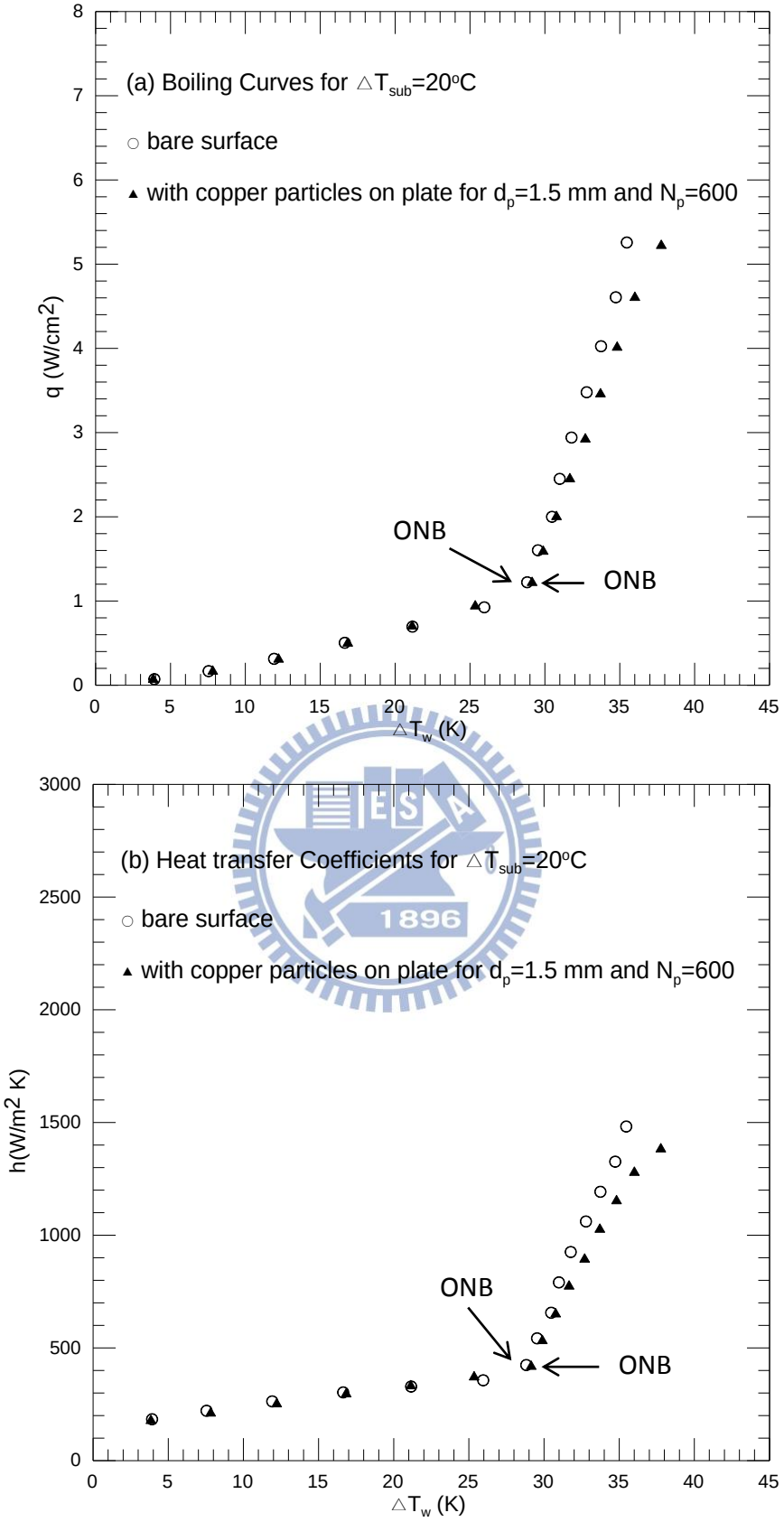

Fig. 4.55 Effects of copper particle diameter and number on subcooled pool boiling curves (a) and boiling heat transfer coefficients (b) for ΔT_{sub}= 20℃ at d_p=1.5 mm and $N_p = 600$.

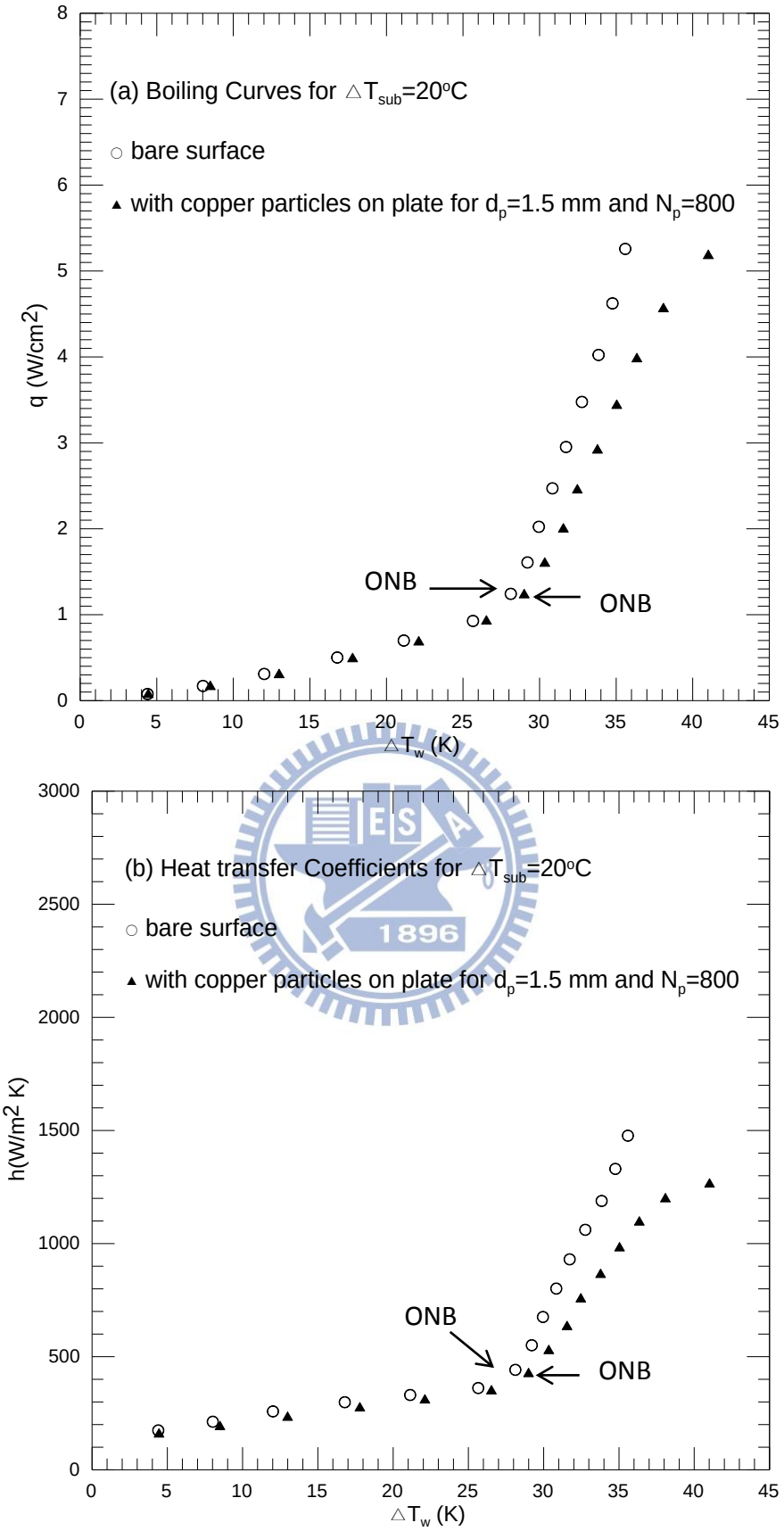

Fig. 4.56 Effects of copper particle diameter and number on subcooled pool boiling curves (a) and boiling heat transfer coefficients (b) for ΔT_{sub}= 20℃ at d_p=1.5 mm and $N_p = 800$.

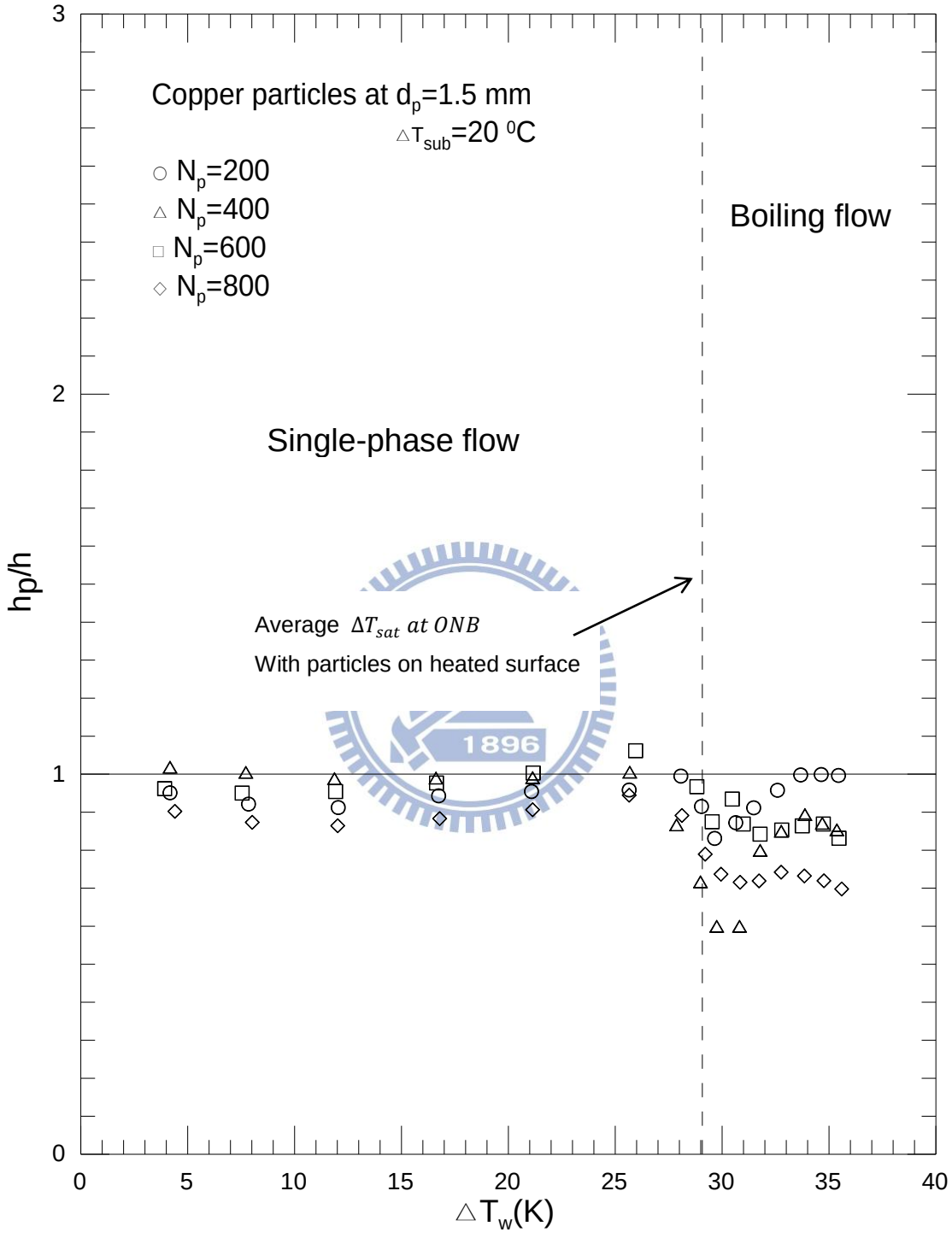

Fig. 4.57 Variations of h_p/h with wall superheat for various total copper particle numbers at d_p=1.0 mm and ΔT_{sub}=20°C.

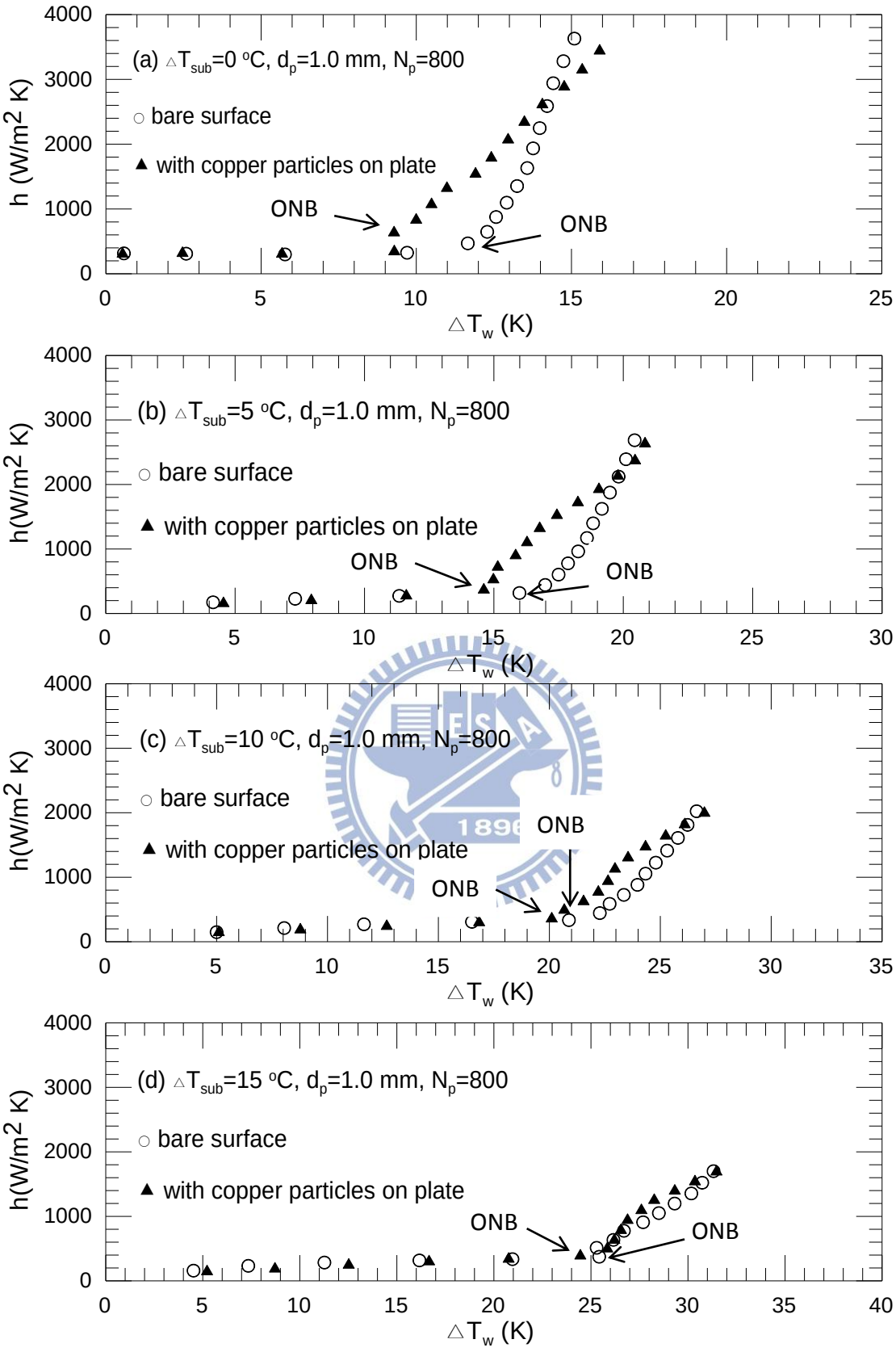

Fig. 4.58 Variations of h with wall superheat for various liquid subcoolings at d_p=1.0 mm and N_p=800.

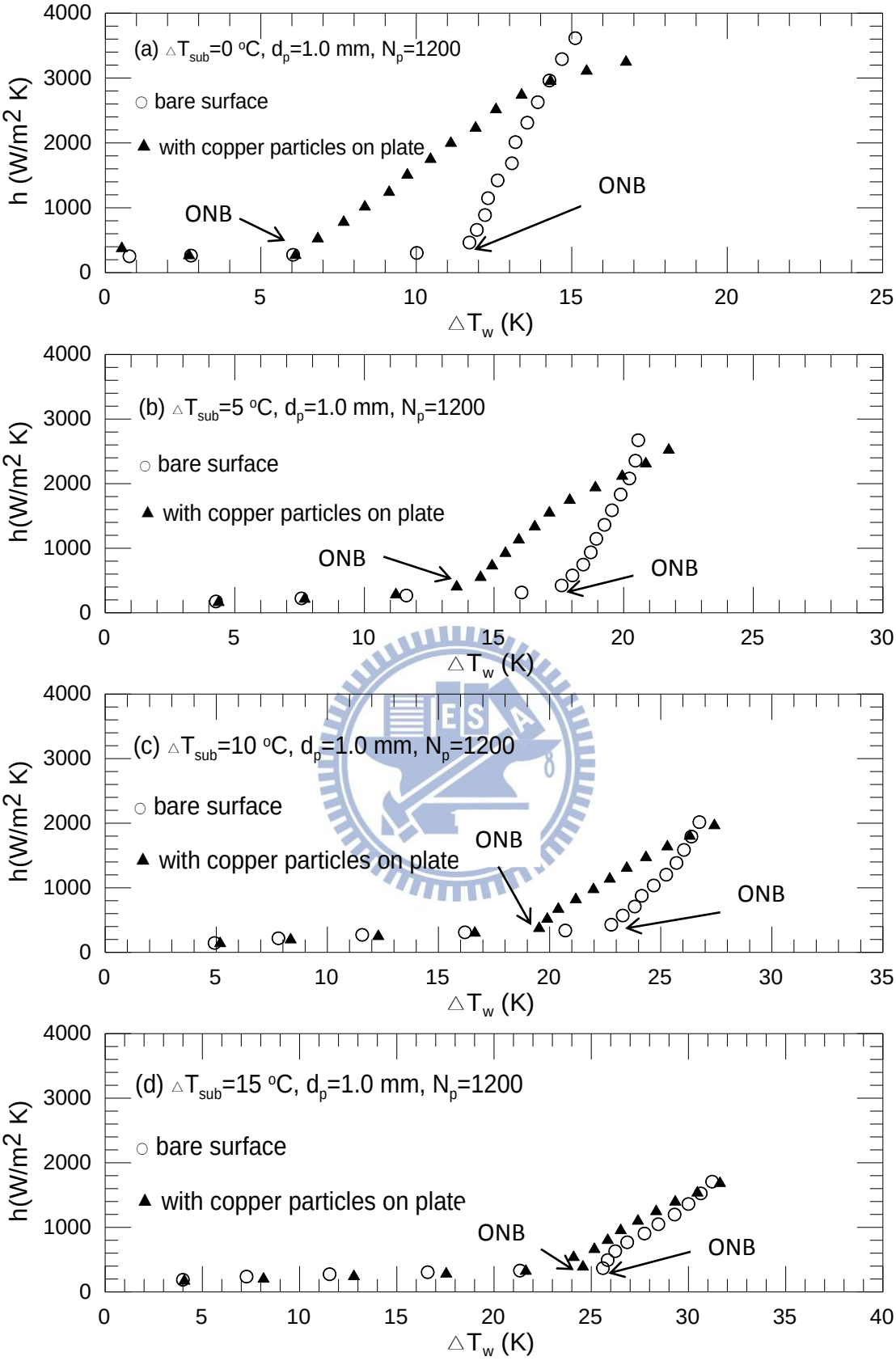

Fig. 4.59 Variations of h with wall superheat for various liquid subcoolings at d_p=1.0 mm and N_p=1200.

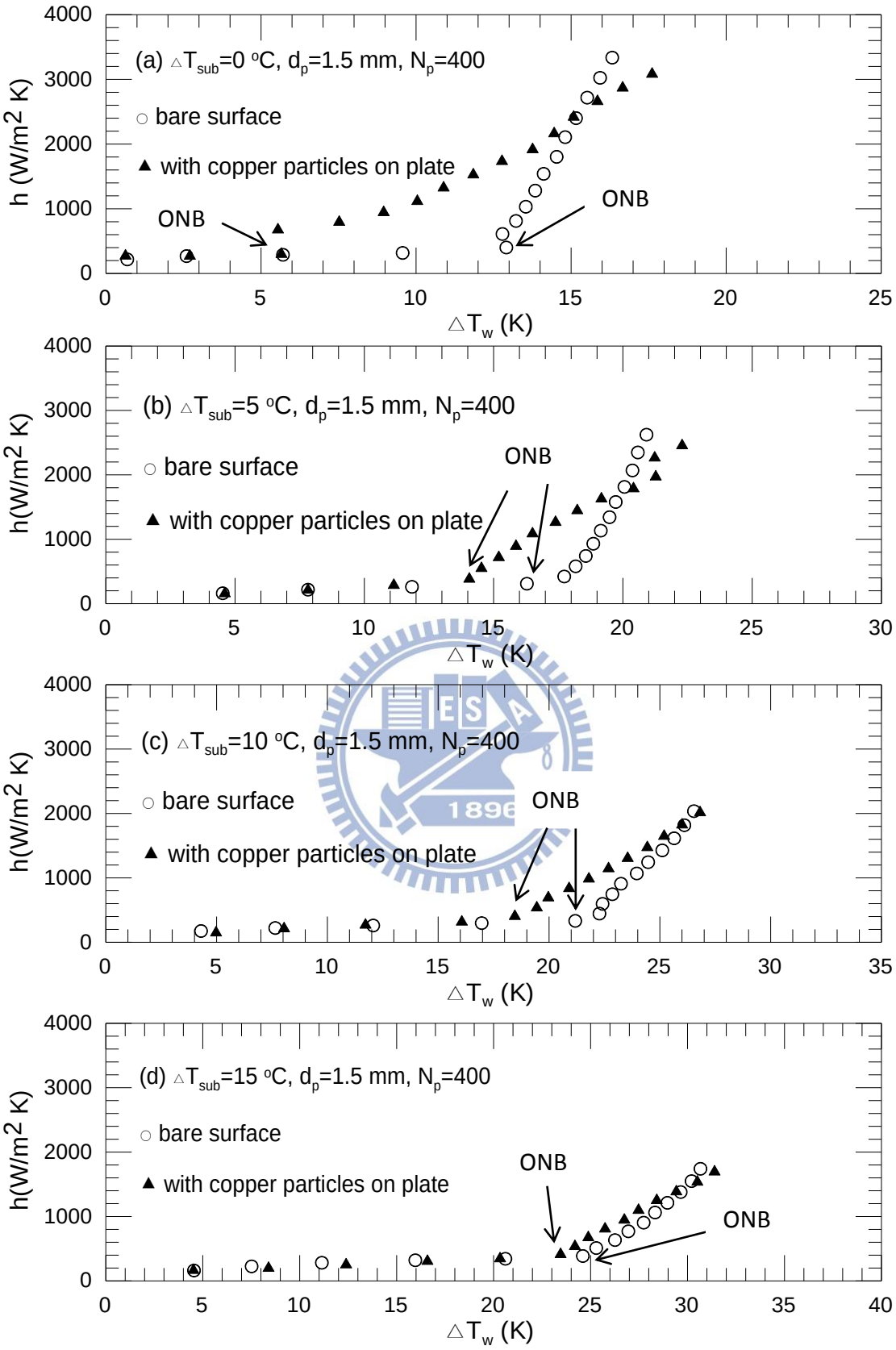

Fig. 4.60 Variations of h with wall superheat for various liquid subcoolings at d_p=1.5 mm and N_p=400.

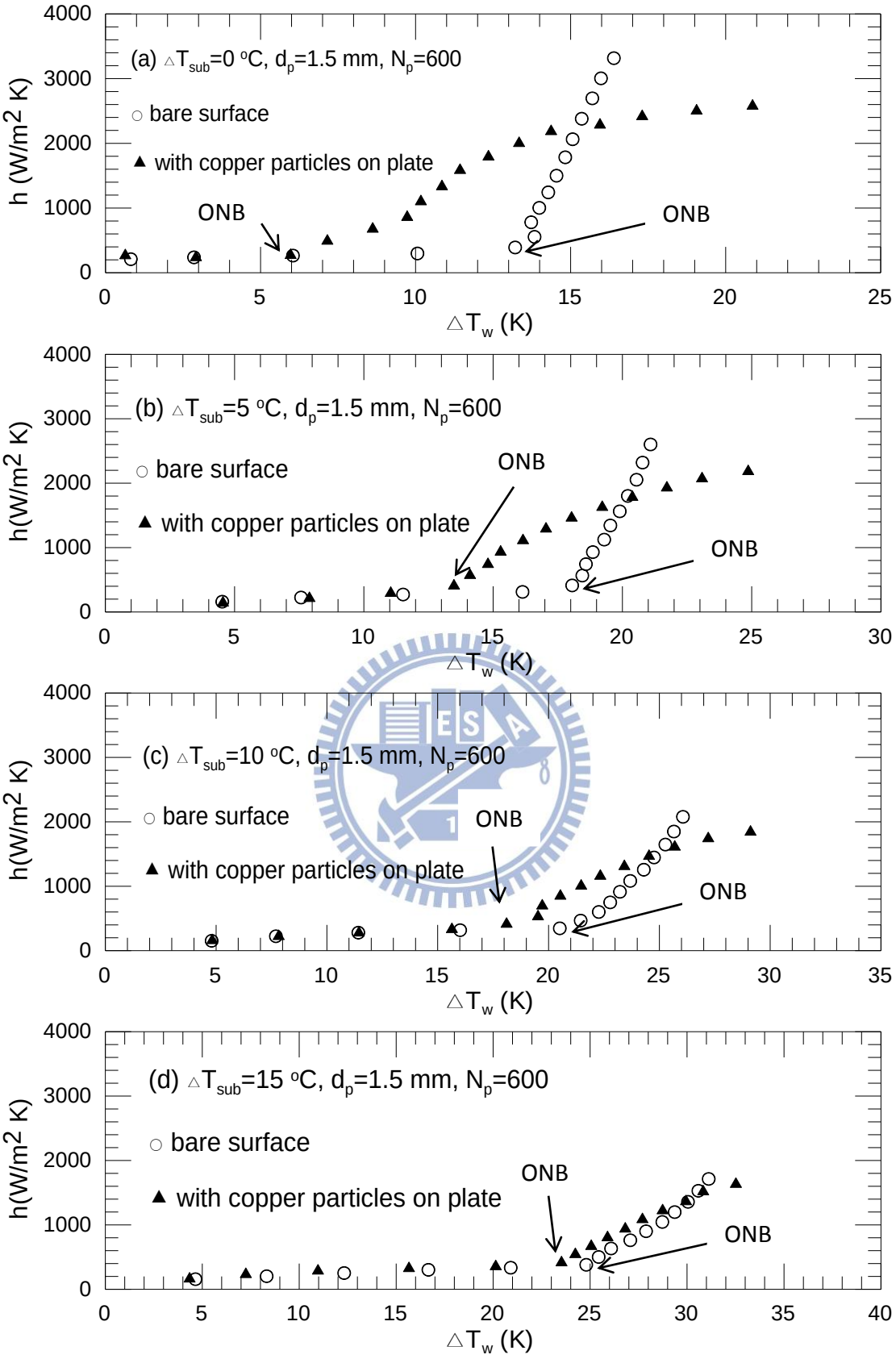

Fig. 4.61 Variations of h with wall superheat for various liquid subcoolings at d_p=1.5 mm and N_p=600.

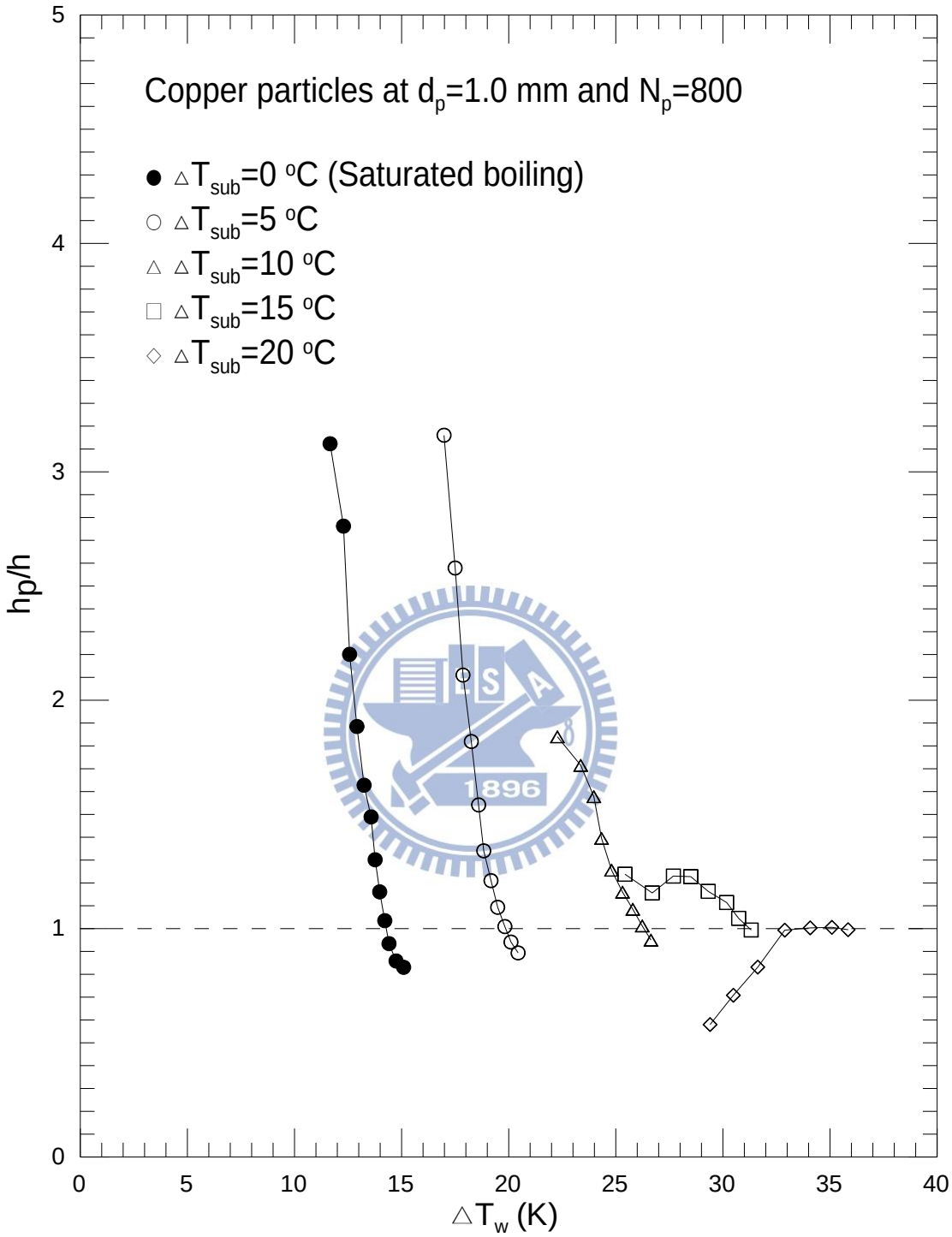

Fig. 4.62 Variations of h_p/h with wall superheat for various liquid subcoolings at d_p=1.0 mm and N_p=800.

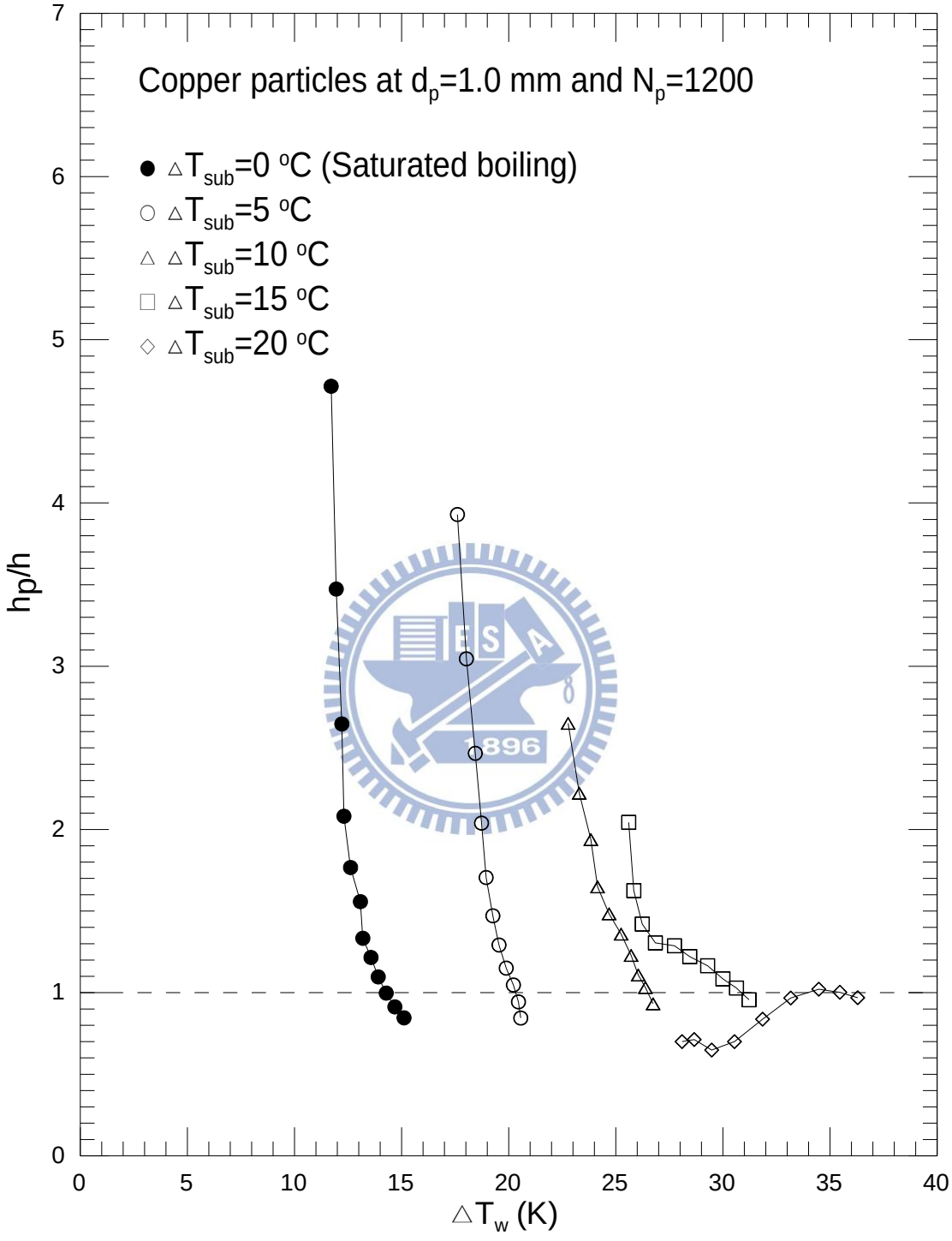

Fig. 4.63 Variations of h_p/h with wall superheat for various liquid subcoolings at d_p=1.0 mm and N_p=1200.

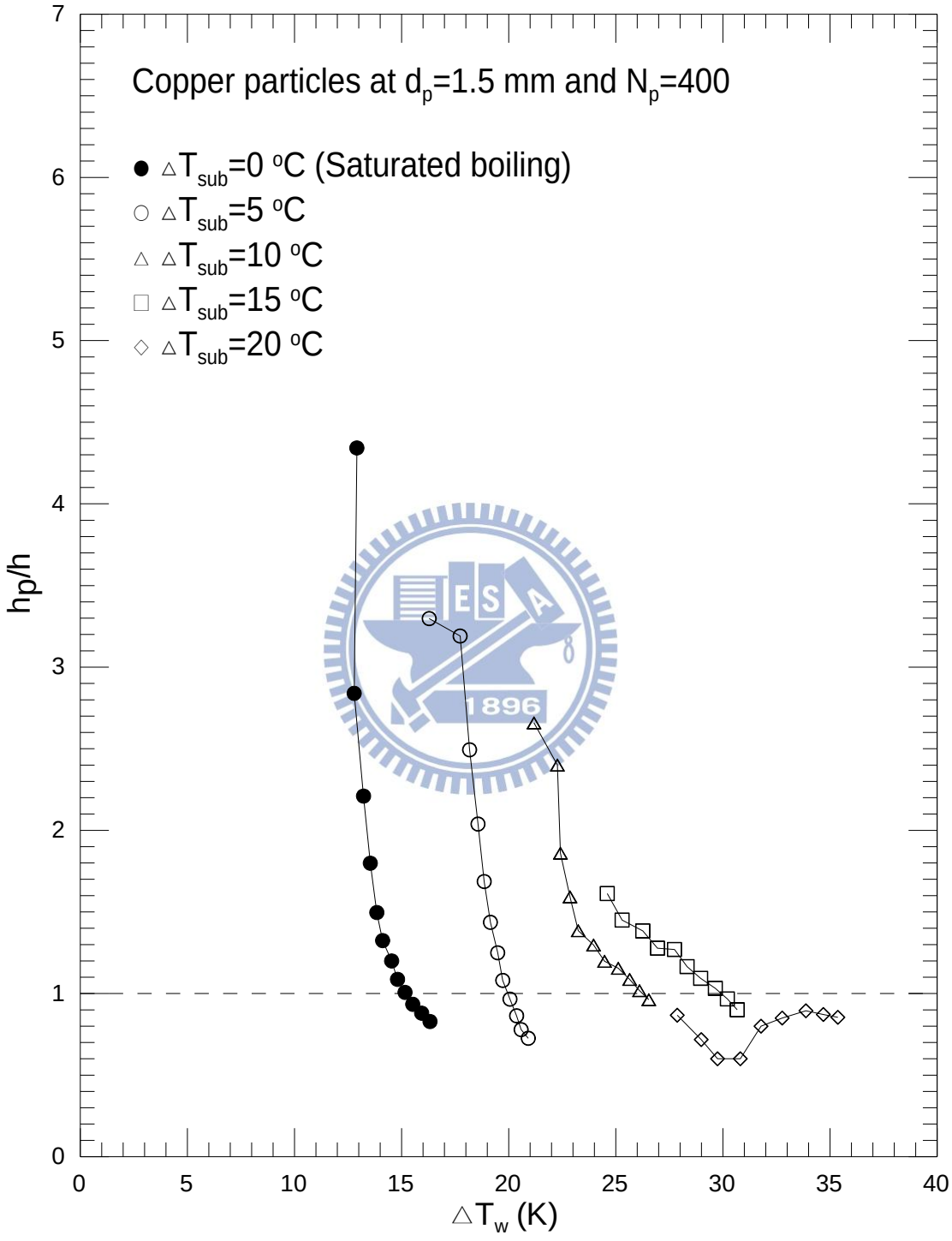

Fig. 4.64 Variations of h_p/h with wall superheat for various liquid subcoolings at d_p=1.5 mm and N_p=400.

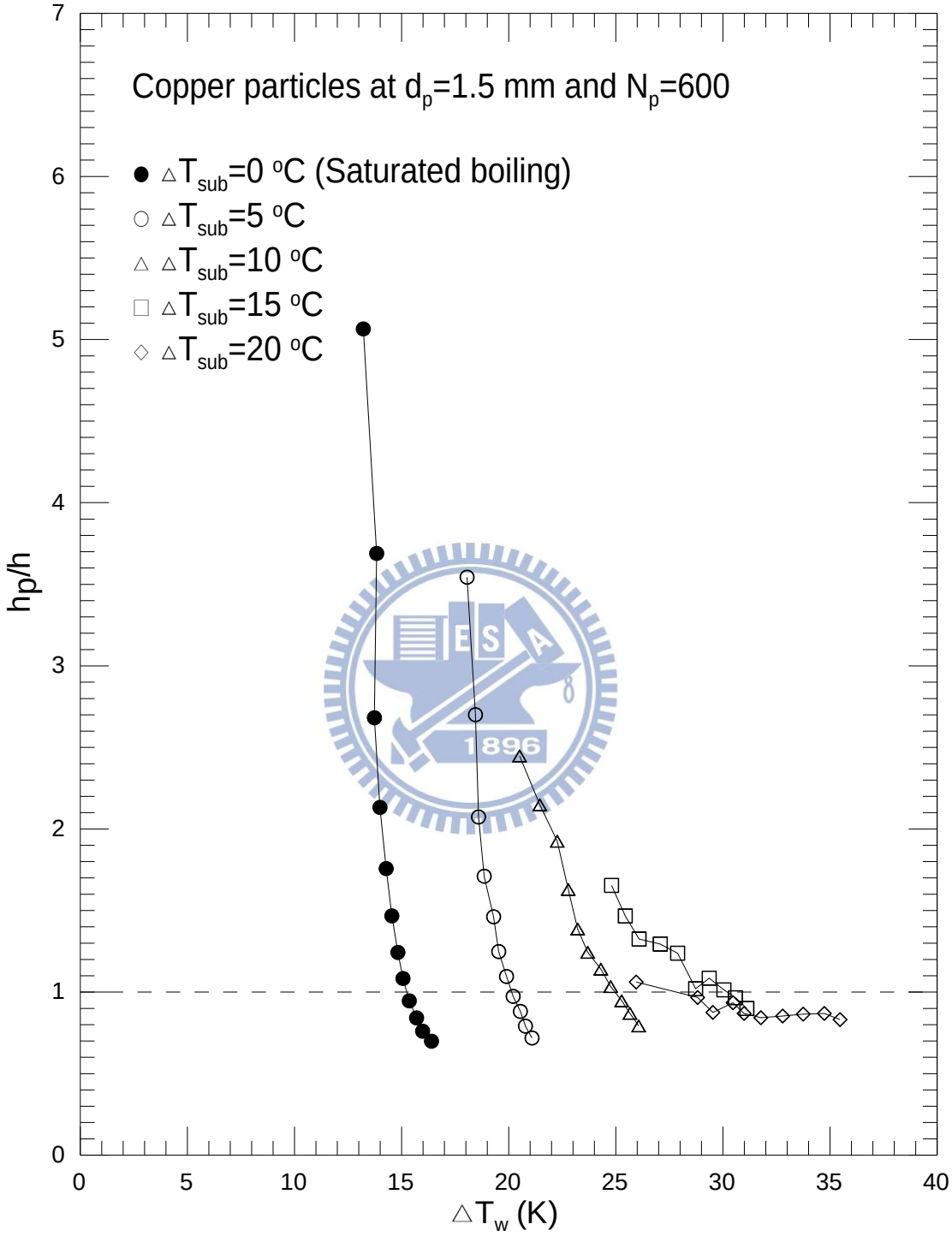

Fig. 4.65 Variations of h_p/h with wall superheat for various liquid subcoolings at d_p=1.5 mm and N_p=600.

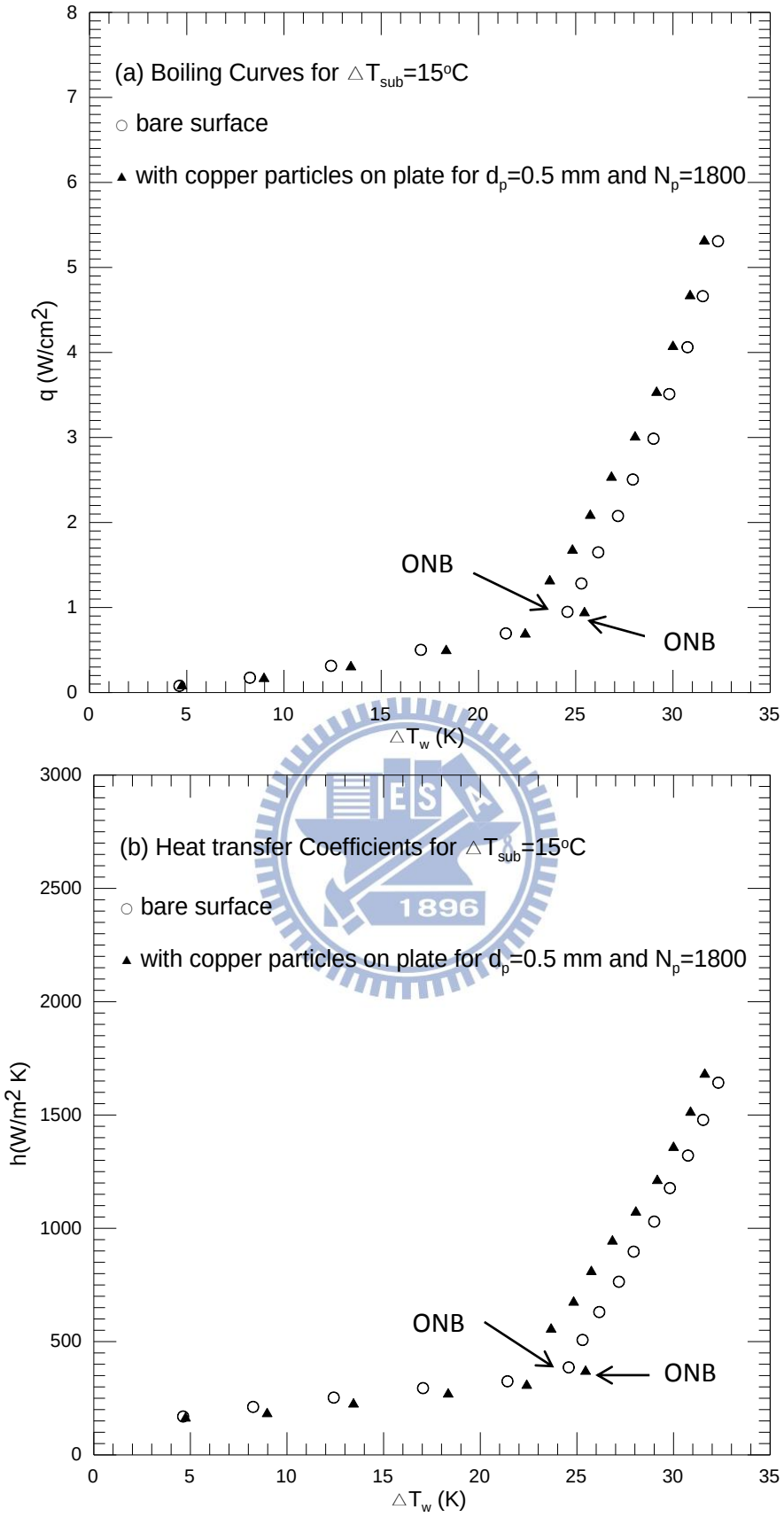

Fig. 4.66 Effects of copper particle diameter and number on subcooled pool boiling curves (a) and boiling heat transfer coefficients (b) for ΔT_{sub}= 15℃ at d_p=0.5 mm and $N_p = 1800$.

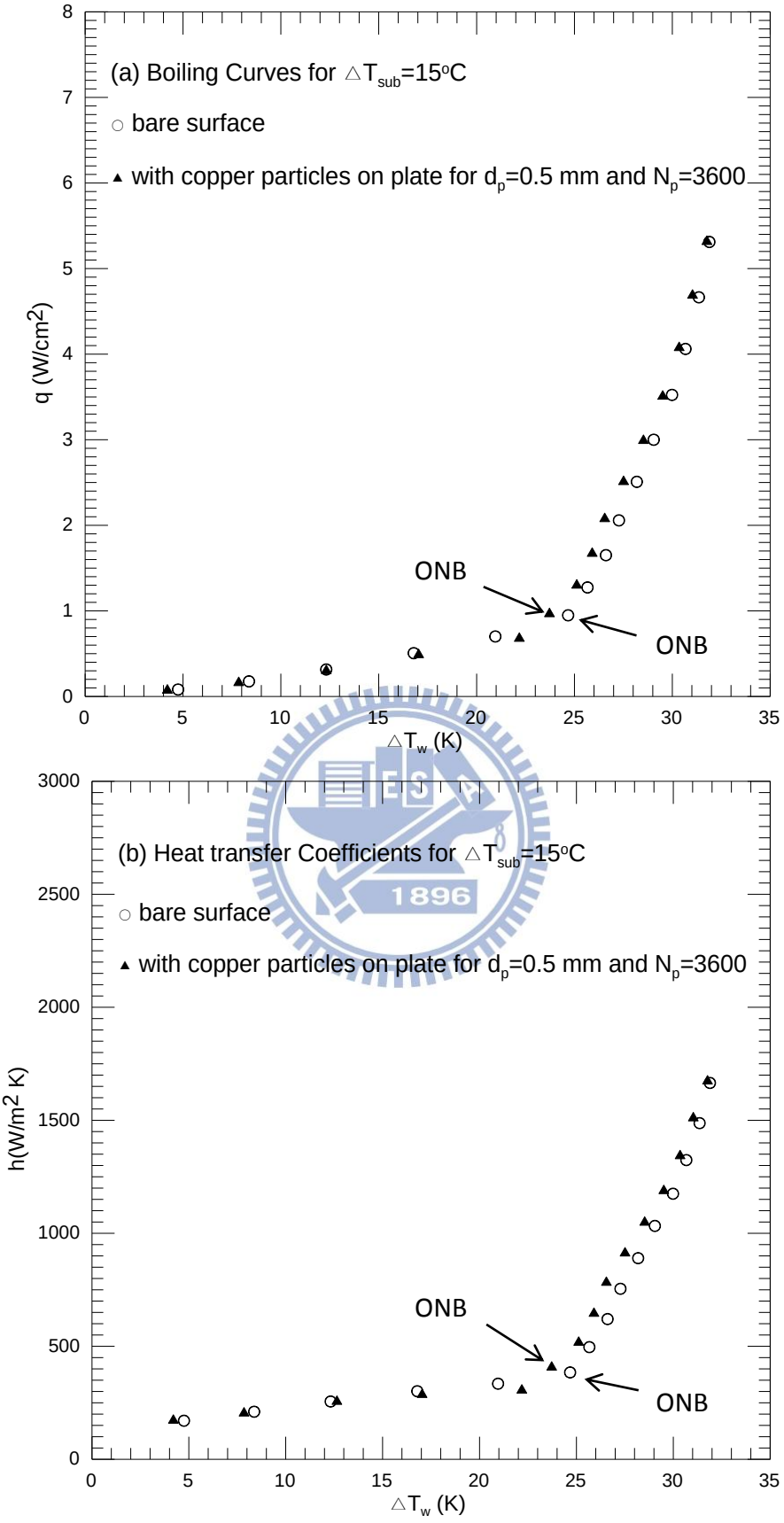

Fig. 4.67 Effects of copper particle diameter and number on subcooled pool boiling curves (a) and boiling heat transfer coefficients (b) for ΔT_{sub}= 15℃ at d_p=0.5 mm and $N_p = 3600$.

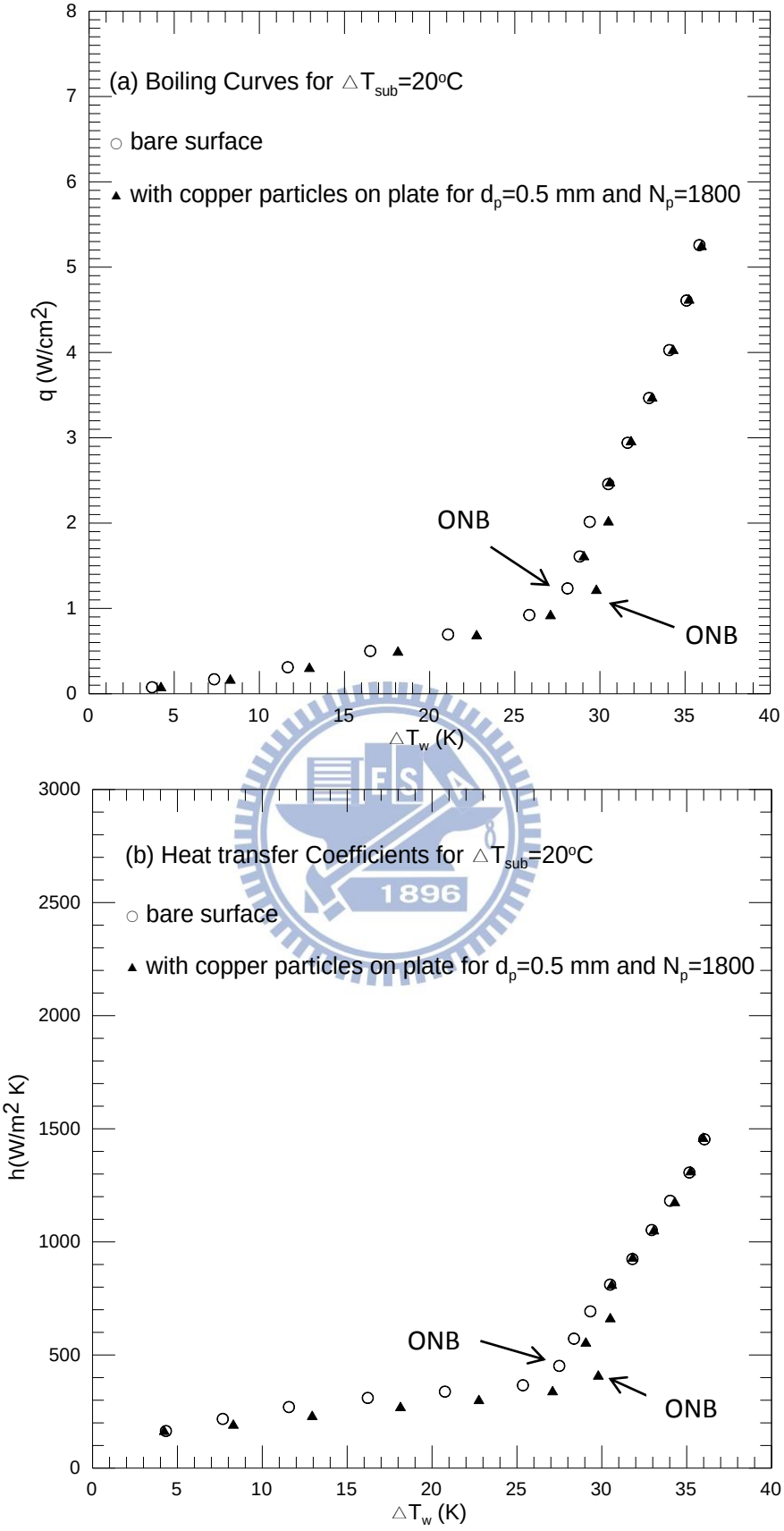

Fig. 4.68 Effects of copper particle diameter and number on subcooled pool boiling curves (a) and boiling heat transfer coefficients (b) for ΔT_{sub}= 20℃ at d_p=0.5 mm and $N_p = 1800$.

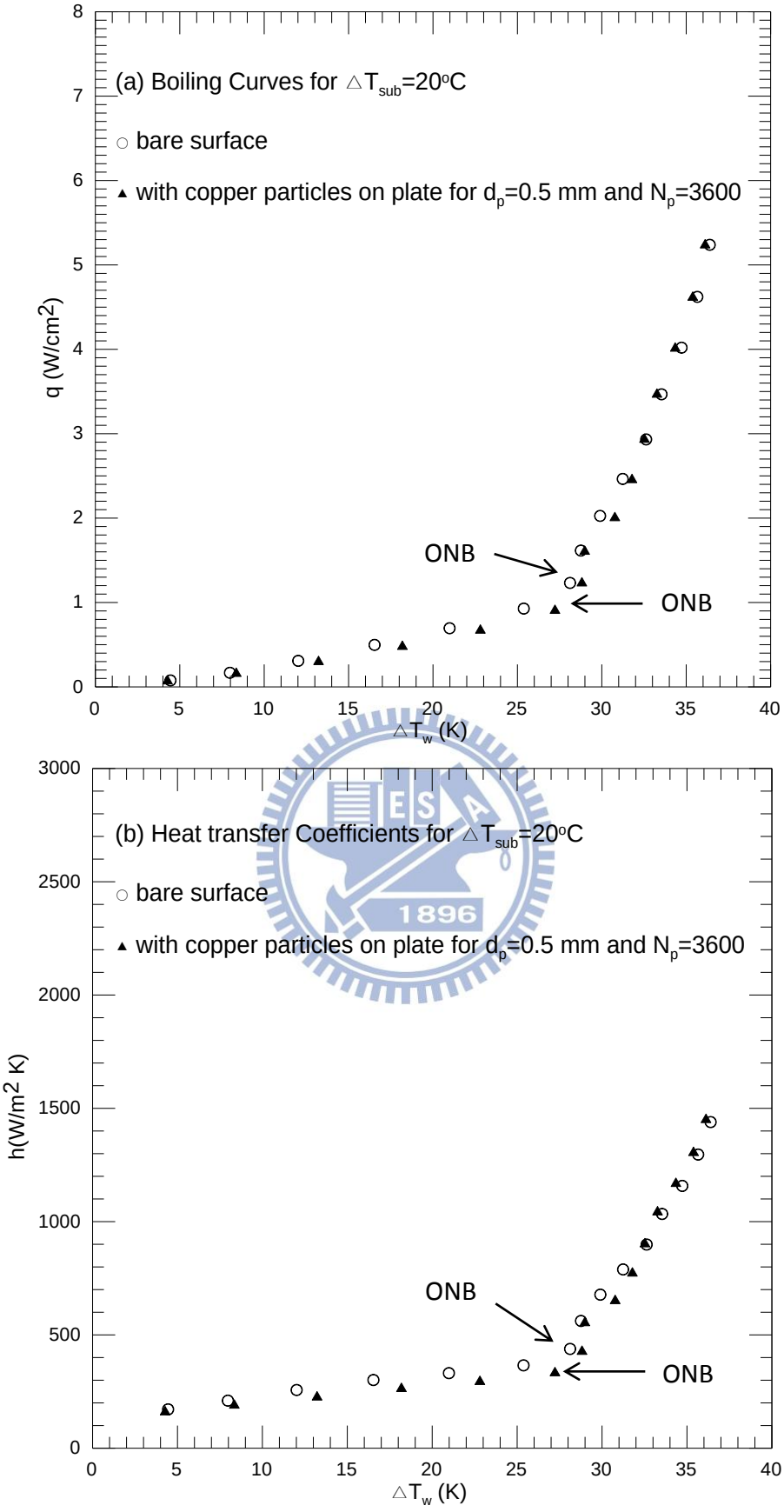

Fig. 4.69 Effects of copper particle diameter and number on subcooled pool boiling curves (a) and boiling heat transfer coefficients (b) for ΔT_{sub}= 20℃ at d_p=0.5 mm and $N_p = 3600$.

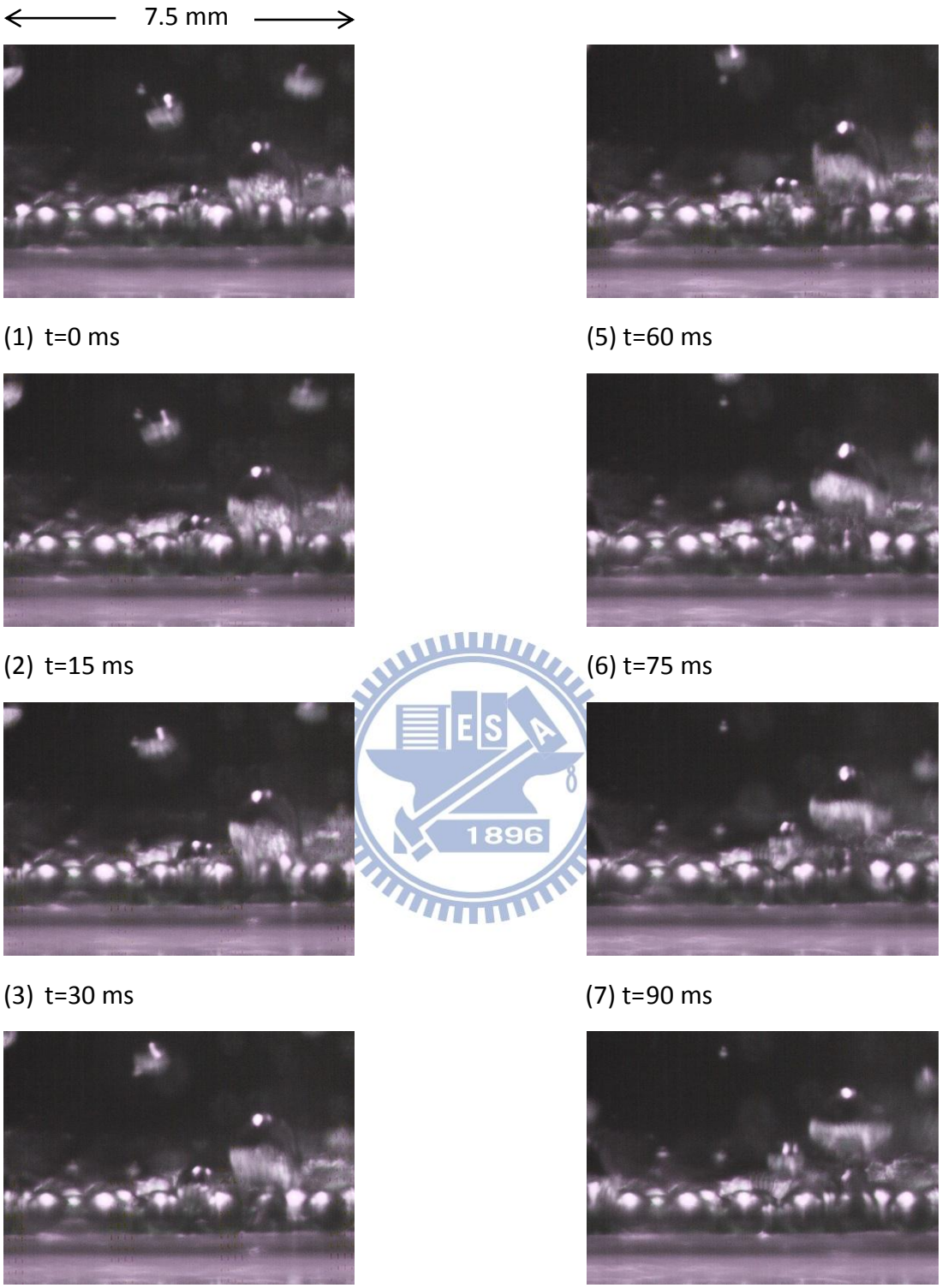

Fig. 4.70 Photos taken from side view of subcooled boiling flow for ΔT_{sub}=5℃ at selected time instants for q= 0.78 W/ cm^2 with copper particles on heated surface at d_p=1.0 mm and $N_p = 600$.

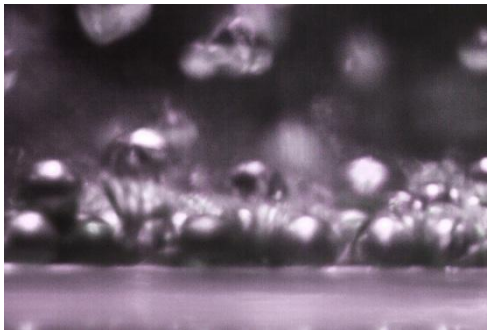

(1) t=0 ms

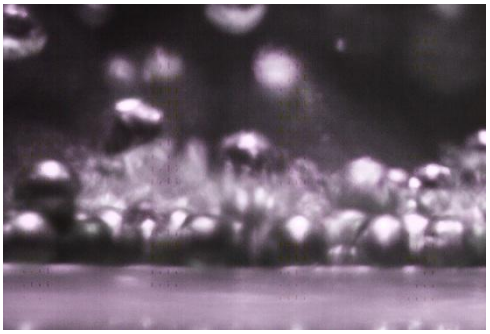

(5) t=60 ms

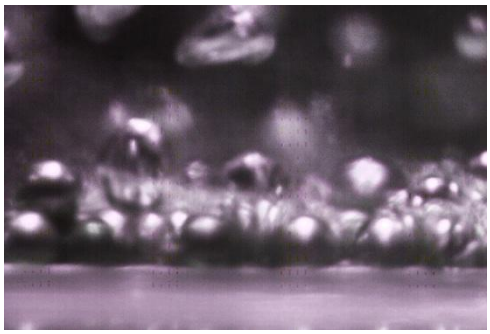

(2) t=15 ms

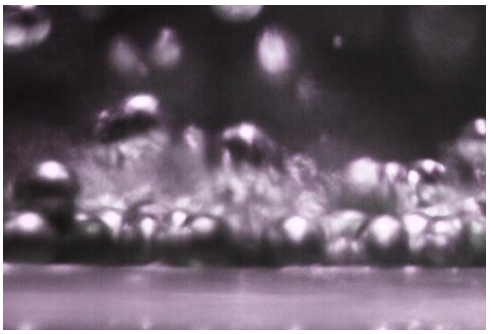

(6) t=75 ms

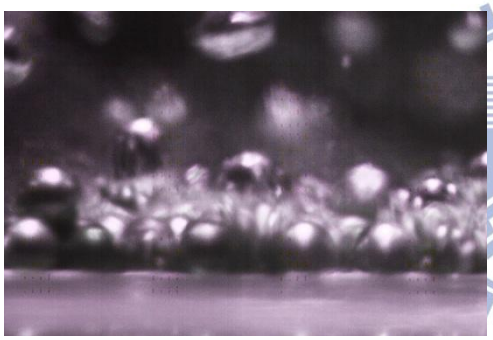

(3) t=30 ms

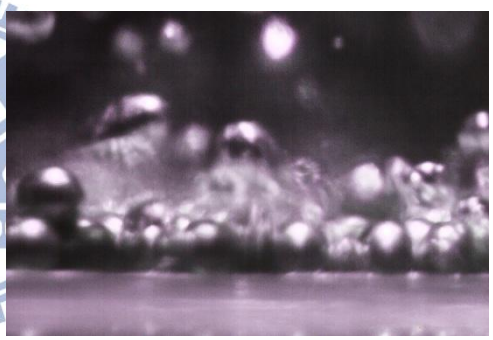

(7) t=90 ms

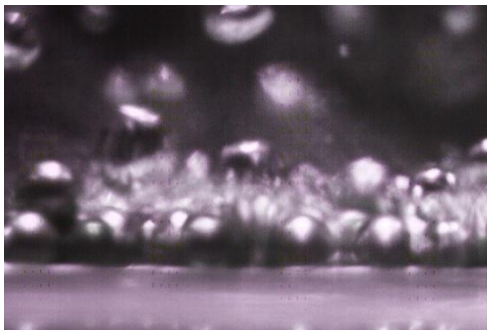

(4) t=45 ms

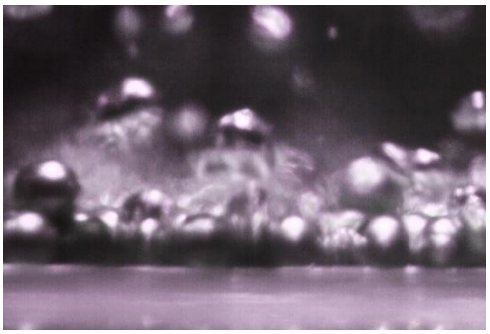

(8) t=105 ms

Fig. 4.71 Photos taken from side view of subcooled boiling flow for ΔT_{sub}=5℃ at selected time instants for q= 2.2 W/ cm^2 with copper particles on heated surface at d_p=1.0 mm and $N_p = 600$.

(1) t=0 ms

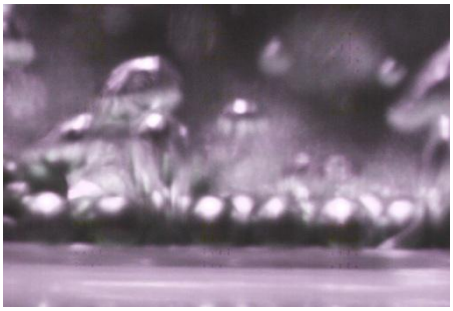

(5) t=60 ms

(2) t=15 ms

(6) t=75 ms

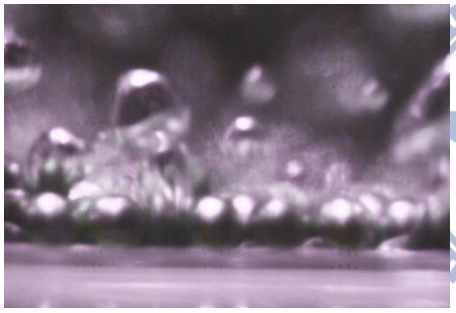

(3) t=30 ms

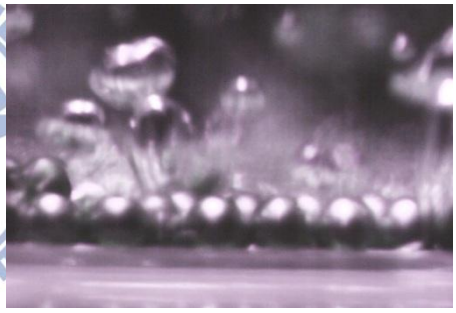

(7) t=90 ms

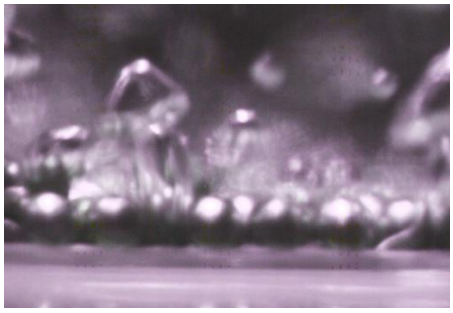

(4) t=45 ms

(8) t=105 ms

Fig. 4.72 Photos taken from side view of subcooled boiling flow for ΔT_{sub}=5℃ at selected time instants for q= 3.1 W/ cm^2 with copper particles on heated surface at d_p=1.0 mm and $N_p = 600$.

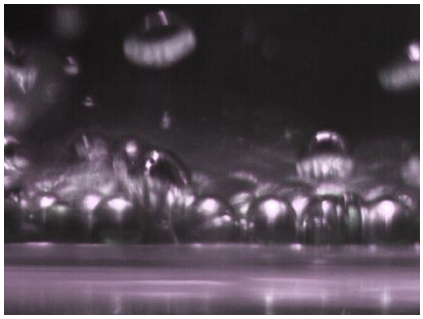

(1) t=0 ms

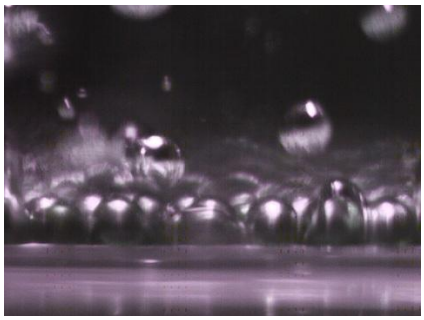

(5) t=60 ms

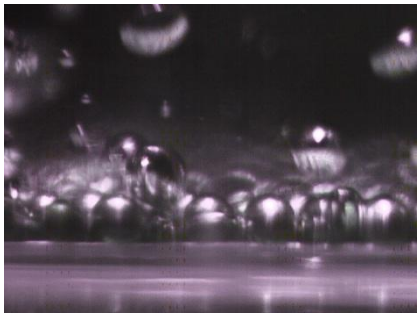

(2) t=15 ms

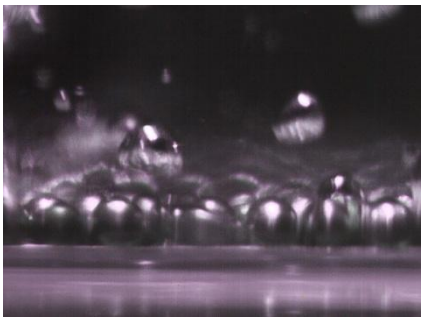

(6) t=75 ms

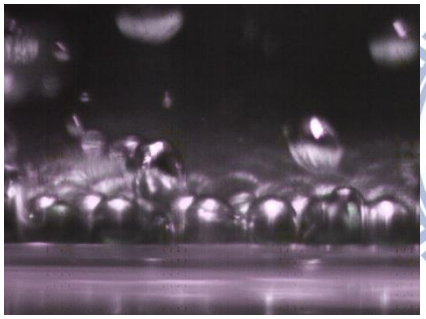

(3) t=30 ms

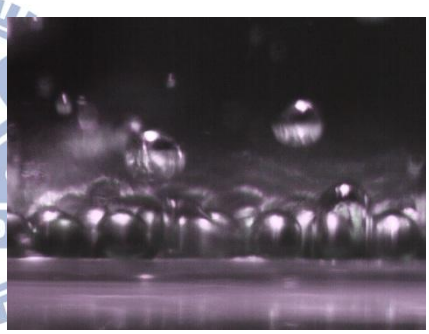

(7) t=90 ms

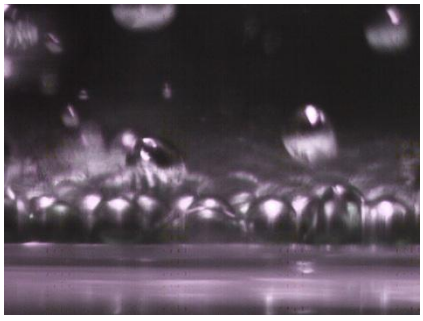

(4) t=45 ms

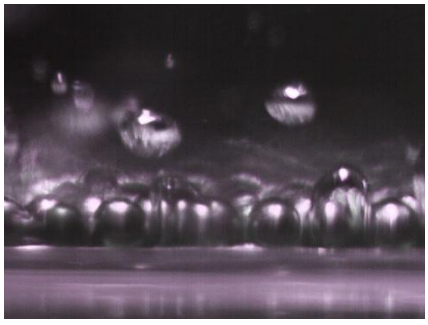

(8) t=105 ms

Fig. 4.73 Photos taken from side view of subcooled boiling flow for ΔT_{sub}=5℃ at selected time instants for q= 1.3 W/ cm^2 with copper particles on heated surface at d_p=1.0 mm and $N_p = 600$.

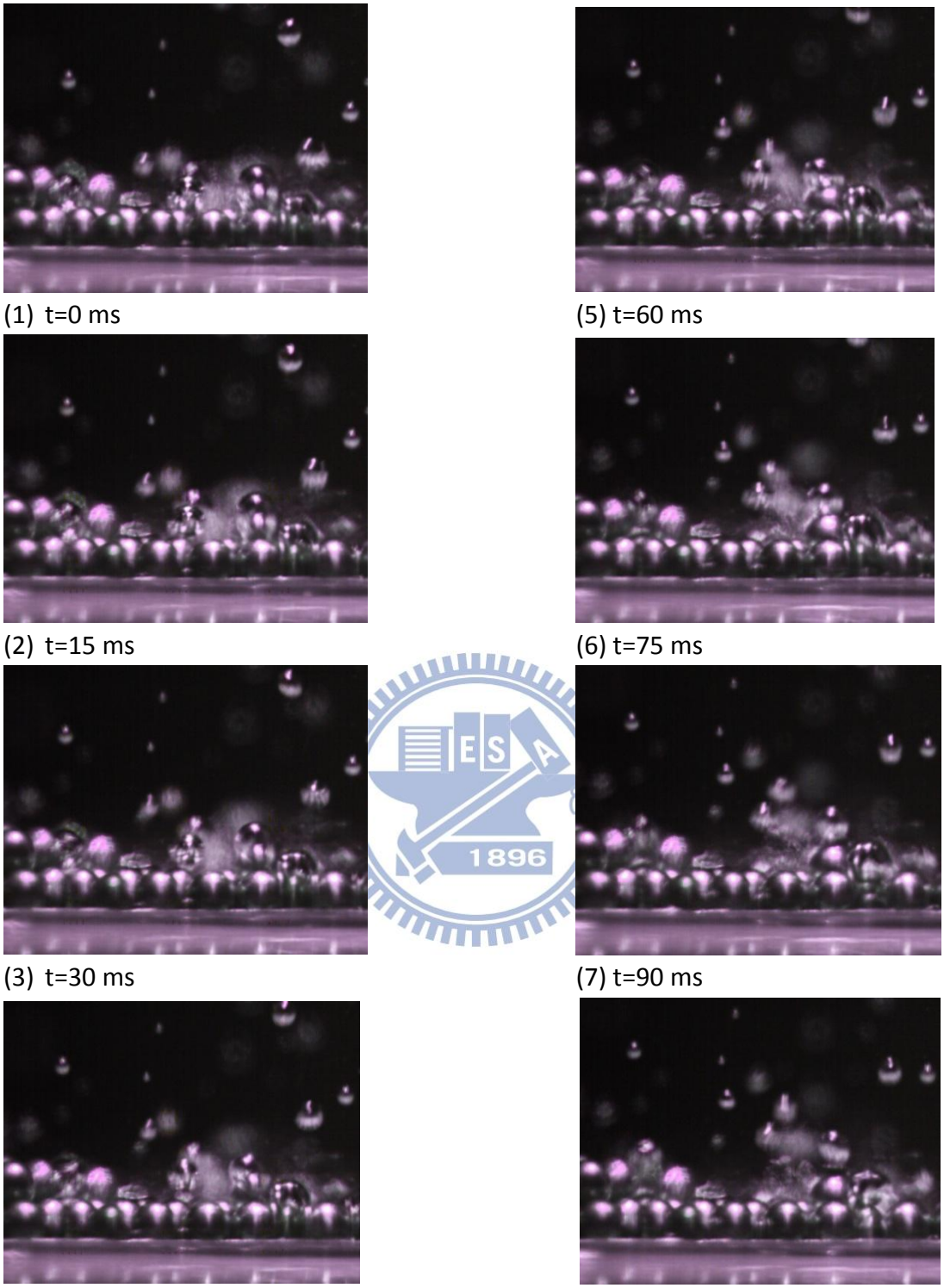

(1) t=0 ms (5) t=60 ms

(2) t=15 ms (6) t=75 ms

(3) t=30 ms (7) t=90 ms

(4) t=45 ms (8) t=105 ms

Fig. 4.74 Photos taken from side view of subcooled boiling flow for ΔT_{sub}=10℃ at selected time instants for q= 1.3 W/ cm^2 with copper particles on heated surface at d_p=1.0 mm and $N_p = 600$.

(1) t=0 ms

(5) t=60 ms

(2) t=15 (s)

(6) t=75 ms

(3) t=30 ms

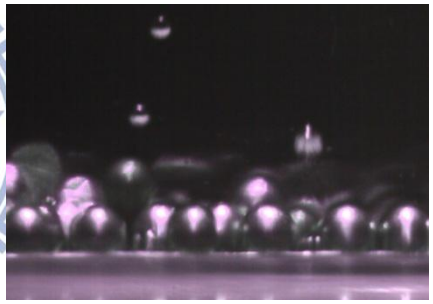

(7) t=90 ms

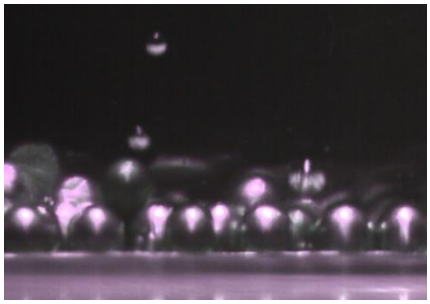

(4) t=45 ms

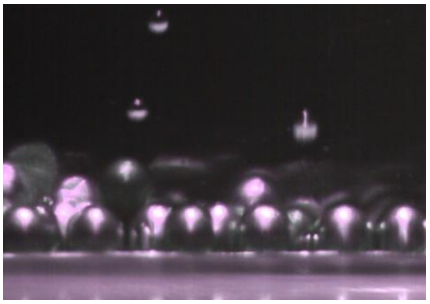

(8) t=105 ms

Fig. 4.75 Photos taken from side view of subcooled boiling flow for ΔT_{sub}=15℃ at selected time instants for q= 1.3 W/ cm^2 with copper particles on heated surface at d_p=1.0 mm and $N_p = 600$.

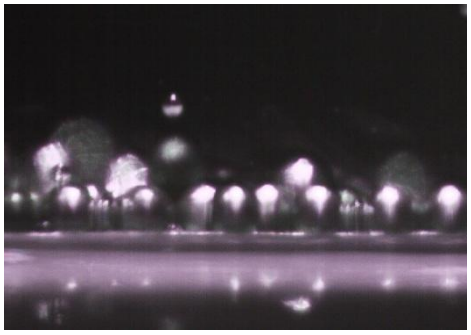

(1) t=0 ms

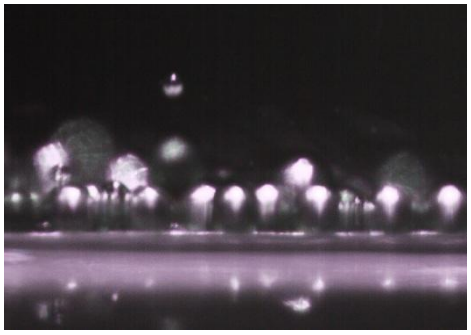

(5) t=60 ms

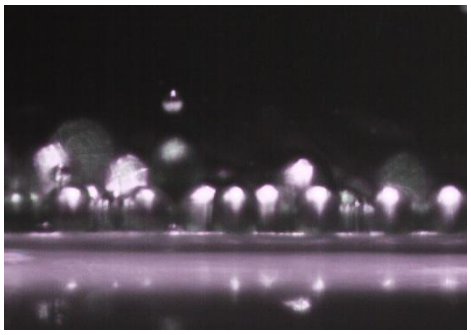

(2) t=15 ms

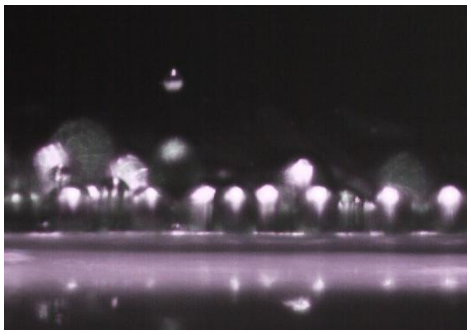

(6) t=75 ms

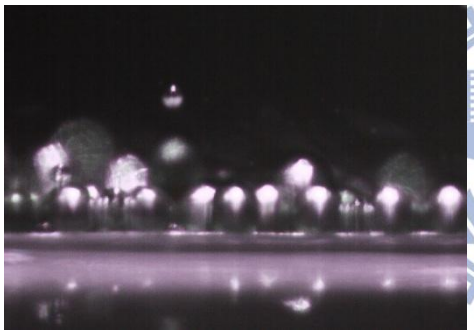

(3) t=30 ms

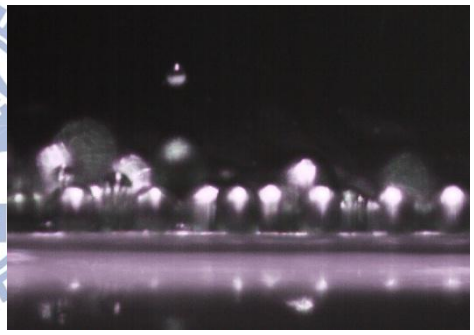

(7) t=90 ms

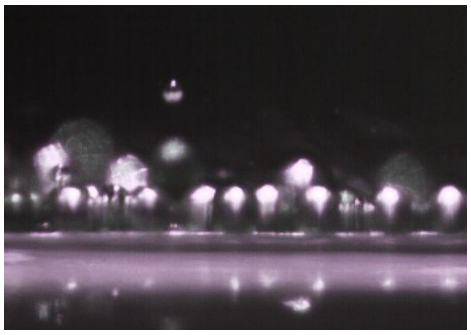

(4) t=45 ms

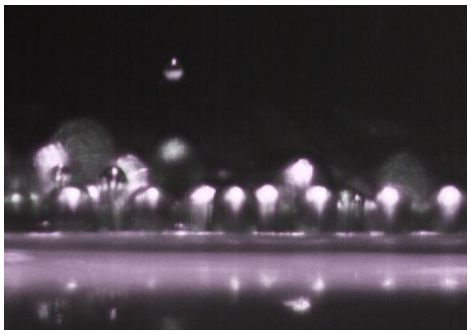

(8) t=105 ms

Fig. 4.76 Photos taken from side view of subcooled boiling flow for ΔT_{sub}=20℃ at selected time instants for q= 1.3 W/ cm^2 with copper particles on heated surface at d_p=1.0 mm and $N_p = 600$

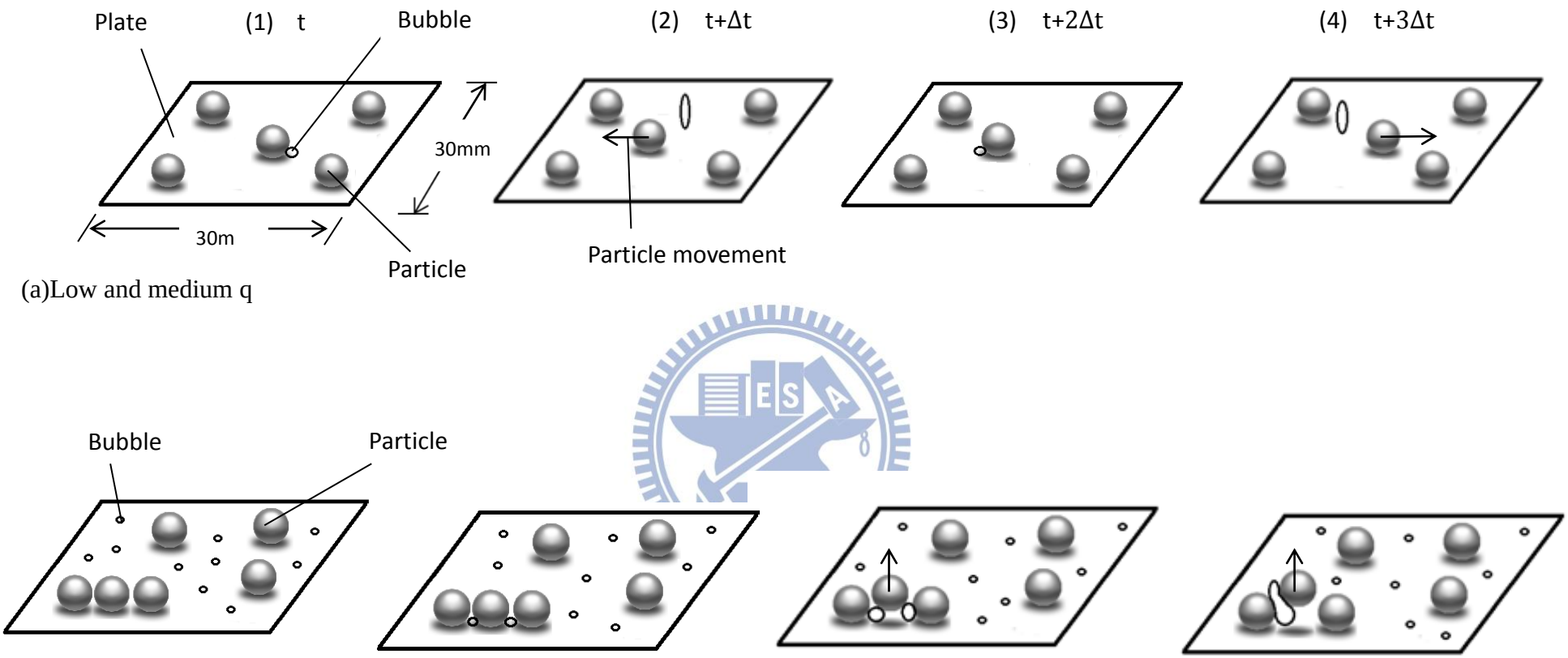

Fig. 4.77 Schematic illustration of particle-bubble interactions in boiling flow on heated surface at (a) low and medium flux and (b) high flux($\Delta t \approx 0.01$ sec.)

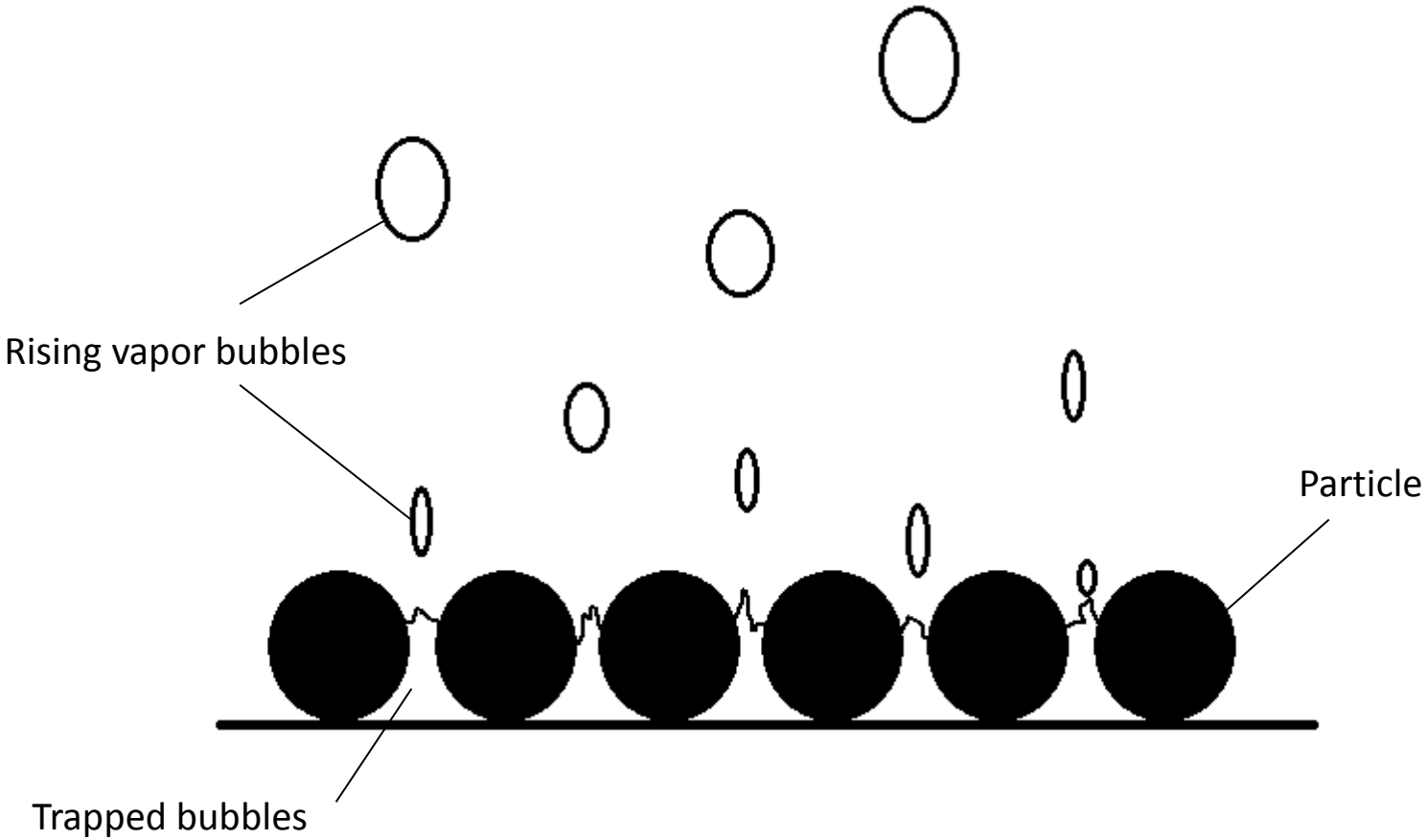

Fig. 4.78 Schematic illustration of retarding bubble growth and departure by particles at high heat flux.

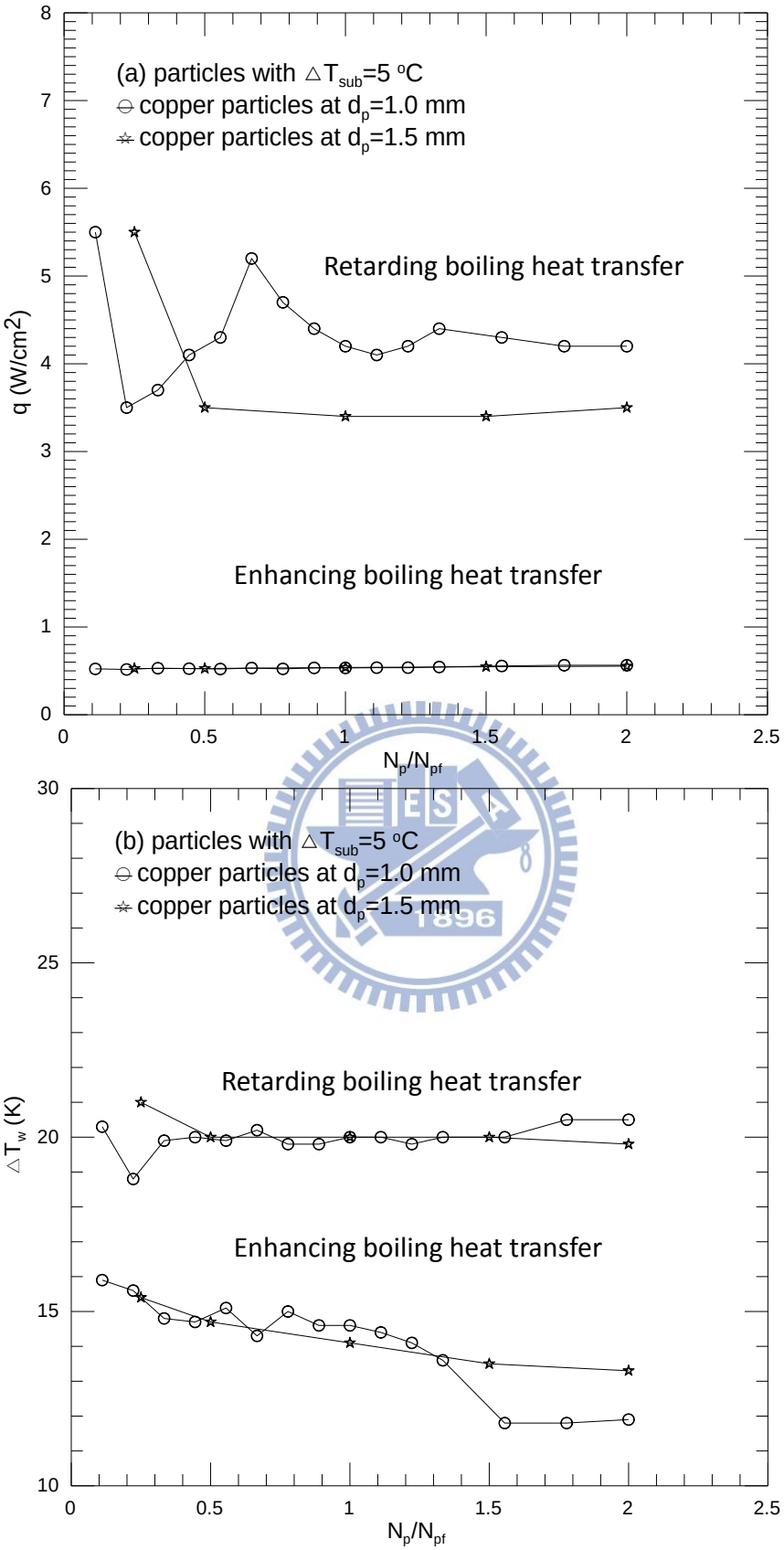

Fig.4.79 Boundaries for boiling heat transfer augmentation and retardation for copper particles with ΔT_{sub}= 5℃ and different d_p and N_p based on (a) q vs. N_p/N_{pf} and (b) ΔT_w vs. N_p/N_{pf}.

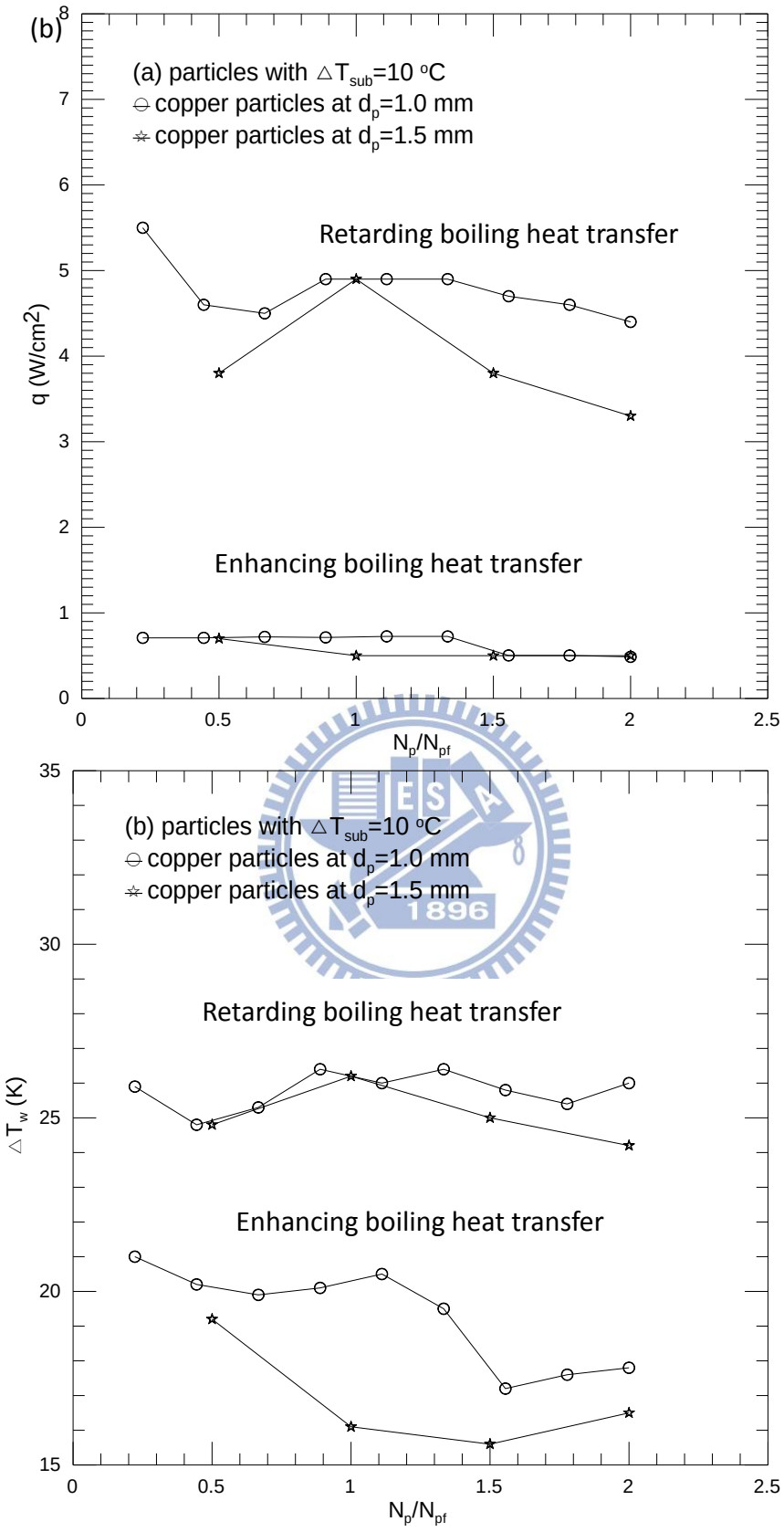

Fig.4.80 Boundaries for boiling heat transfer augmentation and retardation for copper particles with ΔT_{sub}= 10℃ and different d_p and N_p based on (a) q vs. N_p/N_{pf} and (b) ΔT_w vs. N_p/N_{pf}.

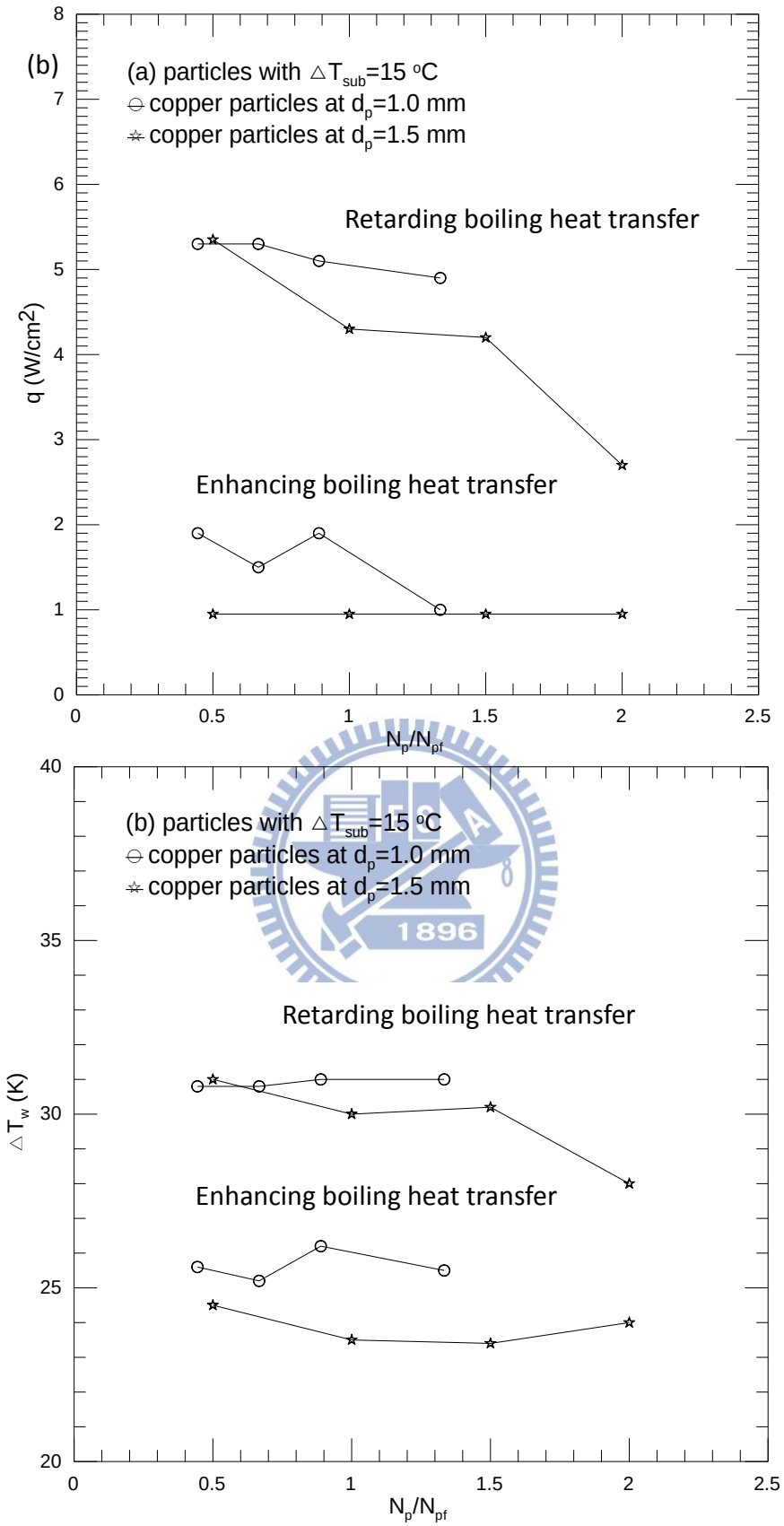

Fig.4.81 Boundaries for boiling heat transfer augmentation and retardation for copper particles with ΔT_{sub}= 15℃ and different d_p and N_p based on (a) q vs. N_p/N_{pf} and (b) ΔT_w vs. N_p/N_{pf}.

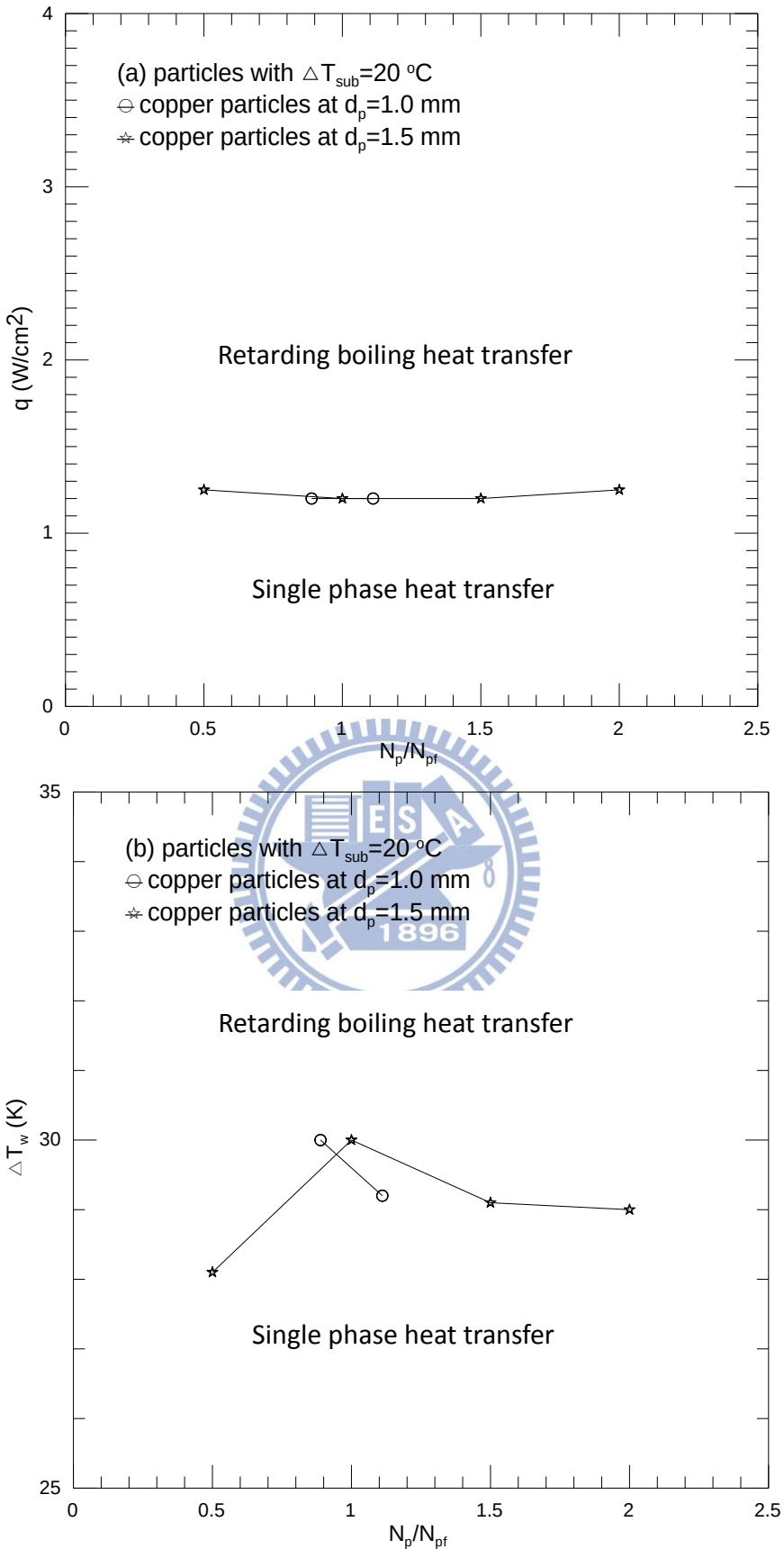

Fig.4.82 Boundaries for boiling heat transfer augmentation and retardation for copper particles with ΔT_{sub}= 20℃ and different d_p and N_p based on (a) q vs. N_p/N_{pf} and (b) ΔT_w vs. N_p/N_{pf}.

CHAPTER 5

CONCLUDING REMARKS

In this study we conduct an experiment to investigate the possible pool boiling heat transfer enhancement in a subcooled boiling flow of FC-72 by placing movable copper particles on the boiling surface. The effects of the liquid subcooling, particle diameter and particle number on the boiling heat transfer enhancement have been examined in detail. The major results obtained from this investigation can be summarized as follows.

(1) The boiling heat transfer enhancement is closely related to the subcooling degree of the working fluid, particle diameter, particle number, and heat flux applied. Specifically, at a higher liquid subcooling the copper particles are less effective in enhancing the boiling heat transfer. At the high ΔT_{sub} of 20℃ the subcooled boiling heat transfer is retarded by the particles especially at a large particle number.

(2) In a slightly subcooled flow with $\Delta T_{sub} \leq 10$℃ the boiling heat transfer can be significantly enhanced by placing copper particles on the heated plate at low and medium heat fluxes (wall superheats) when the total number of the particles in the flow exceeds 60% of the maximum number of particles forming a single closly packed particle layer. For ΔT_{sub}=5℃ and d_p=1.0 mm the boiling heat transfer can be enhanced up to 300% for a suitable choice of the experimental parameters which is also considered as the best heat transfer enhancement among all cases in the experiment. Even for the particle number in the flow well exceeding N_{pf} the enhancement in the boiling heat transfer can be rather significant. Besides, the wall superheat for the incipient boiling can be substantially reduced by the moving

copper particles.

(3) At high heat flux (wall superheat) placing the particles in the flow can substantially retard the boiling heat transfer especially for the large particles. For ΔT_{sub}=5℃ the boiling heat transfer retardation can be 20% for the small copper particles and up to 30% for the large copper particles.

(4) Interactions between the particles and bubbles are very strong in the case of ΔT_{sub}=5℃ and 10℃ at medium and high heat fluxes which result in two opposite effects of enhancing and retarding boiling heat transfer.

(5) At a higher liquid subcooling the bubbles departing from the heated surface are fewer and smaller. The resulting force from the bubble motion acting on the particles is weaker, causing a smaller boiling heat transfer enhancement by the particle movement for a higher ΔT_{sub}.

References

1. G. Xu, B. Guenin, M. Vogel, “Extension of air cooling for high power processors”, Proceedings 9th Intersociety Conference on Thermal Phenomena 1 (2004) 186-193.

2. C. M. Wei, “Enhancement of FC-72 Pool Boiling Heat Transfer by Movable Particles on a Horizontal Plate” , M.S. Theses, Department of Mechanical Engineering, National Chuao Tung University, Hsinchu, Taiwan (2013).

3. S. Nukiyama, “The maximum and minimum values of the heat *Q* transmitted from metal to boiling water under atmospheric pressure”, Journal Japan Society of Mechanical Engineers 37 (1934) 367-374.
(Translated in Int. J. Heat Mass Transfer 9 (1966) 1419-1433).

4. A Bar-Cohen, “Thermal management of air-and liquid-cooled multichip modules”, IEEE Transactions on components, hybrids, and manufacturing technology 10 (2) (1987) 159-175.

5. W. J. Miller, B. Gebhart, N. T. Wright, “Effects of boiling history on a microconfigured surface in a dielectric liquid”, Int. Commun. Heat Mass Transfer 17 (4) (1990) 389-398.

6. J. Y. Chang, S. M. You, “Enhanced boiling heat transfer from micro-porous surfaces: effects of a coating composition and method”, Int. J. Heat Mass Transfer 40 (18) (1997) 4449-4460.

7. S. Vemuri, Kwang J. Kim, “Pool boiling of saturated FC-72 on nano-porous surface”, Int. Commun. Heat Mass Transfer 32 (2005) 27-31.

8. K. N. Rainey, S. M. You, “Pool boiling heat transfer from plain and microporous, square pin-finned surfaces in saturated FC-72”, Trans. ASME J. Heat Transfer 122 (3) (2000) 509-516.

9. K. N. Rainey, S. M. You, “Effect of pressure, subcooling, and dissolved gas on pool boiling heat transfer from microporous, square pin-finned surfaces in FC-72”, Int. J. Heat Mass Transfer 46 (1) (2003) 23-35.

10. H. Honda, H. Takamatsu, J. J. Wei, “Enhanced boiling of FC-72 on silicon chips with micro-pin-fins and submicron-scale roughness”, Trans. ASME J. Heat Transfer 124 (2) (2002) 383-390.

11. J. J. Wei, L. J. Guo, H. Honda “Experimental study of boiling phenomena and heat transfer performances of FC-72 over micro-pin-finned silicon chips”, Heat and Mass Transfer 41 (8) (2005) 744-755.

12. L. Zhang, M. Shoji “Nucleation site interaction in pool boiling on the artificial surface”, Int. J. Heat Mass Transfer 46 (2003)513-522

13. C. K. Yu. , D. C. Lu. and T. C. Cheng “Pool boiling heat transfer on artificial micro-cavity surface in dielectric fluid FC-72 ”, J. Micromech. Microeng. 16 (1989)752-759

14. Chen Li, G. P. Peterson and Y. Wang “Evaporation/Boiling in Thin Capillary Wick (I) –Wick Thickness Effects” Transaction of the ASME 128 (2006) 1312-1319

15. Chen Li, G. P. Peterson “Evaporation/Boiling in Thin Capillary Wick (II) –Effects of Volumetric Porosity and Mesh Size” Transaction of the ASME 128 (2006) 1320-1328

16. T. M. Anderson, I. Mudawar, “Microelectronic Cooling by Enhanced Pool Boiling of a Dielectric Fluorocarbon Liquid”, Trans. ASME J. Heat Transfer 111 (3) (1989) 752-759.

17. J. P. O’Connor, S. M. You, “A Painting Technique to Enhance Pool Boiling Heat Transfer in Saturated FC-72”, Trans. ASME J. Heat Transfer 117 (2) (1995) 387-393.

18. J. P. O’Connor, S. M. You, D. C. Price, “A Dielectric Surface Coating Technique to Enhance Boiling Heat Transfer from High Power Microelectronics”, IEEE Transactions on components, packaging and manufacturing technology Part A 18 (3) (1995) 656-663.

19. J. Y. Chang, S. M. You, “Boiling heat transfer phenomena from micro-porous and porous surfaces in saturated FC-72”, Int. J. Heat Mass Transfer 40 (18)

(1997) 4437-4447.

20. J. Y. Jung, H. Y. Kwak, “Effect of surface condition on boiling heat transfer from silicon chip with submicron-scale roughness”, Int. J. Heat Mass Transfer 49 (23-24) (2006) 4543-4551.

21. H. Honda, J. J. Wei, “Enhanced boiling heat transfer from electronic components by use of surface microstructures”, Experimental Thermal and Fluid Science 28 (2-3) (2004) 159-169.

22. K. N. Rainey, S. M. You, “Effects of heater size and orientation on pool boiling heat transfer from microporous coated surfaces”, Int. J. Heat Mass Transfer 44 (14) (2001) 2589-2599.

23. K. N. Rainey, S. M. You, S. Lee, “Effect of pressure, subcooling, and dissolved gas on pool boiling heat transfer from microporous surfaces in FC-72” Trans. ASME J. Heat Transfer 125 (1) (2003) 75-83.

24. H. M. Chou, R. F. Horng, Y. S. Liu, J. L. Wong, “The effect of grooved pattern on enhanced boiling heat transfer in a cylindrical tank base with a constant surface area”, Int. Comm. Heat Mass Transfer 29 (7) (2002) 951-960.

25. S. Hasegawa, R. Echigo, S. Irie, “Boiling characteristics and burnout phenomena on heating surface covered with woven screens”, Journal of Nuclear Science and Technology 12 (11) (1975) 722-724.

26. J. Y. Tsay, Y. Y. Yan, T. F. Lin, “Enhancement of pool boiling heat transfer in a horizontal water layer through surface roughness and screen coverage”, Heat and Mass Transfer 32 (1-2) (1996) 17-26.

27. J. W. Liu, D. J. Lee, A. Su, “Boiling of methanol and HFE-7100 on heated surface covered with a layer of mesh”, Int. J. Heat Mass Transfer 44 (1) (2001) 241-246.

28. A. A. Watwe, A. Bar-Cohen and A. McNeil, “Combined Pressure and Subcooling Effects on Pool Boiling from a PPGa Chip Package”. InterSociety Conference on Thermal Phenomena (1996).

29. A. Franco, E. M. Latrofa, V. V. Yagov, “Heat transfer enhancement in pool boiling of a refrigerant fluid with wire nets structures”, Experimental Thermal and Fluid Science 30 (3) (2006) 263-275.

30. H. M. Kurihara, J. E. Myers, “The effects of superheat and surface roughness on boiling coefficients”, A.I.Ch.E. Journal 6 (1) (1960) 83-91.

31. M. Shi, Y. Zhao, Z. Liu, “Study on boiling heat transfer in liquid saturated particle bed and fluidized bed”, International Journal of Heat and Mass Transfer 46(2003) 4695-4702.

32. M. Matijevic, M. Djuric, Z. Zavargo, M. Novakovic, “Improving Heat Transfer with Pool Boiling by Covering of Heating Surface with Metallic Spheres”, Heat Transfer Engineering 13(3)(1992) 49-57.

33. Mohamed S., El-Genk, J. L. Parker, “Pool Boiling in Saturated and Subcooled HFE-7100 Dielectric Fluid form a Porous Graphite Surface”, Inter Society Conference on Thermal Phenomena USA (2004) 655-662

34. A Coulibaly, X. Lin, J. Bi, M. Christopher, “Bubble Coalescence at Constant Wall Temperatures During Subcooled Nucleate Pool Boiling”, Experimental Thermal and Fluid Science 44(2013) 209-218

35. T. Harada, H. Nagakura, T.Okawa, “Dependence of Bubble Behavior in Subcooled Boiling on Surface Wettability”, Nuclear Engineering and Design 240(2010) 3949-3955

36. D. Wen, Y. Ding, “Experimental investigation into the pool boiling heat transfer of aqueous based γ-alumina nanofluids”, J. Nanoparticle Res.7 (2) (2005) 265-274.

37. I. C. Bang, S. H. Chang, “Boiling Heat Transfer Performance and Phenomena of Al2O3-water Nano-fluids from a Plain Surface in a Pool”, Int. J. Heat Mass Transfer 48 (12) (2005) 2420-2428.

38. J. H. Jeong, Y. C. Kwon, “Effects of ultrasonic vibration on subcooled pool boiling critical heat flux”, Heat Mass Transfer (2006) 42 : 1155-1161.

39. M. Cipriani, P. Di Marco, W. Grassi, “Effect of an externally applied electric field on pool film boiling of FC-72”, HEAT TRANSFER ENGINEERING 26 (2010) : 3-13.

40. Y. V. Navruzov, P. V. Mamontov, A. V. Stoychev, “Subcooled liquid Pool Boiling Heat Transfer on a Vibration Heating Surface”, Heat Transfer Research 24 (6) (1992) 771-776.

41. S. J. Kline, F. A. McClintock, “Describing uncertainties in single sample experiments”, Mechanical Engineering 75 (1953) 3-8.

42. R. J. Moffat, “Contributions to the theory of single-sample uncertainty analysis”, Journal of Fluids Engineering 104 (2) (1982) 250-260.

43. E. Radziemska, W. M. Lewandowski, “The effect of plate size on the natural convective heat transfer intensity of horizontal surfaces”, Heat Transfer Engineering 26 (2) (2005) 50-53.